Heavy Ion Laboratory

ANNUAL REPORT 2022

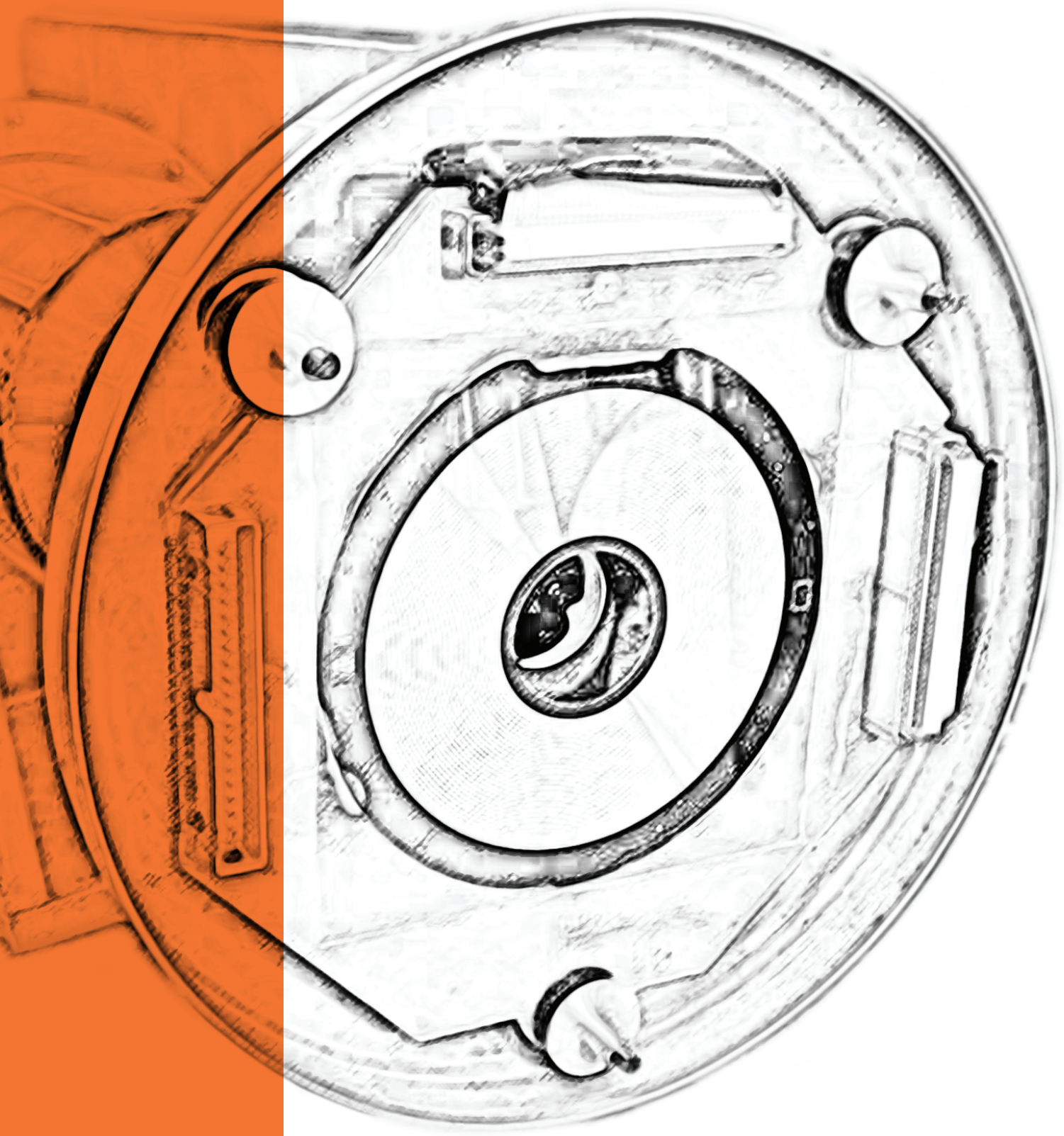

UNIVERSITY OF WARSAW

HIL
Heavy Ion Laboratory

Heavy Ion Laboratory

University of Warsaw

Annual Report

2022

Warszawa, June 2023

Various information concerning the Laboratory is distributed via the HIL mailing list.
In order to subscribe to the list please visit the page
`http://mail.slcj.uw.edu.pl/mailman`

Annual Report of the
Heavy Ion Laboratory, University of Warsaw
ul. Pasteura 5a, 02-093 Warszawa, Poland
phone (+48)22-8222123, (+48)22-5546000
fax (+48)22-6592714
`http://www.slcj.uw.edu.pl`

Editors:
Justyna Samorajczyk-Pyśk, Marzena Wolińska-Cichocka,
Andrzej Tucholski, Nicholas Keeley,
e-mail: raport@slcj.uw.edu.pl
ISSN 1895-6726

Cover design:
Rafał Klęk

On the cover:
Silicon Coulomb excitation Array (SilCA) based on the Double-sided Silicon Stripped Detector (DSSD) for charged particles, placed in the new scattering chamber designed and constructed at the Heavy Ion Laboratory, University of Warsaw.

Contents

Introduction

Early 2022 looked promising. The pandemic was slowly subsiding and towards the end of the previous year, 2021, a large international experiment, HIL088, could already be carried out at HIL. Furthermore, the good news concerning the approval of the EURO-LABS project came to us in January, allowing the Laboratory to receive funds to host foreign research groups within the Transnational Access programme. The year indeed began in a very promising way for nuclear science in Europe. Unfortunately, the situation dramatically changed in February, when the news regarding Russia's attack on Ukraine left everyone in great shock as the world suddenly stopped and looked in that direction. We anxiously waited for news from our Ukrainian HIL users and friends from the institutes in Kiev and Kharkov. Soon, the bold decision was taken by the Polish authorities to withdraw Poland from the list of countries contributing to the Joint Institute for Nuclear Research in Dubna, which was only one of many severe consequences of the war. For our Laboratory, this meant the discontinuation of many common projects on the development of experimental equipment and the termination of important technical cooperation in the field of accelerator physics. However, despite the war in Ukraine, 2022 brought a number of papers summarising the activities of Ukrainian and Kazakh research groups performed using beams from the U-200P cyclotron. It is worth highlighting the publications by A. T. Rudchik et al., Phys Rev. C 106, 014615 (2022) and S.V. Artemov et al., Eur. Phys. J. A 58, 24 (2022).

In the shadow of war right on our eastern border, a very successful spring experimental campaign was carried out in Warsaw. The results of Coulomb excitation experiments and lifetime measurements using a plunger brought to HIL from the University of Cologne confirmed that the time of the pandemic had been well used to prepare the cyclotron for operation. Among the experiments performed, the project to study ^{110}Cd using the Coulomb excitation method led by Dr Katarzyna Wrzosek-Lipska, initiated in 2015 at HIL, was continued in a very successful run at home, followed by a series of measurements abroad proposed by the team from HIL in cooperation with the University of Guelph, Canada and CEA Saclay, France, carried out at ANL, USA, using the GRETA array and at LNL, Italy, using the AGATA spectrometer.

The HIL Programme Advisory Committee met in April 2022 for the first time with its new member composition. All nine proposals presented at the PAC meeting received the PAC's recommendation and filled the laboratory's work schedule until the beginning of 2023. Four of them were addressed to the NEEDLE setup (NEDA & EAGLE), a newly constructed detection array at HIL.

During the summer our Laboratory was surprised by further bad news from the Ministry of Science about the suspension of funding for the Warsaw cyclotron. With the lack of funds to cover the expenses necessary to conduct the autumn experimental campaign, it was necessary to suspend the activity of the accelerator to prevent increasing the Laboratory's deficit. This was particularly painful for our foreign users, as they could not benefit from the support of their research projects from the EURO-LABS TNA program launched on September 1, 2022. Fortunately, our research work could continue based on funds from grants and international cooperation. Thanks to the outstanding efforts of the team of Dr Grzegorz Jaworski and Dr hab. Marcin Palacz, the neutron detectors of NEDA were installed in the EAGLE frame and a fully digital readout for the NEEDLE setup was successfully developed. The construction of the new "Warsaw DSSD" chamber was also completed and bench-tested at HIL, to be installed soon after at IJCLab in Orsay

near Paris for the physics campaign scheduled for the first months of 2023. Furthermore, radiobiological projects at HIL were carried out in a newly equipped dedicated isotope laboratory and cooperation with the JPET team from the Jagiellonian University also developed successfully.

Finally, thanks to the support of the Rector of the University of Warsaw, Prof. Alojzy Z. Nowak and many other kind people, in the last days of December we obtained funds for the operation of the Warsaw Cyclotron. This allowed us to look to the new year with hope. Today we know that the beginning of 2023 was very successful at HIL, which keeps us excited about the future. Keep on going!

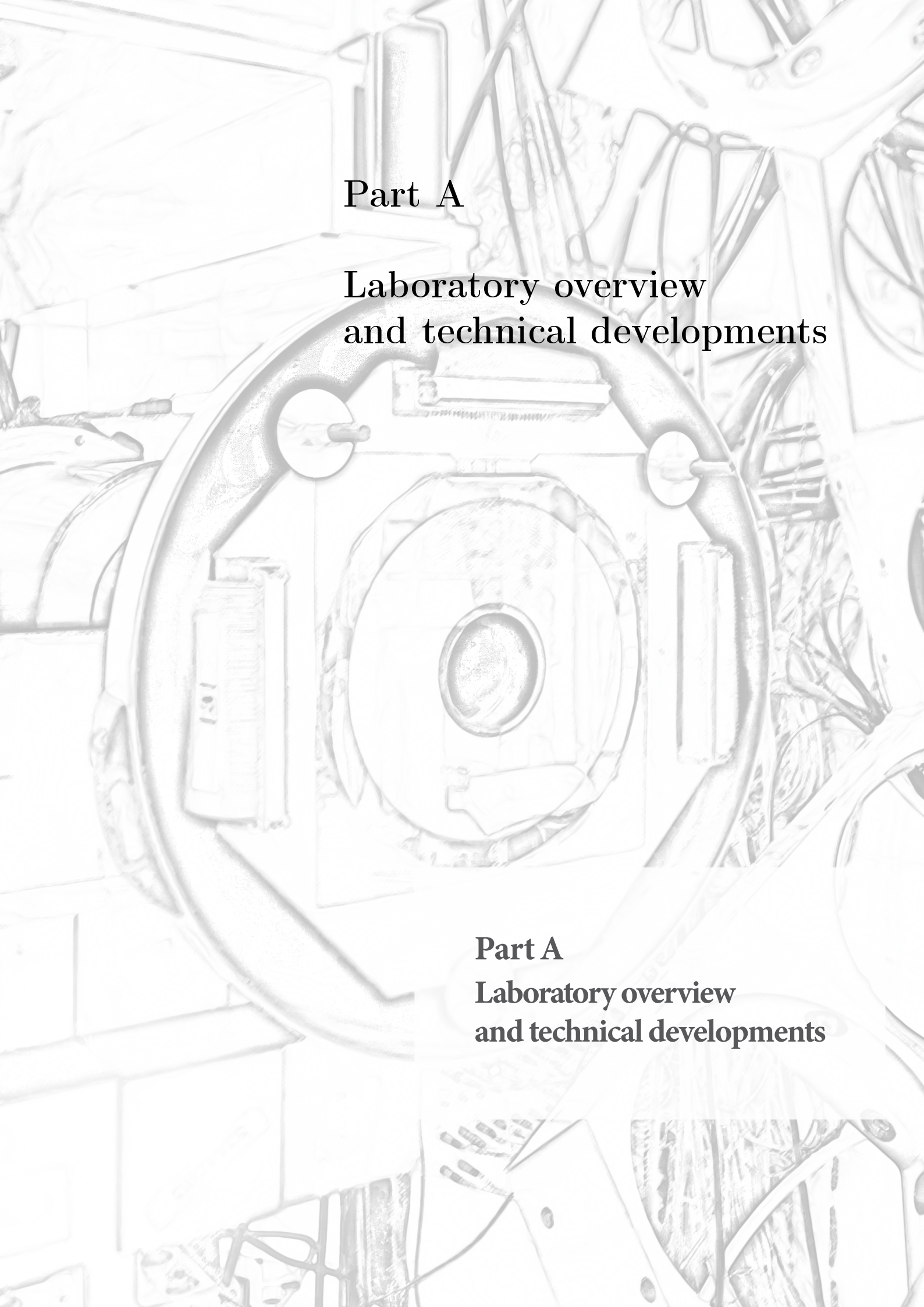

Part A

Laboratory overview and technical developments

Part A
Laboratory overview and technical developments

A.1 Cyclotron operation in 2022 and tasks carried out in order to improve the cyclotron infrastructure and efficiency

J. Choiński, P. Gmaj, A. Górecki, A. Bednarek, T. Bracha, A. Jakubowski, P. Jasiński, W. Kalisiewicz, M. Kopka, W. Kozaczka, P. Krysiak, K. Łabęda, K. Makowski, I. Mazur, J. Miszczak, B. Paprzycki, K. Pietrzak, B. Radomyski, O. Saeed Mohamed Nassar, K. Sosnowski, Ł. Standyło

Heavy Ion Laboratory, University of Warsaw, Warszawa, Poland

Operation:

The main activity of the technical team, especially in the first half of the year, was to provide ion beams for experiments recommended by the PAC and approved by the HIL Director. Works related to the development of thecyclotron infrastructure were also not neglected, and ares discussed in further articles in this Report. The development of work on large modernization projects was strongly limited due to the lack of adequate financing in 2022. Hence, the main effort was put into maintenance of the cyclotron infrastructure and the replacement of worn out elements.

ECR Ion sources:

The 14.5 GHz ECR ion source operated for the needs of the cyclotron and experiments without any problems. In the meantime the old 10 GHz ECR ion source was upgraded. New water pipes for the water cooling system of the source were installed. The source has been completely disassembled and each part has been checked and replaced with a new one. Small adjustment of the position of the puller and the whole extraction carried out. A new RF coupler without a long tube was designed, built and tested in the source. The new type of RF coupler allows the mounting of an oven to produce a Nickel beam. The first prototype of such an oven was built and tested with a positive result. The final structure will be built next year. At the end of the year new coils for the source were wound.

Cyclotron:

At the beginning of the year a slight modification was made to the duant "A" puller's position, plus a small adjustment in the magnetic field of the central part of the cyclotron. All work was aimed at improving the efficiency of the cyclotron and preparing the machine for upcoming experiments. Taking advantage of the opening of the cyclotron, the shape of the cyclotron center was modernized in order to install a new inflector.

Experiments:

In 2022 five experiments recommended by the PAC were performed: HIL093, HIL094, HIL103, HIL087 and HIL102.

- HIL093 Probing shapes and structures in ^{100}Ru via Coulomb excitation (20.03-05.04.2022)

- HIL094 Electromagnetic structure of low-lying states in ^{110}Cd – complementary Coulomb excitation measurements with a ^{14}N beam (06-13.04.2022)
- HIL103 Semiconductor detectors for low-energy heavy ions (30.05-03.03.2022)
- HIL087 Lifetime studies in neutron-deficient ^{172}Os using the RDDS technique EAGLE + Cologne Plunger (20-30.06.2022)
- HIL102 Search for chiral to not chiral transition by lifetime measurement of I=10^{+} state in ^{128}Cs with a plunger technique (04-10.07.2022).

The remaining experiments planned for implementation in 2022 and recommended by the Experimental Committee had to be postponed due to various limitations caused by the pandemic and problems with financing the work of the Laboratory in the second half of the year. As every year, in October the students' workshop was held, but without the participation of the cyclotron.

A.2 Modernization of the spiral inflector

J. Choiński, B. Radomyski, M. Antczak, P. Jasiński, W. Kalisiewicz, R. Kopik, K. Łabęda, B. Paprzycki

Heavy Ion Laboratory, University of Warsaw, Warszawa, Poland

As a result of cooperation between the HIL team and the JINR accelerator team in Dubna the U-200P cyclotron has been equipped with a spiral inflector. The accumulated experience from the operation of the inflector convinced us that modernizing it was worth the effort .

We had a number of goals in mind: replacing a damaged inflector should be possible without venting the accelerator, the periods of inflector operation between replacements should be extended, the transmission of the ion beam through the inflector should be improved, thus increasing the beam current from the cyclotron.

In the original design, the high voltage to the inflector electrodes was supplied from the bottom of the inflector, through a special base, with wires running in the cyclotron valley, from the side wall of the cyclotron vacuum chamber. If the inflector was to be replaced, the accelerator had to be vented and the top half of the cyclotron had to be lifted to access the inflector. The downtime for the replacement of the inflector and recovery of the cyclotron vacuum was about 1 week.

In the first stage of the modernization the HV supply route from the side wall of the cyclotron chamber was replaced with a HV supply from the top of the cyclotron, through the existing channel in the upper magnet beam. Previously, this channel housed the internal PIG ion source. As a result lifting of the upper part of the accelerator is no longer needed, and the entire cyclotron recovery process was shortened to 3 days.

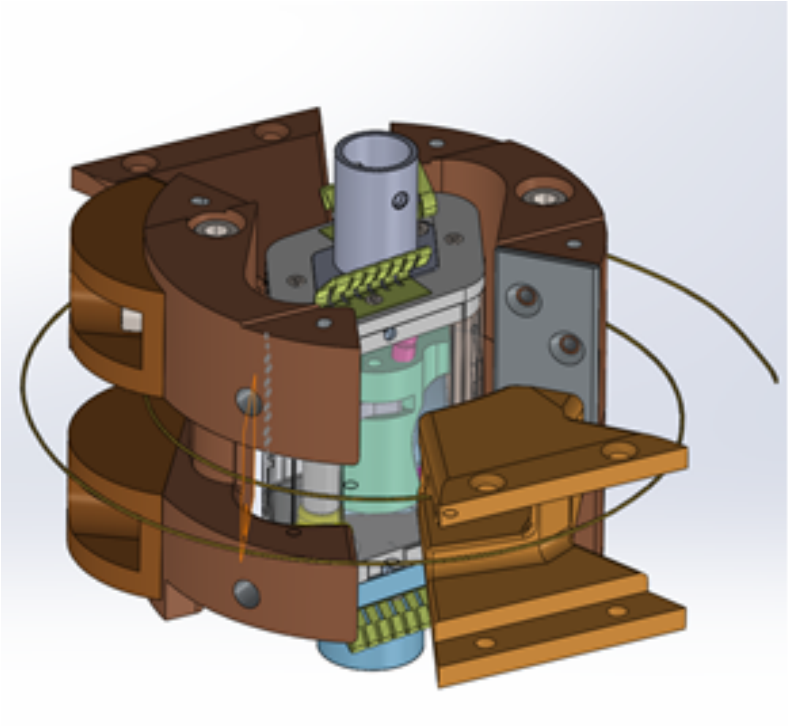

Figure 1: The inflector, puller and central part of the U-200P cyclotron.

The powering the inflector from the top of the cyclotron made it possible to introduce a number of additional modifications. These modifications were made in stages to both the inflector and the cyclotron. The modifications are listed below:

- the shape of the electrodes and their mounting in the inflector housing has been corrected;
- the method of powering the electrodes within the housing has been changed;
- the external height of the inflector has been changed, so that it is possible to find the optimal entry of the ion beam into the medial plane of the cyclotron by changing the height of the inflector;
- a change in the position of the inflector exit relative to the duant puller was obtained by modifying the elements of the cyclotron center and the puller and the shape of the inflector housing, see Figure 1.

Currently, it is possible to change the angle of the inflector position relative to the puller by an angle of $\pm 8^{\circ}$ relative to its original position. Changes in the vertical and horizontal position of the inflector are carried out by a dedicated mechanical setup installed on the top of the magnet above the vertical channel of the cyclotron. In the first quarter of 2023, tests of one of the versions of the new inflector were carried out. The intensity of the ion beam at the exit from the cyclotron has increased by a factor of approx. 40%. The working time of the new inflector is comparable to the original inflector. Further testing of new versions of the inflector will continue in 2023. Ultimately, our goal is to introduce a version that will allow replacement of the inflector without venting the cyclotron .

A.3 An internal, well cooled, target station for the U-200P cyclotron suitable for irradiation of different types of targets

J. Choiński, B. Radomyski, M. Antczak, T. Bracha, P. Jasiński, R. Kopik, K. Łabęda, J. Miszczak, Ł. Świątek

Heavy Ion Laboratory, University of Warsaw, Warszawa, Poland

For several years now, the Heavy Ion Laboratory has been involved in medical radioisotope production, mostly Astatine-211, utilizing the alpha-particle beam from the U-200P cyclotron. The production station is attached to the cyclotron vacuum chamber, see Figure 1.

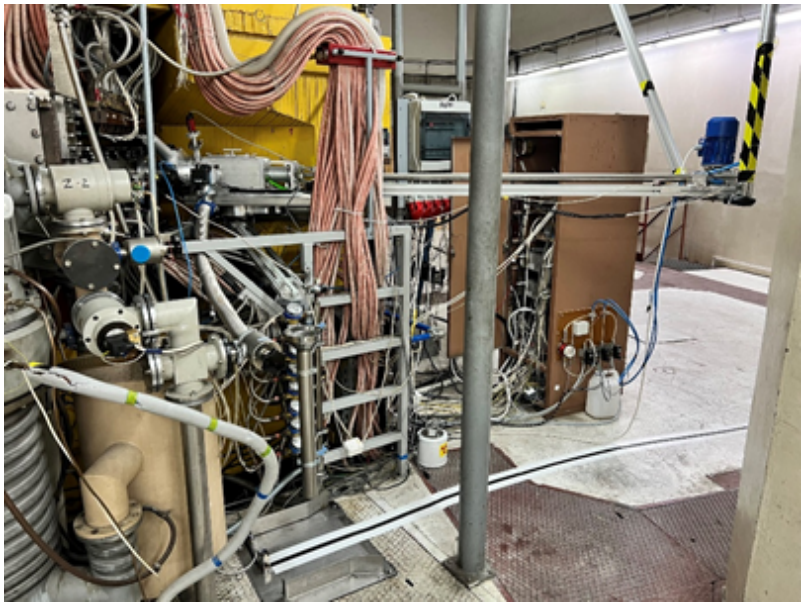

Figure 1: A view of the target station for the U-200P cyclotron

A very simple station, which was designed 28 years ago for a carbon target irradiation utilizing internal beams of the cyclotron, has been replaced with a new one. Several weaknesses of the old system, like a very poor water cooling system of the target, or purely manual operation influenced the decision to design a new irradiation station.

The new station, with tilted target, allows a target to be irradiated material with maximal available current of the internal beam. The rage of available irradiation radii of the target can vary from 70 cm up to the maximum extraction radius, 85 cm. More details are available in [1].

In the new station, the steps that still need to be performed manually are limited to three operations: opening of the vacuum chamber of the station, installation of the target in the target head, and closing of the vacuum chamber of the station. All other activities are performed remotely/automatically with the help of PLC and dedicated computer software with a graphical user interface (GUI).

During a target irradiation beam current and water cooling temperature are monitored on-line.

Figure 2: A view of the designated path

After the irradiation is completed, the target is remotely released from the target head, and using a conveyor belt is sent to a shielding container placed on a remotely controlled cart. The cart, with its cargo, moves away autonomously from the cyclotron area into the maze of the cyclotron bunker along a designated path, see Figure 2. There, the operator closes the target container and prepares this shipment for further treatment of the irradiated target.

The first production experiment with the new station is expected during 2023.

Bibliography

[1] J. Choiński *et al.*, HIL Annual Report (2019) 16.

A.4 A standalone station with automatic loading, dedicated to the PETtrace cyclotron

J. Choiński, T. Bracha, J. Kowalska, B. Radomyski, A. Stolarz, Ł. Świątek, R. Tańczyk
Heavy Ion Laboratory, University of Warsaw, Warszawa, Poland

The Radiopharmaceutical Production and Research Center, built and launched by the Heavy Ion Laboratory has a dual activity. Part of the Center is leased to an external company and is used for daily production of radiopharmaceuticals such as fluorodeoxyglucose ^{18}F-FDG and choline based on fluorine ^{18}F using a standard station for the production of ^{18}F. The center also has the possibility to produce two other typical radioisotopes for PET scanners, i.e. ^{11}C and ^{15}O using dedicated stations. In the intervals between regular production of ^{18}F the PETtrace machine, together with a dedicated external station for the irradiation of targets in metal and powder form, is used by the HIL team for research on the production of various other radioisotopes. They are used for synthesizing/labelling of bio-chemical compounds with potential application as radiopharmaceuticals.

This research work is currently carried on in cooperation with teams from the Institute of Nuclear Chemistry and Technology in Warsaw and from the Jagiellonian University, Kraków. The above-mentioned institutions began a joint research project entitled "Development of three-photon emitting radiotracers for positronium imaging" as a consortium launched on 2022-07-21, under the OPUS-2022 edition, contract No. UMO-2021/43/B/ST2/02150, where the Jagiellonian University, Faculty of Physics, Astronomy and Applied Computer Science is the leading unit.

The HIL team contribute to the project with radioisotope production performed using homemade dedicated standalone external target system for the irradiation of targets, composed of both metallic pieces/foils or powder (elemental or compound)[1, 2], Fig. 1.

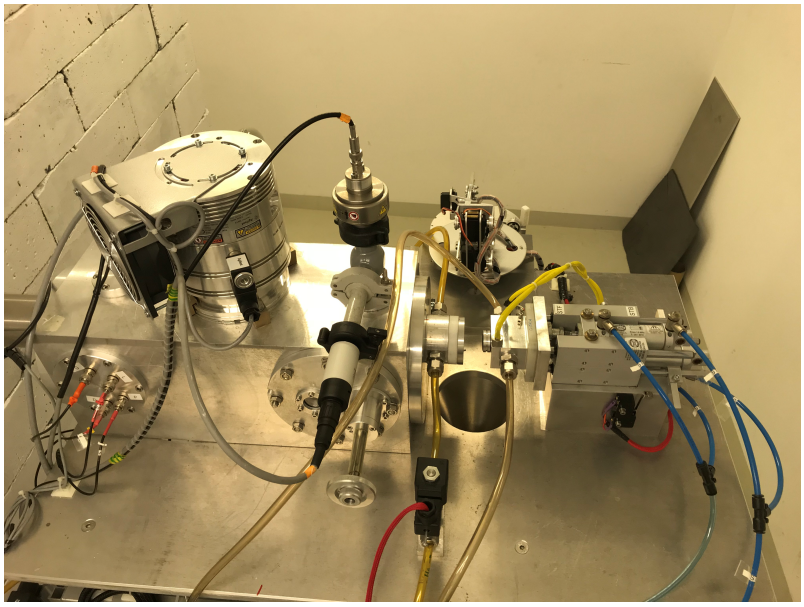

Figure 1: The standalone station connected to the PETtrace cyclotron

In order to increase the efficiency of the radioisotope production (achieving the highest activity of the produced radioisotope in the same irradiation time) we have worked on

a target holder modification allowing the use of a slanted target. At this very moment the target optimization concerns the production of the scandium isotope ^{44}Sc.

This system is fully remotely controlled and protected by Polish patent no. 227402. The external target system is connected to the cyclotron via a dedicated beam line. The target station is isolated from the cyclotron by a protective wall which ensures safe working conditions for the center staff. After irradiation the target drops into a lead container and is evacuated from the cyclotron vault on a remotely controlled trolley. Last year we performed a dozen target irradiations for research groups cooperating with us, producing ^{43}Sc, ^{44}Sc, ^{89}Zr, ^{135}La isotopes.

Bibliography

[1] J. Choiński *et al.*, HIL Annual Report (2021) 18.
[2] J. Choiński *et al.*, HIL Annual Report (2020) 14.

A.5 Status of the EAGLE array

M. Palacz, T. Abraham, G. Jaworski, M. Kisieliński, M. Kowalczyk, W. Okliński for the EAGLE collaboration

Heavy Ion Laboratory, University of Warsaw, Warszawa, Poland

The central European Array for Gamma Levels Evaluations (EAGLE) is an array of High Purity Germanium (HPGe) detectors located at HIL [1], see also [2]. Up to 30 HPGe detectors with anti-compton shields can be installed in the EAGLE frame, and the setup can be augmented with various ancillary devices.

The Heavy Ion Laboratory operates a number of HPGe detectors on loan from GAMMAPOOL [3]. At present, 15 complete sets of a HPGe detector and its anti-compton shield are allocated by GAMMAPOOL to HIL. HIL also owns 19 smaller detectors with anti-compton shields, which may also be installed in the frame of EAGLE. The detectors located at HIL are routinely serviced in-house [4].

Four experiments were run with EAGLE in the first half of 2022. They are covered in separate contributions to this Annual Report. These were:

- "Probing shapes and structures in ^{100}Ru via Coulomb excitation" [7];
- "Electromagnetic structure of low-lying states in ^{110}Cd — complementary Coulomb excitation measurements with a ^{14}N beam" [8];
- "Lifetime studies in neutron-deficient ^{176}Pt using the RDDS technique EAGLE + Cologne Plunger" [9];
- "Search for chiral to not chiral transition by lifetime measurement of I=10^+ state in ^{128}Cs with a plunger technique" [10].

The installation of the NEDA detector array at HIL [11] was started in December 2021 and the array became available for experiments in connection with EAGLE in January 2023. On this occasion a new data acquisition system for EAGLE was developped, based on CAEN V1725S(B) digitizers and the XDAQ system.

A new automatic control system for filling the intermediate LN_2 tank of EAGLE was built and installed in 2022 — see the contribution of Ref. [12].

Bibliography

[1] J. Mierzejewski *et al.*, Nucl. Inst. and Meth. **A659** (2011) 84.
[2] M. Palacz *et al.*, HIL Annual Report 2019, page 12.
[3] T. Abraham *et al.*, HIL Annual Report 2016, page 17.
[4] T. Abraham *et al.*, HIL Annual Report 2017, page 14.
[5] M. Kowalczyk, HIL Annual Report 2017, page 16.
[6] T. Abraham *et al.*, HIL Annual Report 2018, page 51.
[7] I. Piętka *et al.* this Report, page 63.
[8] P. Garret *et al.* this Report, page 66.
[9] C. Fransen *et al.*, this Report, page 69.
[10] A. Nałęcz-Jawecki *et al.* this Report, page 72.
[11] G. Jaworski *et al.*, this Report, page 18.
[12] T. Abraham *et al.*, this Report, page 28.

A.6 Installation of NEDA at HIL

G. Jaworski[1], M. Palacz[1], A. Goasduff[2], M. Kowalczyk[1], P. Kulessa[1], I. Kuti[3], M. Matuszewski[1], B. Radomyski[1], N. Toniolo[2], T. Abraham[1], G. Colucci[1], A. Fijałkowska[4], K. Hadyńska-Klęk[1], M. Komorowska[1], R. Kopik[1], L. Lappo[5], A. Malinowski[6] P.J. Napiorkowski[1], W. Okliński[1,4], A. Otręba[4], S. Panasenko[1], W. Poklepa[4], J. Samorajczyk-Pyśk[1], K. Wrzosek-Lipska[1], K. Zdunek[6]

1) Heavy Ion Laboratory, University of Warsaw, Warszawa, Poland
2) INFN, Laboratori Nazionali di Legnaro, Legnaro, Italy
3) Institute of Nuclear Research (ATOMKI), Debrecen, Hungary
4) Faculty of Physics, University of Warsaw, Warszawa, Poland
5) Faculty of Physics, Warsaw University of Technology, Warszawa, Poland
6) Faculty of Chemistry, University of Warsaw, Warszawa, Poland

For several decades now, γ-ray spectroscopy methods have been extensively applied to studies of the structure of proton-rich nuclei. Excited states in such nuclei can be populated in fusion-evaporation reactions in which the nuclei of interest are produced by the emission of a few particles from the compound nucleus (CN). The arrays of HPGe detectors employed have to be coupled to ancillary devices, which allow accurate identification of the reaction products. In particular, when most proton-rich nuclei are studied, the reaction channels with neutron emission from the CN lead to the most exotic, and most interesting nuclear structures, produced with very small cross sections. To identify such reaction channels, large arrays of liquid scintillator detectors like the Neutron Wall [1, 2] and the Neutron Shell [3] were constructed and used in the past.

Note that a clean tagging on multiple neutrons is especially difficult and important, as a single detected neutron tends to scatter in more than one detector, which mimics detection of a larger number of neutrons. On the other hand, the cross section typically drops by an order of magnitude with each additional neutron emitted, so events with a larger number of neutrons detected are exceptionally rare. Cuts on the distance, time and amount of light produced in the scintillator are thus required to distinguish true multiple neutrons from scattering.

Based on the decades of experience with the above mentioned arrays, following extensive R&D work a new neutron multiplicity filter NEDA [4] was constructed. The new array is optimised for high efficiency, excellent capabilities in distinguishing neutrons and gamma rays, as well as proper determination of the multiplicity of neutrons. It should also work at high counting rates. Thanks to these features, NEDA is apt to work as an ancillary device to modern γ-ray spectrometers. Indeed, within its first physics campaign in 2018 [5–7], NEDA was connected to AGATA at GANIL [8], presenting excellent performance. In this contribution, we report on the installation of NEDA at the Heavy Ion Laboratory, in conjunction with the EAGLE γ-ray spectrometer [9].

The EAGLE frame can host up to 30 HPGe detectors and ancillary devices. In the configuration with NEDA, see Fig. 1, triplets of neutron detectors were placed at each of the 15 forward faces of the frame (with respect to the beam direction), at a distance of about 450 mm from the target. Fifteen HPGe detectors were located at backward angles, filling the remaining empty faces. An additional seven NEDA detectors have been mounted downstream of the frame, about 650 mm from the target, forming a "forward wall" to detect neutrons emitted at small ϑ angles with respect to the beam axis. A new electronics and data acquisition system was also developed and installed. The NEDA equipment was moved to HIL in December 2021, and the installation was completed in January 2023.

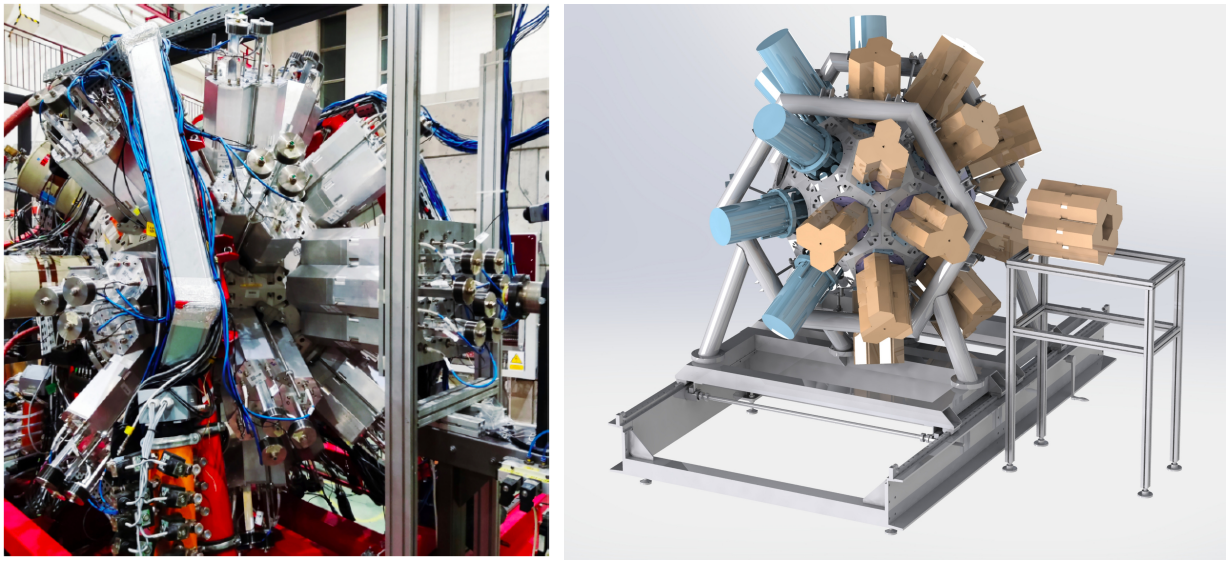

Figure 1: The NEEDLE setup at HIL. Beam direction: from left to right. In the rendering: dewars of HPGe detectors (brown/blue), NEDA detectors (silver/brown).

The new aggregate of the detectors is nick-named NEEDLE. It is expected to have a γ-ray photopeak efficiency of 1.4% for γrays at 1.3 MeV, and about 20% and 2% efficiency to detect and identify one and two neutrons, respectively. These numbers are based on the measurements for HPGe detectors, evaluation of the data acquired with NEDA at GANIL, and on Geant4 simulations.

NEEDLE can be equipped with additional ancillary devices, for example a charged particle detector, an electron spectrometer, and a plunger. Work on the installation together with NEEDLE of the DIAMANT charged particle detector [10] has already been started. The Köln plunger [11] has been previously used in several experiments with EAGLE, and it does not require any modifications to function together with NEDA. The ULESE conversion electron spectrometer [12] is available for experiments at HIL, and it can be mounted in the EAGLE frame if one of the HPGe detectors or a NEDA triple is removed.

A number of possible physics cases to be studied with NEEDLE were proposed and discussed during a dedicated workshop [13]. The Programme Advisory Committee at its meeting on 7 April 2022 recommended three projects for realisation using NEEDLE.

The installation and use of NEDA at HIL are supported by the National Science Centre, Poland (NCN), grant No. 2020/39/D/ST2/00466.

Bibliography

[1] Ö. Skeppstedt *et al.*, Nucl. Inst. and Meth. **A421** (1999) 531.
[2] J. Ljungvall, M. Palacz, J. Nyberg, Nucl. Inst. and Meth. **A524** (2004) 741.
[3] D.G. Sarantites *et al.*, Nucl. Inst. and Meth. **A530** (2004) 473.
[4] J.J. Valiente-Dobon *et al.*, Nucl. Inst. and Meth. **A927** (2019) 81.
[5] G. Jaworski *et al.*, Acta Phys. Pol. **50**(3) (2019) 585.
[6] B. Cederwall *et al.*, Phys. Rev. Lett. **124** (2020) 062501.
[7] X. Liu *et al.*, Phys. Rev. C **104** (2021) L021302.
[8] E. Clément *et al.*, Nucl. Inst. and Meth. **A855** (2017) 1.
[9] J. Mierzejewski *et al.*, Nucl. Inst. and Meth. **A659** (2011) 84.
[10] J. Scheurer *et al.*, Nucl. Inst. and Meth. **A 385**, (1997) 501.
[11] A. Dewald *et al.*, Prog. Part. Nucl. Phys. **67**, (2012) 786.
[12] J. Perkowski *et al.*, Rev. Sci. Inst. **85**, (2014) 043303.
[13] NEDA@HIL prePAC Workshop, `https://www.slcj.uw.edu.pl/en/needle-workshop/`

A.7 SilCA – Silicon Coulomb excitation Array at the Heavy Ion Laboratory

K. Hadyńska-Klęk[1], P.J. Napiorkowski[1], J. Iwanicki[1], J. Mierzejewski[2], S. Panasenko[1], C. Hiver[3], A. Iwanicki[1], M. Komorowska[1], S. Królikiewicz[4], G. Pasqualato[3], J.N. Wilson[3], K. Wrzosek-Lipska[1].

1) Heavy Ion Laboratory, University of Warsaw, Warszawa, Poland
2) Żolimajster Co. Jan Mierzejewski, Poland
3) Irene Joliot Curie Laboratory, Orsay, France
4) Warsaw University of Technology, Faculty of Mechatronics, Warsaw, Poland

Coulomb Excitation experiments were among the first performed around the commissioning time of the Warsaw Cyclotron in the 'nineties. Several particle detection systems were used for the purpose, the most recent being the PiN diode array housed within the so-called Munich chamber.

To increase particle detection efficiency, a new scattering chamber has been built to accommodate an annular DSSD array (Double-Sided Silicon Strip Detector). The detector is axially symmetric with a central hole of 1.6 cm radius and an outer radius of 4.2 cm. The new chamber is constrained to a 10 cm radius to be compatible with several gamma detection arrays including the EAGLE set-up at HIL [1]. It features a modular design that allows for easy rearrangement of the detector and targets inside. A 3D project drawing of the new reaction chamber is presented in Fig. 1.

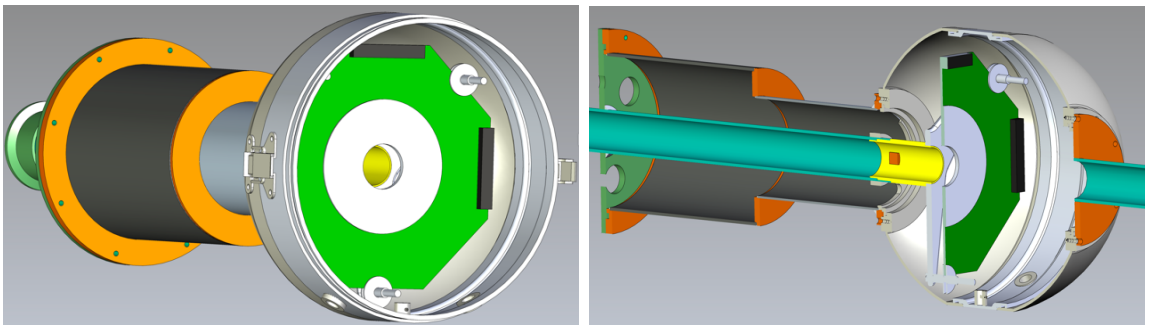

Figure 1: 3D project drawing of the new reaction chamber.

Currently, the chamber is used in a simplified configuration consisting of:

- Two hemispheres, spin-formed from soft aluminum sheet;
- Central ring (turned from hard aluminum);
- Motorised rotating and automated target changer (3D-printed);
- Analogue camera with LED illumination;
- Large-diameter side-arm housing signal connections;
- Small diameter side arm for exit of outgoing beam.

The DSSD array is placed at backward angles and (depending on the distance from the target) covers the following angles:

- 125-152° for 3 cm,
- 133-158° for 4 cm,
- 140-162° for 5 cm.

The array was first commissioned at HIL in October 2022 using a ^{241}Am α source. The signal from 5.1 MeV alpha particles registered in the DSSD array was transmitted using Mesytec MPR-16 preamplifiers and Mesytec MDU-16 differential-to-single-end converters to a CAEN V1725SB digitizer module for readout (64 sectors (32 channels) and 32 rings (16 channels)). The obtained FWHM of 50 keV corresponds to 1% resolution at 5 MeV (see Fig. 2).

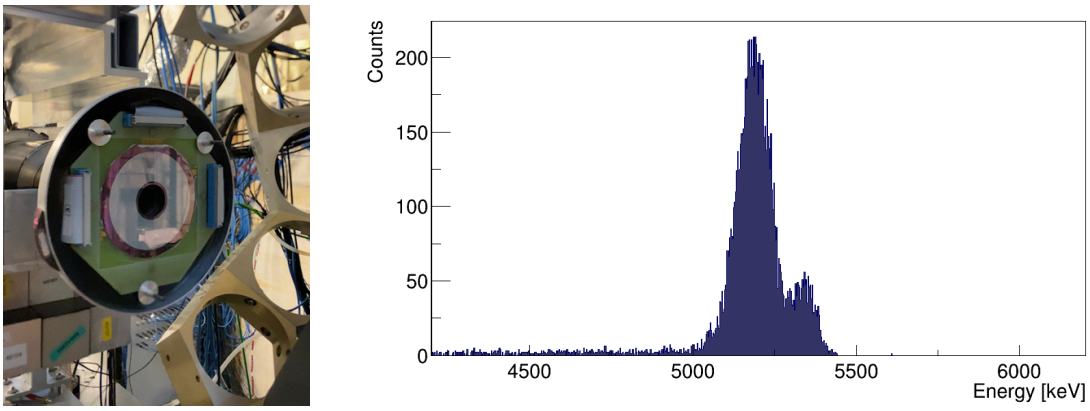

Figure 2: A DSSD detector placed inside the chamber (left panel) and a spectrum of 5.1 MeV alpha particles emitted by the ^{241}Am source (right panel.)

The central ring of the scattering chamber is versatile and was designed to be easily exchanged with another one equipped with another device, depending on the experimental requirements. Currently, the central ring is equipped with an automatic target changer, allowing it to accommodate a 3D-printed wheel with six independent spots, which can be filled with either different targets, quartz glass, or an empty frame for beam focusing. The target changer is remotely controlled using an external driver, allowing one manually to position the wheel in the programmed spot. In addition, in the present configuration, an on/off LED source of light and a camera are positioned downstream on the same ring, allowing for monitoring of the status of the targets in use. Furthermore, a 3D-printed holder for radioactive sources for calibration purposes has ben to prepared and can be placed on the changer instead of a target wheel, see Fig. 3.

The new Coulomb excitation array was shipped and in-beam commissioned at the ALTO facility of the Irene Joliot-Curie Laboratory, Orsay, France, in December 2022. It was placed in the center of the setup consisting of the ν-ball2 HPGe clover array [2] and the PARIS $LaBr_3$ (CeBr) + NaI phoswich high-energy γ scintillator calorimeter [3]. A Coulomb excitation reaction with a ^{16}O beam of 66 MeV energy scattered from a ^{197}Au target was successfully measured. The commissioning experiment was followed by a series of measurements, including: "Evidence for enhanced collectivity in ^{58}Fe examined through Coulomb excitation" (G. Pasqualato et al.,) and "Detailed spectroscopy of fission isomers in uranium isotopes" (J.N. Wilson et al.,). In the latter, the DSSD array was shielded against emitted fission fragments by a 10 μm thick aluminum foil, and the detector was used to register light ions exclusively (protons, deuterons, and alpha particles). The final

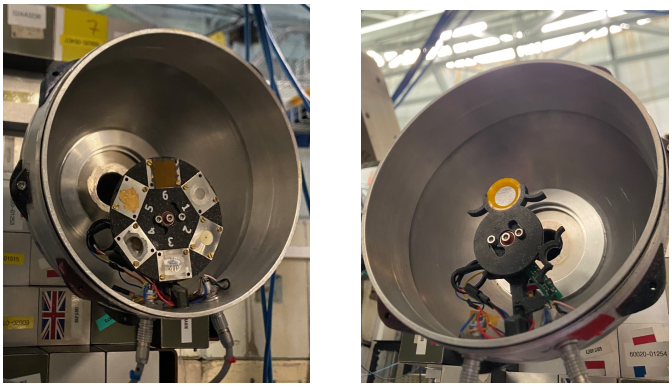

Figure 3: The chamber with the target wheel (left panel) and the holder for radioactive sources (right panel.)

experiment run in this campaign was dedicated to the Coulomb excitation of ^{40}Ca by ^{197}Au target. The collected online spectrum is presented in Fig. 4.

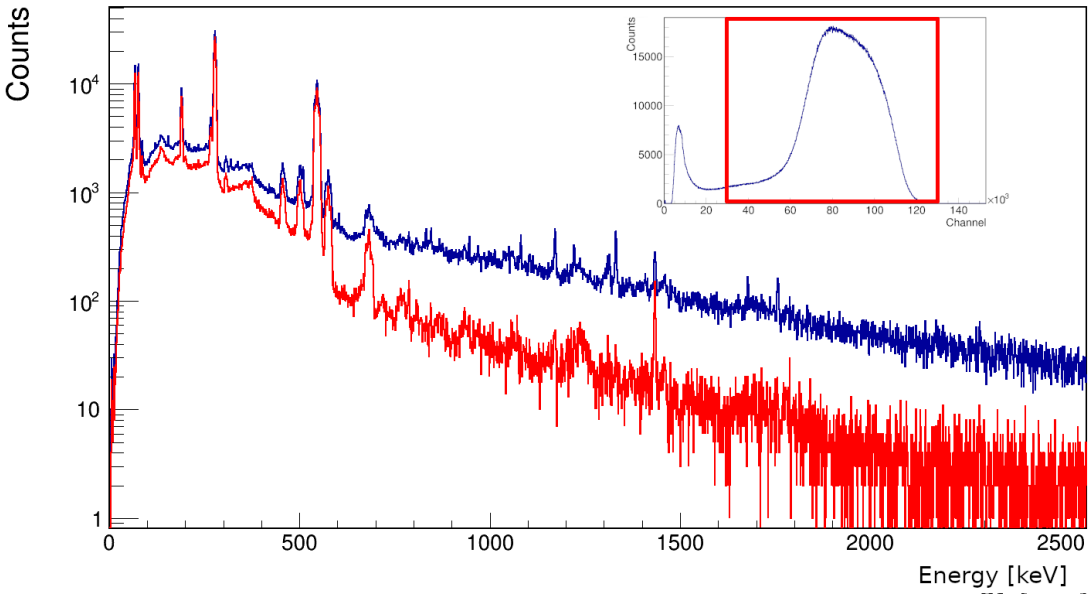

Figure 4: A comparison of online spectra from the Coulomb excitation of ^{40}Ca by a ^{197}Au target: a raw online spectrum (blue) and a spectrum gated on a particle energy range corresponding to back-scattered ^{40}Ca (red). The inset: a non-calibrated energy spectrum collected in one of the DSSD sectors with the back-scattered ^{40}Ca energy gate.

The chamber is in the process of redesign to accommodate a set of side detectors mounted in the forward hemisphere, extending from around 90 degrees towards lower angles. This configuration requires another set of signal feed-through elements (the small diameter forward arm will be replaced with a large one) and a linear target changer.

Bibliography

[1] J. Mierzejewski et al. Nucl. Instr. Meth. A659, 84, (2011).
[2] M. Lebois et al. Nucl. Instrum. Meth. A, 960 163580 (2020).
[3] A. Maj et al., The PARIS project, Acta Phys. Pol. B 40 (2009) and F. Camera and A. Maj, PARIS White Book, ISBN 978-83-63542-22-1 (2021) 565.

A.8 Foil production of soft metals

A. Stolarz, J. Kowalska,

Heavy Ion Laboratory, University of Warsaw, Warszawa, Poland

Production of targets of soft malleable metals with thicknesses around 1-2 μm is a challenging procedure. Foils of soft metals such as Pb, Sn, Cd, etc, although soft and malleable can be easily produced down to 2-3 mg/cm^2 ($\sim$2.5 – 3.5 μm, depending on the material density) by mechanical reshaping i.e., by rolling between stainless steel sleeves. However achieving lower thicknesses becomes problematic due to the strong sticking/adhesion of the rolled material to the steel sheet which results in the foil rending or the appearance of pinholes in the produced foil.

Foils with a thickness of around 1 mg/cm^2 for many metals can be produced by applying a rolling multipack, i.e., double steel sleeves [1], but this is not a satisfactory approach in the case of soft metals. Much better results can be achieved using interlayers such as a film of silicon oil [2] or plastic foils e.g. Melinex (Mylar) [3, 4] or Teflon [4, 5]. In both cases removing the rolled material from the rolling pack is very delicate (due to adhesion forces these foils can be easily damaged) and time consuming (e.g. leaving the whole pack in alcohol after a few passes through the rolls over night to remove the foil and further its cleaning-rinsing in alcohol in the case of the use of silicon oil).

Completing an order for targets of ^{110}Cd, ^{106}Cd ($\sim$1 mg/cm^2) and ^{120}Sn ($\sim$2 mg/cm^2) requested for Coulomb excitation measurements carried out at HIL, LNL (Italy) and Isolde, (CERN) we applied a thin Cu foil as interlayer. An attempt to apply the techniques with use of a plastic interlayer (test on natural material) failed as Cd at thicknesses close to those requested could not be removed from the backing (see Fig. 1). Taking into account that Sn is much softer and more adhesive to the steel sandwich there was no approach with the use of Teflon sheets.

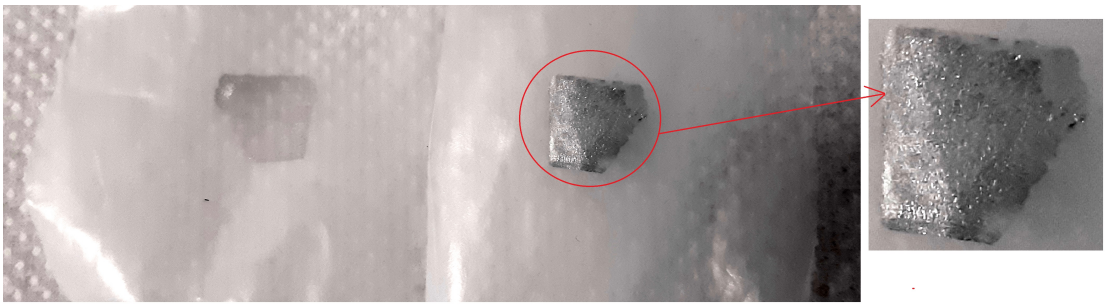

Figure 1: natCd rolled between Teflon sheets. On the far left - shadow of the Cd foil composed of micro/nano grains ripped out of the main foil.

The protective Cu foil was 10 μm thick. Since Cu is very soft and plastic it allows separation of the rolled material from the backing by tearing the Cu foils and not the fragile rolled material.

Material initially rolled directly in the stainless steel sheets down to $\sim$2 μm for Cd and 15 μm for Sn was placed between Cu foils and then between a stainless steel pack. Application of such composition of the rolling pack allowed preparation of 0.8 μm Cd (testing with natCd) and 2 μm Sn foils (Fig. 2).

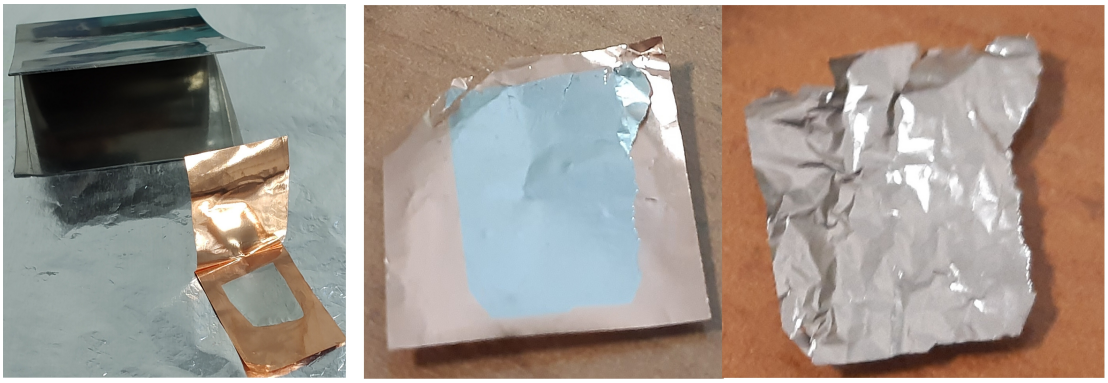

Figure 2: Sn before removing from the Cu sandwich (left) and Cd on Cu backing and after separating from the Cu backing (right)

Bibliography

[1] F.J. Karasek, Report AERE-R **5097** (1965) 111.
[2] G. Manente, R. Pengo, Nucl. Inst. and Meth. **A282** (1989) 140.
[3] J.B. Reynolds, Report AERE-R **5097** (1965) 108.
[4] K.M. Glover, F.J.G. Rogers, T.A. Tuplin, Nucl. Inst. and Meth. **102** (1972) 443.
[5] C.K. Gupta, *et al.*, AIP Conference Proceedings **1962**, (2018), 030013.

A.9 Investigation of very high radiation hardness of a 10 μm silicon self-biased detector - preliminary research.

A.J. Kordyasz[1] Z. Szefliński[1], M. Paluch-Ferszt[1], K.Z. Krutul-Bitowska[1], P.J. Napiorkowski[1], M. Kowalczyk[1], Ł. Kordyasz[2]

1) Heavy Ion Laboratory, University of Warsaw, Warszawa, Poland
2) Sonictech, Mokra 3c, 05-092 Kiełpin, Poland

The problem of detector radiation hardness is very important for experimental physics. This field of investigation is strongly pushed by the search for adequate detectors for use with the upgraded intensity at the LHC and future EIC colliders, but radiation resistant detectors are also being investigated for laser inducted fusion reactions, or studies connected with the search for double beta decay. In an attempt to improve detector radiation hardness special detector technologies and new materials like diamond [1] or silicon carbide [2] have been tried. Thick self-biased silicon detectors were developed by Y. Kim et al., in 1986 [3], however, our work is concentrated on thin self-biased silicon detectors [4, 5]. The aim of this work is to test a thin (10 μm) epitaxial silicon strip detector operated in a built-in-field bias potential. It seems to be more resistant to radiation damage due to the extremely low bias potential generated by the internal built-in-field potential and the low strip detector thickness. The low strip detector thickness prevents doping of the detector material since heavy ions are not stopped in it [6].

The thin strip detector was constructed using epitaxial silicon n^+ - n structure of epitaxial layer resistivity about 300 $\Omega\cdot$ cm and thickness about 10 μm obtained by anodic dissolution of thick 400 μm n^+ substrate using a HF jet [7]. The strip detector n^+ - n - p^+ junctions were obtained using B^+ implantation through an Al mask in the form of a comb [5] into the epitaxial n type side using the low-temperature technique [8]. To reduce the detector electric capacitance (by maximally decreasing the strip length), the large-area self-biased strip detector (in the form of thin 10 μm epitaxial membrane with n^+ - n - p^+ junctions) was broken down into smaller strip detector pieces (small self-biased strip detectors with n^+ - n - p^+ junctions). Fig. 1 show part of a 10 μm strip detector, from which a small detector was obtained.

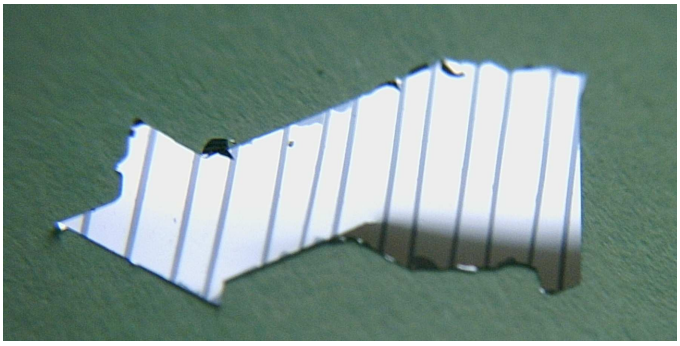

Figure 1: Part of a 10 μm strip detector with about 1 mm wide strips (with an evaporated thin layer of Al contacts) separated by very narrow distances (blue color of silicon). From this part of the strip detector a small ΔE detector containing only one strip was broken off. Mechanical stresses on the surfaces of the 10 μm thin epitaxial layer cause its deformation, which results in the surface of the thin strip detector element not being perfectly flat.

The selected strip detector without a deformed thin epitaxial layer was mounted in a detector housing supplied with a collimation entrance window of diameter 1 mm (to register particles only from one strip). After gluing 25 μm silver wire contacts to the strip detector Al surfaces using two component silver paste hardened at a temperature of about 80°C, the self-biased thin strip detector operating with an internal built-in-field potential (without any external bias potential), was ready to work with α particles and heavy ions.

Previously tests with a 23 μm self-biased detector were performed with Rutheford scattering of 90 MeV, ^{14}N ions on a Au target. They showed proper working of the detector with a total maximum, available dose of about $7.1{\cdot}10^{11}$ ions/cm^{-2} [9]. To increase the available dose of 90 MeV ^{14}N ions on the thin strip detector we irradiated it with the beam, directly in the Faraday Cup presented in Fig. 2.

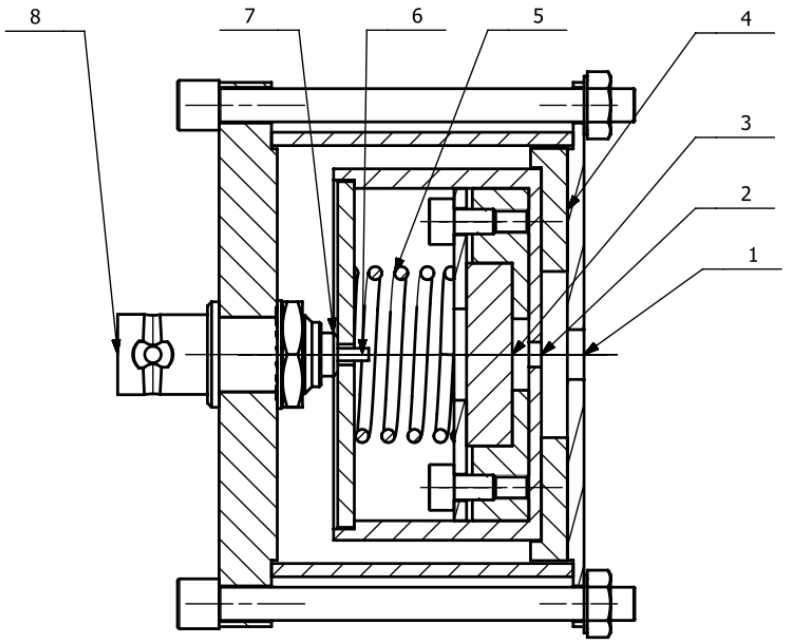

Figure 2: Faraday Cup for irradiation of the thin detector by heavy ions. Description of the figure: 1. Hole with diameter of 6 mm (beam collimator), 2. Hole with diameter of 3 mm (beam collimator), 3. Si detector collimated to a diameter of 1 mm with Al foil 120 μm thick, 4. Teflon insulator, 5. Spring holding the detector down, 6. Central metal part of the BNC connector, 7. Teflon insulator for the BNC connector, 8. Input to the BNC connector.

Before and after irradiation with ^{14}N ions measurements with 5.487 MeV α particles from a ^{241}Am source with a $E-\Delta E$ in were performed. The $E-\Delta E$ telescope was composed of the 10 μm self-biased ΔE strip detector followed by a thick silicon E detector. Results are presented in Fig. 3 which shows the response of the single ΔE strip detector collimated to 1 mm for α particles.

We used for the measurement a very intense, thick ^{241}Am source with a large component of α particles at low energy.

Detector irradiation was performed at the Exposure Station on beam - line A at the Heavy Ion Laboratory of Warsaw University.

The performed spectral measurements (Fig. 3) showed proper operation of the $E-\Delta E$ telescope, which enables their use in nuclear physics to identify light charged particles and

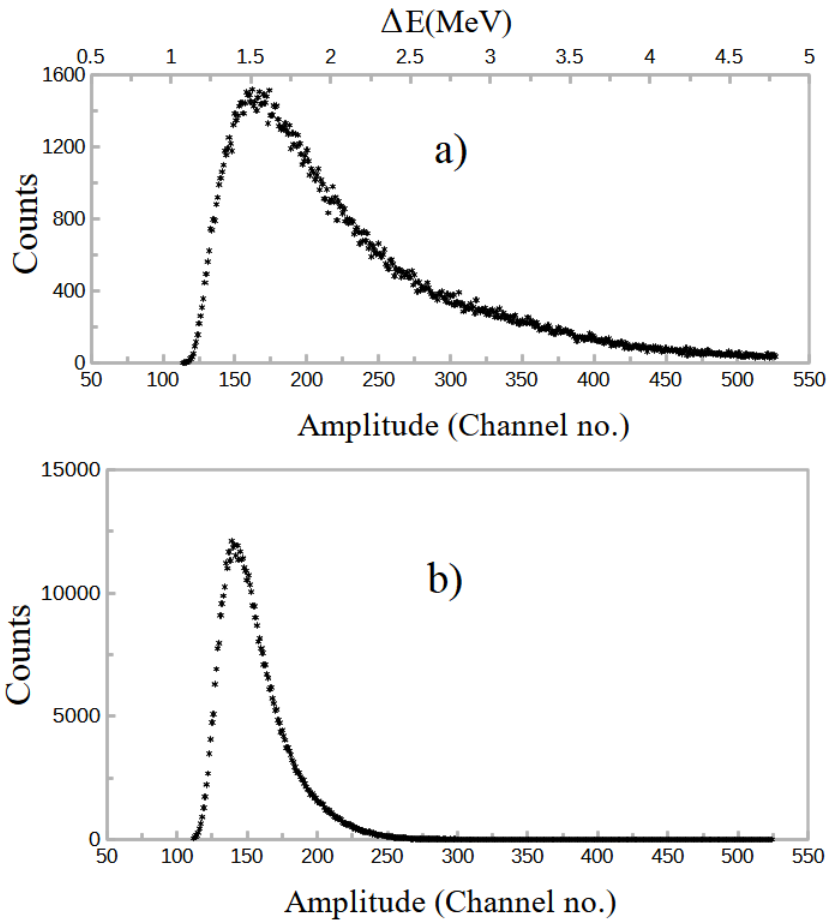

Figure 3: Response of α particles from ^{241}Am registered in the single collimated strip 10 μm ΔE strip detector. Energy calibration was performed using a) part of the picture, which presents the energy lost of α particles registered in the 10 μm ΔE detector before irradiation by heavy ions. Part b) presents the results after irradiation of the detector with the 90 MeV ^{14}N ions and a total dose of about $2.5{\cdot}10^{16}$ ions/cm^{-2}.

heavy ions. However, the decrease of the pulse-height of the thin ΔE detector versus heavy ion dose should be taken into account.

In future work the dependence of the control measurement with 5.487 MeV α particles from ^{241}Am source as a function of dose with irradiation by 90 MeV ^{14}N ions up to destruction of the thin detector energy spectrum should be achieved.

Bibliography

[1] R J Tapper, Rep. Prog. Phys. **63**, (2000) 1273.
[2] M. H. Kushero et al., Materials **14**, (2021) 568.
[3] Y. Kim et al., IEEE Transactions on Nuclear Science **33**, (1986) 321.
[4] A. J. Kordyasz et al., Nucl. Instr and Meth. A **539**, (2005) 262.
[5] A. J. Kordyasz et al., Acta Phys. Pol. B. **47**, (2016) 979.
[6] M. Moll; IEEE TRANSACTIONS ON NUCLEAR SCIENCE, VOL. 65, (2018) 1561.
[7] A. J. Kordyasz et al., Nucl. Instr. And Meth. in Phys. Res. A **570**, (2007) 336.
[8] A. J. Kordyasz et al., Eur. Phys. J A **51**, (2015) 15.
[9] A. J. Kordyasz et al., Heavy Ion Laboratory Annual Report, (2018) 69.

A.10 A new automatic system for refilling the LN_2 tank at EAGLE

T. Abraham, M. Antczak, J. Miszczak, M. Kowalczyk, M. Kopka, K. Pietrzak, R. Ratyński, P. Krysiak, A. Jakubowski, R. Kopik, M. Palacz, Ł. Świątek, W. Kozaczka

Heavy Ion Laboratory, University of Warsaw, Warszawa, Poland

The Central European Array for Gamma Levels Evaluations (EAGLE) is an array of High Purity Germanium (HPGe) detectors located at HIL [1, 2]. The HPGe detectors require liquid nitrogen cooling to function [3]. The cooling is provided by an automatic system that refills the dewars. The system replenishes the LN2 in the dewars twice a day. The liquid nitrogen for the system is fed from a 240-litre tank located near the EAGLE setup. With 15 HPGe detectors mounted, the tank needed to be manually refilled every second day.

Utilizing the fact that the feeding tank was connected to a large (10000-litre) LN2 tank outside the building via a vacuum-insulated pipe, it was not difficult to automate the process of refilling the 240-litre tank. Two additional cryogenic electro-valves were built into the existing infrastructure, and an exhaust line with a Pt100 temperature sensor was added. The new automated system is controlled by a program running on a Raspberry Pi computer, as shown in Figure 1.

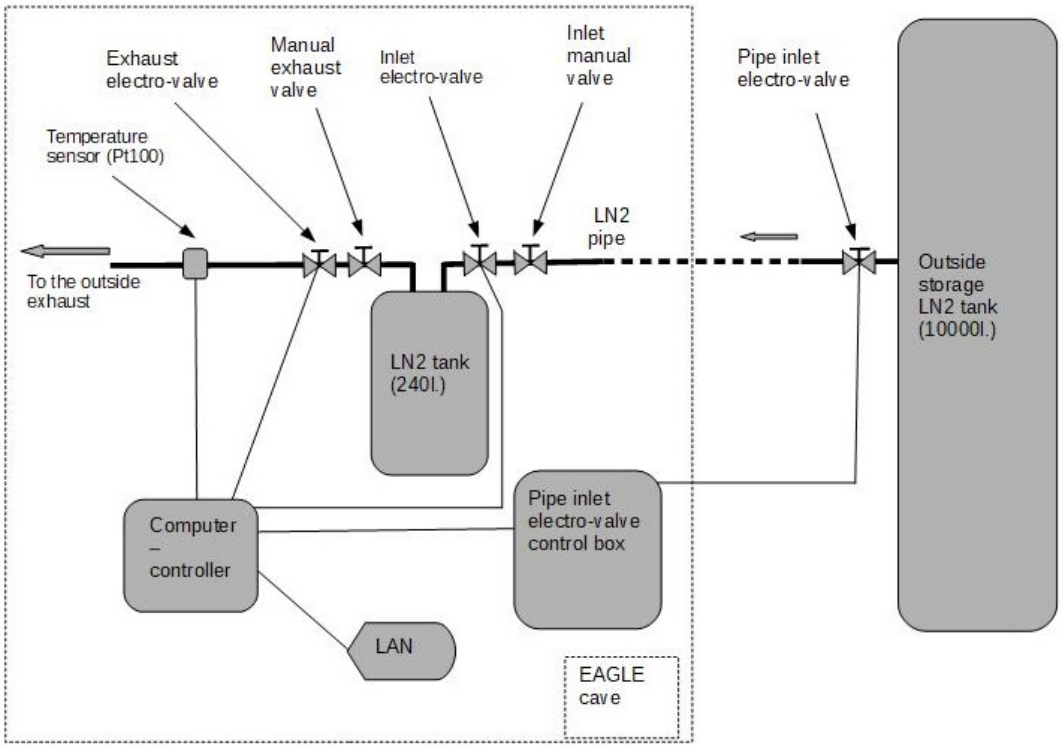

Figure 1: Schematic of the LN_2tank automatic refilling system

The program ("zalewacz") settings are stored in a text file ("ustawienia.cfg") where one can configure parameters such as the hour of refilling, time between refills (in 24-hour

steps), maximum time of refilling, temperature threshold at the exhaust sensor indicating a full tank, and up to three email addresses where information about each LN2 resupply is sent. All important events are saved in a log file.

The system, which was successfully activated in October 2022, has been operating without any issues for over six months now.

Bibliography

[1] J. Mierzejewski *et al.*, Nucl. Inst. and Meth. **A659** (2011) 84.
[2] J. Mierzejewski *et al.*, HIL Annual Report (2010) 24.
[3] H. Mierzejewski *et al.*, HIL Annual Report (2010) 26.

A.11 The PALS (Positron Annihilation Lifetime Spectroscopy) setup at HIL.

S. Panasenko
Heavy Ion Laboratory, University of Warsaw, Warszawa, Poland

Introduction

Positron Annihilation Lifetime Spectroscopy (PALS) is a non-destructive research method and is widely used in materials science. PALS is based on measuring the time interval between positron creation and annihilation signals.

The purpose of the work carried out is to create a working PALS installation using existing equipment, measure and compare the characteristics of an analog time interval conversion system and a digital recording system, determine the main time parameters of the systems and the possibility of using the setup, together with opportunities for improvement.

Description

The detection unit consists of: gamma or positron source, 2 gamma detectors (PMT + scintillator) and protection against Compton radiation, High-voltage PMT power supply. This unit is used in both analog and digital registration systems. Positron source ^{22}Na - calibration source in a plastic container. Compton shielding is located between the detectors. The signal from the PM anodes goes directly to the inputs of the registration system.

The installation consists of a detection unit and an analog or digital conversion and registration system.

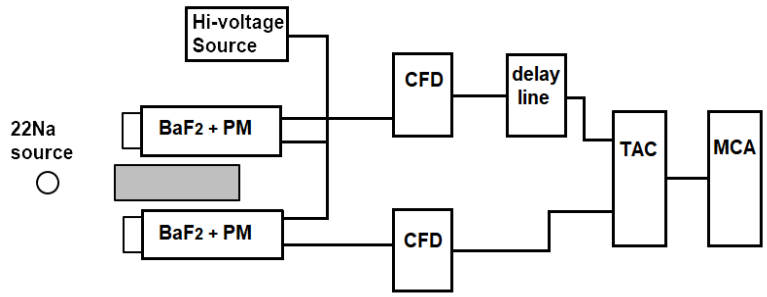

Figure 1: Installation with analog registration system

The analog registration system (Fig. 1) based on CFD consists of:
2 blocks ORTEC 935 Constant-Fraction Discriminator;
Cable delay line (switchable delay unit);
ORTEC 566 Time-to-Amplitude Converter;
Amplitude Analyzer MCA.

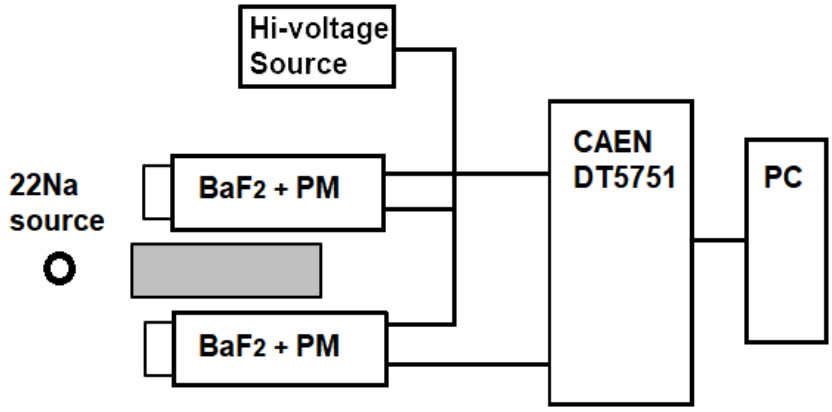

Figure 2: Installation with digital registration system.

The digital registration system (Fig. 2) includes a CAEN DT5751 digitizer with a sampling rate of 1GS/s, 10 bit, 4 Channels per board and PC with CoMPASS 2.0.1 software [1]. The digital system allows measurements in Leading edge and CFD modes and changges in the configuration of the system without changing the external connections. The CoMPASS software acquires energy and timing, can configure the digitizer, calculate and show the statistics, save the data files (raw data, lists, waveforms, spectra) and can work off-line with saved files.

Measurements with ^{22}Na

The subsequent setup of registration systems for operation with ^{22}Na in the lifetime spectroscopy mode consists in setting the thresholds for the 1274.5 keV triggering and 511 keV annihilation gamma quanta. A properly configured system allows registration of the maximum number of useful events with a minimum background.

The first series of measurements was carried out with an analog recording system. After tuning, measurements were taken with a duration of 443900 s and 316750 s. The measurement results for 443900 s are shown in Fig. 3. The resulting spectrum shape agrees with the typical spectra of PALS implementations. The second measurement with a duration of 316750 s was carried out 2 months after the first one. Fig. 4 shows both 443900 s and 316750 s measurements. The slight discrepancy is due to the adjustment of the system.

The second series of measurements was carried out with a digital registration system. The measurement results for 405016 s are shown in Fig. 5

Results

The measurements carried out showed that the analog and digital registration systems have a comparable native temporal resolution, 35 ps and 72 ps, respectively. The intrinsic temporal resolution of the detection system was about 527 ps and 510 ps, respectively, which is much worse than the time resolution of the registration systems and does not allow full use of their capabilities. This resolution of the detectors is probably due to the properties of the PMTs and scintillators. A comparison of long-term measurements showed that, despite the fact that the intrinsic time resolution is worse, the digital registration

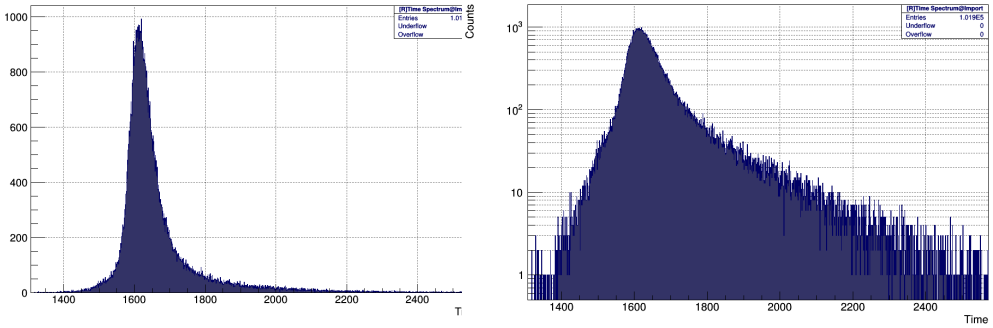

Figure 3: ^{22}Na, 443900 s, measurement with the analog registration system, linear and log scale counts, relative scale time.

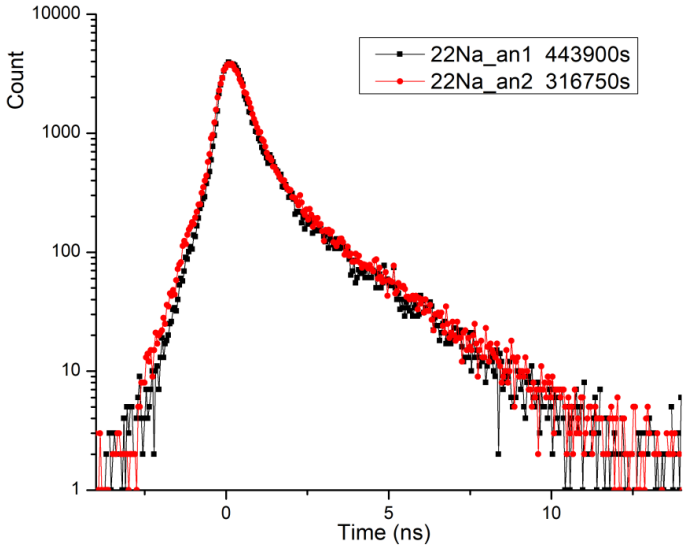

Figure 4: ^{22}Na, with the analog registration system, comparison of 443900 s and 316750 s measurements, corrected scales.

system gives better results, which is associated with the possibility of obtaining many parameters simultaneously and more accurate settings. The possibility of using the setup for PALS is strongly limited by the inherent resolution and does not allow measurements with metals and semiconductors, for which the characteristic process times are less than 300 ps. An attempt to analyze the data of long-term measurements with a ^{22}Na source by the PALSfit3 [2] program showed a large uncertainty in the results obtained.
The maximum value of the CoMPASS software for the digital registration system scale of 45 ps/div is set by the manufacturer, which limits the use of this software.
Measurements with an ADC with a frequency of 2 GHz showed that an increase in the digitization frequency does not lead to a proportional increase in the measurement accuracy. Of great importance is the coordination of the parameters of the signal source - the detector and the digitizer. The assembled PALS installation has shown its performance and can be used for educational purposes. Better time resolution and a dedicated positron source are

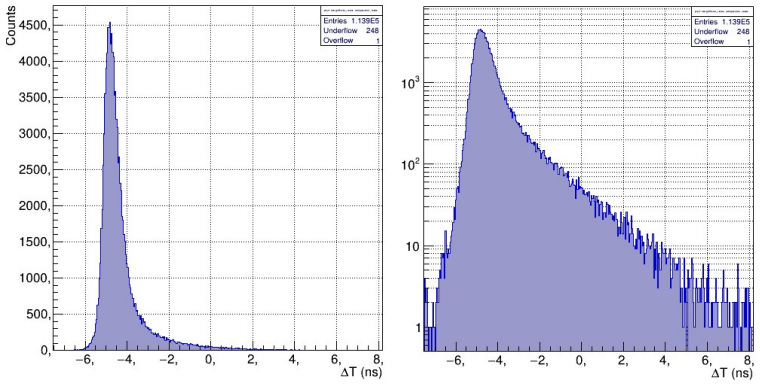

Figure 5: ^{22}Na, with the digital registration system, measurement time 405016 s, linear and log scale, (ΔT - relative scale).

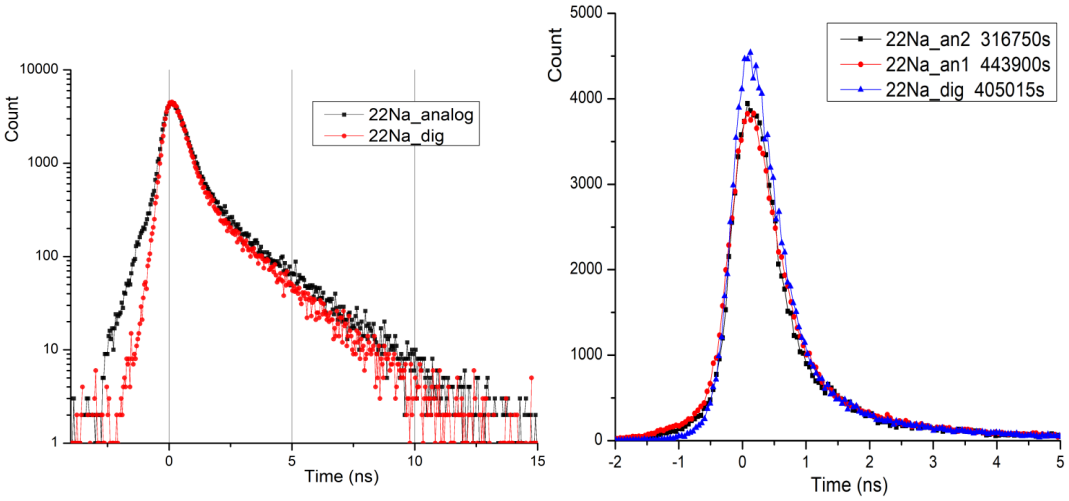

Figure 6: ^{22}Na, comparing analog and digital measurements.

needed to investigate the properties of materials. Improving the time resolution includes changing both the recording hardware and the recording and processing software. Equipment upgrades include replacing the scintillator and PMT with a faster one, or SiPM, developing specialized programs, using a positron source with a thin window, etc. As shown in [3], smaller scintillators have better time resolution.

The project was supported by the IDUB Programme within the framework of the competition: New Ideas - Ukraine.

Bibliography

[1] CAEN Application Note AN3251, Time Measurements with CAEN Waveform Digitizers. Viareggio, 2015.
[2] http://palsfit.dk PALSfit3 is a computer program for the analysis of positron lifetime spectra.
[3] The JOINBON SiPM for the readout of LySO crystals: a Multi Voltage Threshold approach Journal of Instrumentation, Volume 15, July 2020, N. D'Ascenzo et al 2020 JINST 15 C07006.

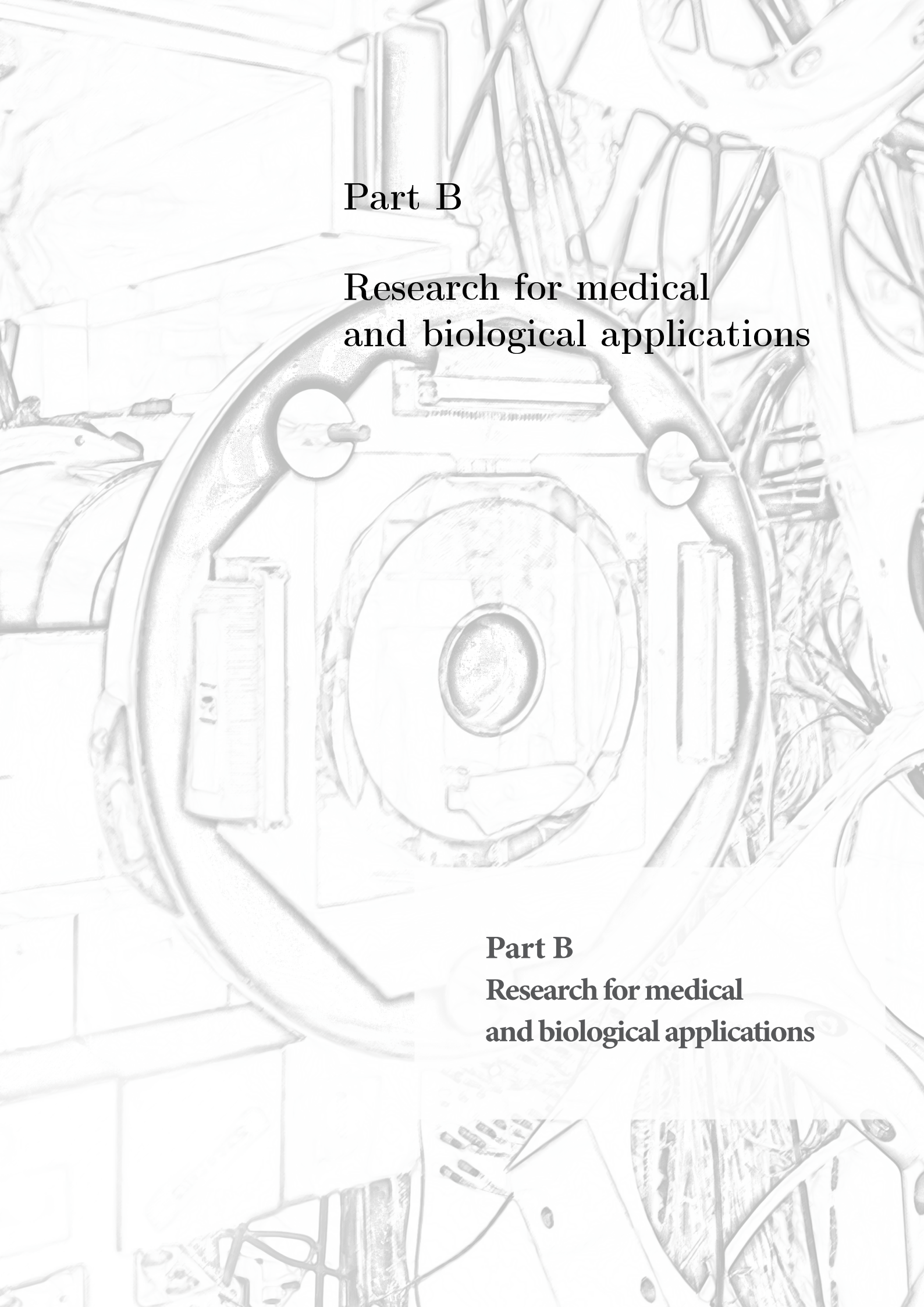

Part B

Research for medical and biological applications

Part B
Research for medical and biological applications

B.1 Determination of radionuclidic impurities in the production of 18F labeled radiopharmaceuticals.

J. Sykuła[1], K. Kilian[2], A. Trzcińska[2]

1) Faculty of Physics, University of Warsaw, Warszawa, Poland
2) Heavy Ion Laboratory, University of Warsaw, Warszawa, Poland

Radiopharmaceuticals labeled with the ^{18}F isotope are the most commonly used research tracers for diagnosis using positron emission tomography. During the production of a radioisotope, long-lived impurities are formed in side reactions. They may constitute an additional dose burden for the patient from ionizing radiation. Therefore, assessing the level of radiopharmaceutical contamination and analyzing the distribution of impurities in the synthesis process is an exciting research topic, also crucial for patient safety. The main purpose of the work is to identify and quantify the emerging radionuclidic impurities in the production of ^{18}F for the production of [^{18}F] fluorodeoxyglucose (FDG) radiopharmaceuticals and [^{18}F] fluorocholine (FCH) and safety assessment of the final product.

Apparatus

The identification of isotopes in the samples was based on gamma spectroscopy. The measurements were carried out using a high purity germanium (HPGe) detector model Canberra BE2825. The detector was connected to a computer through an Ortec 672 amplifier and analog-digital converter. A Tukan8k multi-channel analyzer was used for data acquisition and analysis. The detector together with the sample was placed in a shield made of lead bricks about 5 cm thick, which minimized the influence of background radiation.

Samples

Elements of the [^{18}F] FDG and [^{18}F] FCH synthesis kits, as well as recovered enriched water, production waste, and finished products were taken or analysis. The ^{18}F isotope was produced in the GE PetTrace cyclotron by bombarding for 120 min a liquid target [^{18}O]H_2O with 16.5 MeV protons at a beam current of 40 μA - 60 μA. The target material was in a niobium body with windows made of HAVAR foil. The following samples were analyzed:

- for the production of [18F]FDG:
  - 11 Accel Plus QMA Sep-Pak anion exchange columns,
  - 22 Sep-Pak C-18 carbon columns, 2 columns from each synthesis set,
  - 11 Sep-Pak Alumina N Plus aluminum columns,
  - 11 samples of the finished product ^{18}FDG,
  - 5 samples of recovered water spiked with [^{18}O]H_2O,
  - 5 samples of post-production waste,
- for the production of [18F]FCH:
  - 9 Accel Plus QMA Sep-Pak anion exchange columns,
  - 9 samples of 4 element set Sep-Pak Plus Silica chromatography columns,
  - 9 Sep-Pak Plus CM silica columns,
  - 9 Sep-Pak Plus C18 carbon columns,

- 7 samples of the finished product ^{18}FCH,
- 7 samples of recovered water spiked with [^{18}O]H_2O,
- 7 samples of post-production waste.

The full set of samples from the synthesis of the radiopharmaceutical consisted of all the above-mentioned elements from a single synthesis. For the [^{18}F]FCH, 7 complete sets, and for the [^{18}F]FDG 5 complete sets were tested.

Results

^{18}F production

Total activity from identified radionuclide contaminants throughout the production process or ^{18}F was 139 ± 15 kBq at the end of bombardment (EOB). This is about 0.0001% of the activity of ^{18}F EOB. The dominant isotopes were ^{52}Mn and ^{56}Co.

[^{18}F]FDG

The lowest activity of radionuclide impurities was determined in the final product samples [^{18}F]FDG. The average sum of impurity activities in the samples of the final [^{18}F]FDG product was 35.0 ± 7.9 Bq. More than 99% of the total activity of radionuclide impurities is found in the QMA column and the reclaimed water and does not go to the next stages of the synthesis of the radiopharmaceutical. Figure 1 shows the distribution of radionuclidic impurities at subsequent stages of the radiopharmaceutical synthesis and the detailed results are presented in Fig. 2.

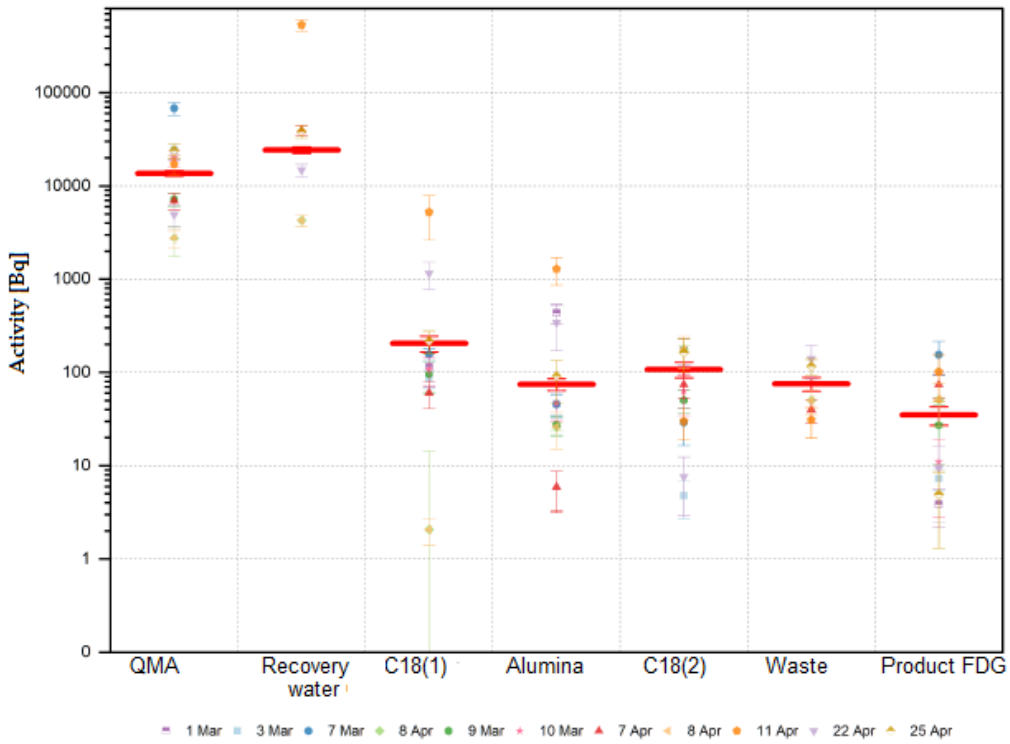

Figure 1: Pattern of total activities of radionuclidic impurities in subsequent steps of the FDG production.

[^{18}F]FCH

The average sum of impurity activities in the samples of the final [^{18}F]FCH product was 18.1 ± 2.8 Bq. This value is 10^{-10} of the activity of the ^{18}F radionuclide at the end of

Isotope	QMA n=11	Recovery water n=5	C18 (1) n=11	Alumina n=11	C18(2) n=11	Waste n=5	Product FDG n=11	Total n=5
^{182}Re	348 ± 41	7.5 ± 2.5	118 ± 37	0.49 ± 0.16	2.65 ± 0.49	6.3 ± 1.3	< 0,2	1770 ± 500
^{183}Re	327 ± 25	12.0 ± 2.2	1.59 ± 0.19	0.273±0.034	1.13 ± 0.15	9.5 ± 1.6	1.10 ± 0.24	140 ± 16
^{184}Re	29.8 ± 3.6	2.51 ± 0.44	2.86 ± 0.63	1.14 ± 0.15	1.96 ± 0.50	1.94 ± 0.32	0.204±0.056	29.1 ± 4.5
^{48}V	0.55 ± 0.23	< 0,3	< 0,3	< 0,3	< 0,3	< 0,3	< 0,3	0.99 ± 0.15
^{51}Cr	435 ± 17	79.7 ± 5.1	3.27 ± 0.14	6.53 ± 0.25	0.631±0.043	1.59 ± 0.13	< 0,3	439 ± 19
^{52}Mn	5640 ± 270	13 700±1000	48.2 ± 6.3	89 ± 17	16.3 ± 2.9	6.0 ± 1.4	10.3 ± 3.9	115 000±12 000
^{54}Mn	10.26 ± 0.44	2.35 ± 0.20	< 0,4	< 0,4	< 0,4	< 0,4	< 0,4	15.2 1,1
^{56}Co	1980 ± 130	9270 ± 940	7.82 ± 0.60	2.45 ± 0.25	2.24 ± 0.45	5.5 ± 1.1	0.95 ± 0.27	9750 ± 940
^{57}Co	37.1 ± 1.6	200 ± 12	0.345±0.023	< 0,2	< 0,2	0.327±0.067	< 0,2	213 ± 12
^{58}Co	503 ± 33	4350 ± 310	1.103±0.048	0.814±0.048	0.87 ± 0.22	1.072±0.082	< 0,2	4610 ± 320
^{95m}Tc	1140 ± 140	4200 ± 1500	7.7 ± 1.5	3.32 ± 0.59	2.33 ± 0.54	4.05 ± 0.87	< 0,2	4500 ± 1500
^{96}Tc	2710 ± 260	0.71 ± 0.20	10.5 ± 2.8	11.6 ± 3.7	10.1 ± 2.0	7.5 ± 1.2	8.6 ± 2.4	2240 ± 330
^{40}K	2.96 ± 0.34	3.19 ± 0.76	4.89 ± 0.25	2.44 ± 0.16	3.70 ± 0.24	4.29 ± 0.45	1.53 ± 0.16	27.3 ± 2.5
^{57}Ni	22.4 ± 8.4	75 ± 17	< 0,2	< 0,2	6.7 ± 1.8	0.50 ± 0.12	< 0,2	720 ± 140
^{7}Be	1.01 ± 0.21	9.6 ± 1.1	< 0,4	< 0,4	< 0,4	< 0,4	< 0,4	32.4 ± 2.7
Sum	13 630 ± 950	24 200±2000	204 ± 39	108 ± 21	75 ± 11	76 ± 13	35.0 ± 7.9	139 000±15 000

Figure 2: Average activities [in Bq] of radionuclidic impurities in FDG production.

irradiation. Figure 3 shows the distribution of radionuclidic impurities at subsequent stages of the radiopharmaceutical synthesis and the detailed results are presented in Fig. 4.

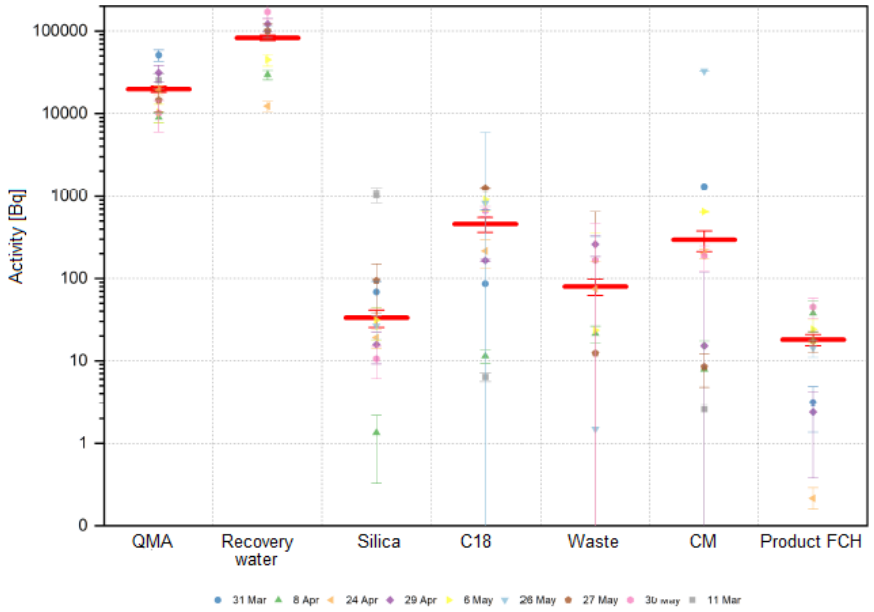

Figure 3: Pattern of total activities of radionuclidic impurities in subsequent steps of the FCH production.

Conclusions

Activity derived from radionuclide impurities in the final product [^{18}F]FDG and [^{18}F]FCH account for 10-7% of the activity of the ^{18}F EOB radioisotope. This is significantly lower than the maximum permissible activity of radionuclidic impurities (0.1%) specified in the European Pharmacopoeia. Thus, both products meet the legal requirements for radionuclidic purity, and the radionuclidic impurities found in the products do not jeopardize patient safety. Contaminants identified in the recovered water had the highest activity both for the production process of [^{18}F]FDG and for the synthesis of [^{18}F]FCH. The activity of impurities in the QMA columns was slightly lower. The total activity of impurities

Isotope	QMA	Recovery water	Silica	CM	C18	Waste	Product FCH	Total
	n=8	n=7	n=9	n=9	n=9	n=7	n=7	n=7
^{182}Re	44.3 ± 6.9	< 0,2	7.4 ± 4.6	27 ± 11	118 ± 31	< 0,2	< 0,2	244 ± 43
^{183}Re	362 ± 39	67 ± 18	9.8 ± 1.4	0.54 ± 0.17	1.35 ± 0.40	1.41 ± 0.34	0.39 ± 0.15	358 ± 41
^{184}Re	35.4 ± 4.7	5.06 ± 0.88	0.62 ± 0.15	1.10 ± 0.27	4.0 ± 1.1	0.104±0.035	0.48 ± 0.20	44.1 ± 5.4
^{48}V	1.84 ± 0.27	< 0,3	< 0,3	< 0,3	< 0,3	< 0,3	< 0,3	2.27 ± 0.36
^{51}Cr	744 ± 30	103.3 ± 5.6	< 0,3	< 0,3	< 0,3	< 0,3	< 0,3	733 ± 27
^{52}Mn	10 120 ± 680	56 400±2700	1.50 ± 0.38	47 ± 15	136 ± 30	59 ± 17	0.82 ± 0.29	65 900 ± 3500
^{54}Mn	10.78 ± 0.52	5.52 ± 0.40	< 0,4	< 0,4	< 0,4	< 0,4	< 0,4	17.03 ± 0.68
^{56}Co	983 ± 73	12 700±1100	0.437±0.091	0.33 ± 0.11	0.230±0.065	0.288±0.037	0.094±0.045	13 700 ± 1100
^{57}Co	24.8 ± 1.3	212.8 ± 8.6	< 0,2	< 0,2	< 0,2	< 0,2	< 0,2	283 ± 11
^{58}Co	788 ± 51	6160 ± 290	0.258±0.020	< 0,2	< 0,2	0.284±0.023	< 0,2	6740 ± 330
^{95m}Tc	760 ± 160	6900 ± 2000	0.28 ± 0.18	0.73 ± 0.27	0.49 ± 0.19	0.59 ± 0.25	0.33 ± 0.17	7700 ± 2100
^{96}Tc	4920 ± 720	< 0,2	4.7 ± 1.8	104 ± 23	71 ± 19	16.2 ± 3.2	< 0,2	4160 ± 710
^{40}K	3.07 ± 0.38	2.65 ± 0.71	0.281±0.064	5.67 ± 0.51	9.17 ± 0.69	1.96 ± 0.26	8.94 ± 0.89	40.5 ± 2.5
^{57}Ni	< 0,2	< 0,2	< 0,2	< 0,2	< 0,2	< 0,2	< 0,2	248 ± 29
^{7}Be	4.50 ± 0.44	< 0,4	< 0,4	< 0,4	< 0,4	< 0,4	< 0,4	2.65 ± 0.68
Sum	19 810±1720	82 800±6000	33.4 ± 8.0	295 ± 83	458 ± 95	80 ± 18	18.1 ± 2.8	100 100 ± 7000

Figure 4: Average activities [in Bq] of radionuclidic impurities in FCH production.

in the remaining stages of the synthesis of both products was an order of magnitude lower. That is, the purification process on the QMA column is crucial for removing impurities at the initial stage of the synthesis and determining the proper quality of the final product. Qualitative analysis of radionuclidic impurities in both synthesis processes shows a similar isotopic composition. In all stages, ^{52}Mn and ^{56}Co dominated, while a significant part was removed from the production process in the cationic form together with the recovered water. The QMA column retained a third impurity in the total activity - the isotope ^{96}Tc in anionic form. During the analysed period the total activity of the radionuclidic impurities remains stable. In individual cases differences were observed due to fundamental changes in production parameters (irradiation of one or two targets), differences in the produced activity at the end of exposure, and service activities in the target system.

B.2 The potential of various types of tea in the green synthesis of selenium nanoparticles

A. Sentkowska[1], K. Pyrzyńska[2]

1) Heavy Ion Laboratory, University of Warsaw, Warszawa, Poland
2) Faculty of Chemistry, University of Warsaw, Warszawa, Poland

Tea extract obtained from Camelia sinensis leaves is consumed worldwide and is valued for its health-promoting properties. Based on the manufacturing process, the main types of tea could be classified as green tea (non-oxidized), white tea (lightly oxidized), oolong tea (partially oxidized) and black tea (fully oxidized) [1]. Each of these types differs in taste, aroma and color of the infusion. More importantly, from the point of view of their use in the synthesis of selenium nanoparticles, their chemical composition is also different. It was proven that the total phenolic content of green and black tea is similar, but there are differences in the types and concentrations of particular flavonoids due to varying degrees of oxidation during production [2]. Generally, epigallocatechin 3-gallate (EGCG), the major constituent of tea catechins, is found in higher concentrations in white tea than in green tea [3]. In this study, the synthesis of selenium nanoparticles using extracts of different kinds of tea is reported. We focused on characterizing the differences in the polyphenol profile and antioxidant capacity among the studied tea infusions as well as examining their potential in the synthesis of SeNPs. The obtained nanoparticles were characetrized using UV-VIS spectroscopy, transmission electron microscopy (TEM), scanning electron microscopy (SEM) and dynamic light scattering (DLS). The use of all

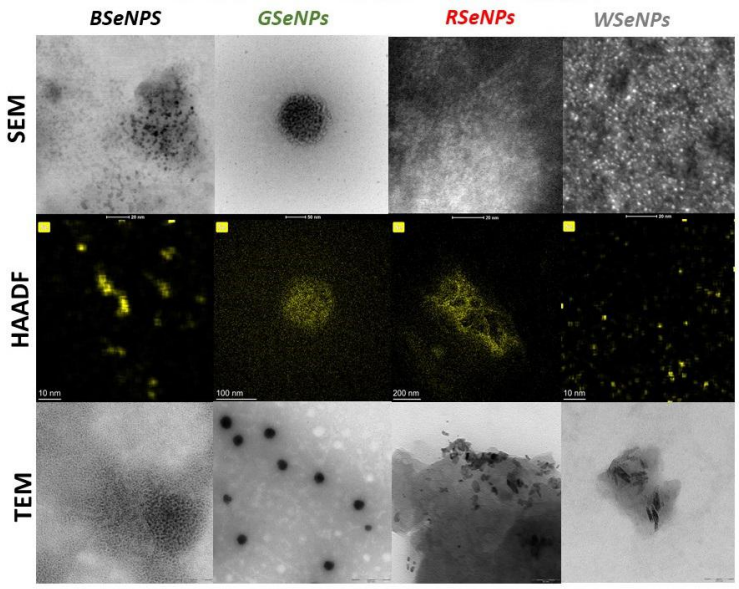

Figure 1: SEM, TEM and TEM (HAADF STEM) of the obtained selenium nanoparticles. Abbreviations: BSeNPs—nanoparticles synthesized using black tea infusions, GSeNPs—green tea, RSeNPs—red tea and WSeNPs—white tea infusion.

analysed tea infusions allowed us to obtain SeNPs. Their SEM, TEM and TEM HAADF STEM are shown in Figure 1. From a dimensional point of view, all synthesized SeNPs were below 100 nm in size, thus they have the potential to be used in medicine. The size of the nanoparticles decreased in the ollowing series: those obtained with green tea

(12.15 nm), red tea (7.781 nm), black tea (4.891 nm) and white tea (3.938 nm). Difficulties in their purification are a potential problem, and a thorough analysis of their parameters (size, shape) should be carried out on purified SeNPs, as the clean-up procedure has a great impact on the physical properties of SeNPs, as we reported previously [3]. The highest ability to neutralize free radicals among teas was shown by green tea (30.43 ± 0.92%), while for nanoparticles obtained from it this value is more than three-times higher (97.42 ± 1.3%). Such huge differences were observed for all teas. The next step in the research on SeNPs synthesized by this method should be to develop a method for their purification or to consider the use of the post-reaction mixture as an oral mixture in a possible therapy with SeNPs.

Bibliography

[1] C. Chupeerach et al. Foods **10** (2021) 117.
[2] V. Stangl et al. Mol. Nutr. Food Res. **50** (2006) 218.
[3] T. Jenny et al. In Tea in Health and Disease Prevention 2013, page 33.
[4] A. Sentkowska, K.Pyrzyńska, Molecules **27** (2022) 2486.

B.3 Effect of thiol addition on selenium stability in beetroot juice

A. Sentkowska[1], K. Pyrzyńska[2]

1) Heavy Ion Laboratory, University of Warsaw, Warszawa, Poland
2) Faculty of Chemistry, University of Warsaw, Warszawa, Poland

Interest in selenium compounds has grown as we have learned more about their role in the human body. Today, it is widely recognized that this element is an essential part of antioxidant enzymes, and plays on important role in scavenging free radicals, regulating their content during biochemical reactions and protecting cells from oxidative stress [1]. One of the selenium sources in diet may be products of plant origin. Most plants can absorb inorganic Se and transform it into organic species, which are less toxic and more bioavailable than inorganic forms. The major selenium-containing amino acids occurring naturally in dietary sources are selenomethionine (SeMet) and Se-methylselenocysteine (MeSeCys). Both display strong antioxidant activities and cytotoxicity against several cancer cells [1]. Detailed knowledge of individual selenium species is important to their potential for human health and to understand the metabolic processes in plants. As we reported earlier, beets and beetroot juices can be a source of selenium [3]. The red beetroot (Beta vulgaris L.) is a well known root vegetable cultivated in all temperate climates. It is consumed as an ingredient in salads and soups or as juice. Beetroot is also used in the food industry as a colorant because it is a great source of betalains, a group of chromoalkaloids, which can be divided into betacyanins (red-violet pigments) and betaxantins (yellow pigments). In recent years, this vegetable has become more popular due to its possible health benefits for humans. Beetroot plants have the ability to accumulate nitrates, which lower blood pressure to improve athletic performance [4]. Pilot studies showed that fifteen days of consumption of beetroot juice by elite runners resulted in improvements in the time to exhaustion [5]. Beetroot also exhibits antioxidant and anti-inflammatory properties. However, data on the concentration of trace elements and minerals in juice prepared from different beetroot varieries are limited. Moreover, there are no adequate reports concerning total selenium content in beetroot juice as well as the concentrations of its speciation forms.

In this work, we present expanded studies on the stability of selenium compounds in beetroot juices as a function of ditiotreitol (DTT) and β-mercaptoethanol (βME) concentration and storage conditions. Two series of both beetroot juices under study were prepared, without and with the addition of reductive thiols, DDT and βME, respectively. They were stored at different temperatures (20°C, 4°C, and -19°C) for various periods of time, and the concentrations of selenium species were then determined. The concentration of SeMet in homemade prepared juice without thiol addition rapidly decreased, regardless of the storage temperature and, after 2 days of storage, its concentration was below the LOD value. By contrast, the concentrations of SeMetO were increased in these juice samples stored at all temperatures in the following order: 20°C < -19°C < 4°C after 8 days. In similar samples of organic beetroot juice, a fast decrease of SeMet concentration was also observed, although after 6 days of storage at 20°C it still retained about 45% of its initial concentration. The MetSeCys was also highly unstable, and the biggest losses of this Se compound were observed for squeezed juice, particularly when stored at room temperature. The concentrations of Se(IV) in both juices under study increased with the time of storage, especially when they were stored in the fridge and freezer for longer than 4 days. This form

of selenium may be one of the postulated products of the oxidation of SeMet (as well as other selenoamino acids) [2]. Generally, the addition of DDT or βME does not increase the concentration of selenomethionine with a possible decrease in SeMetO concentration, as was expected. Moreover, the interpretation of the chromatographic profiles becomes more complicated. To the best of our knowledge, there is no exact explanation regarding the effect of the used thiols, especially in the presence of a sample matrix. Since the samples of the examined juices showed different selenium profiles during storage (with and without the addition of thiols), it appears that changes in speciation have occurred, either from lengthy storage under different conditions or by interaction with the sample matrix, as well as by linked processes. It is very likely that the formed selenoxide may be an equivalent to selenomethionine in biological action, and is metabolized in the same way. However, more studies need to be performed to clear up this problem. Thus, the inclusion of SeMetO in the quantitative determination of SeMet content could be reasonable.

Bibliography

[1] M.P. Rayman Hormones **19** (2020) 9.
[2] R.J. Krause et al. Chem. Res. Toxicol. **19** (2006) 1643.
[3] A. Sentkowska, K. Pyrzyńska Heliyon **6** (2020) e04194.
[4] S.P. Bangar et al. Food Res. Inter. **158** (2022) 11556.
[5] C. Balsalobre-Fernandez et al. PloS One **13** (2018) 1.

B.4 Increasing reaction rates of porphyrins with copper(II) ions for radiopharmaceutical synthesis

M. Pęgier[1], K. Kilian[1], K. Pyrzyńska[2]

1) Faculty of Chemistry, University of Warsaw, Warszawa, Poland
2) Heavy Ion Laboratory, University of Warsaw, Warszawa, Poland

Porphyrins are naturally occurring macrocycles that are able tightly to bind metal ions.The application of both free porphyrins and their complexes with metal ions in non-invasive diagnostics is gaining increasing importance which allows early detection of disturbances or pathological changes caused by diseases. Positron Emission Tomography (PET) with the use of radiopharmaceuticals is one of the most promising medical imaging techniques. Porphyrins are potent fluorophores, biologically compatible, and are known preferentially to accumulate in tumor tissue. The porphyrin-based compounds occurring in nature include the well-known, red-colored heme in hemoglobin, which is responsible for the transport of oxygen, as well as the chlorophylls in some bacteria and plants which are utilized for photosynthesis. Inspired by their role in nature, porphyrins and metalloporphyrins are used not only as agents for tumor diagnostics but also as photosensitizers in photodynamic therapy of cancer (PDT), contrast agents in magnetic resonance imaging, photodynamic antimicrobial chemotherapy, or enzyme models in bioinorganic chemistry [1].

The choice of radionuclide for diagnostic radiopharmaceuticals in PET depends on its nuclear properties (type of radiation, half-life, energy) as well as radionuclide production, the conditions for radiolabeling, and specific activity. ^{64}Cu, with its half-life of 12.7 h, low positron energy (653 keV), and short average tissue penetration range (0.7 mm), has received attention for radiopharmaceutical development due to its favorable nuclear decay properties that make it useful in the labeling of antibodies for immuno-PET applications. It undergoes multiple decay paths, allowing not only PET imaging through positron emission but also offering the possibility of treatment due to the emission of β^- radiation (theranostics). Porphyrins offer potential for applications in nuclear medicine techniques, as ^{64}Cu is a potent radionuclide that can serve as a diagnostic and therapeutic agent. With their natural affinity for tumor tissues, porphyrins can also act as targeting molecules for ^{64}Cu, which can efficiently deliver it to pathological tissues. As potent complexing ligands able tightly to bind ^{64}Cu ions, porphyrins can serve in radiopharmaceutical synthesis [1].

The aim of this work was the optimization of the synthesis of copper complexes with water-soluble porphyrins with cationic and anionic functional groups for potential application in radiopharmaceutical synthesis [2]. Efforts were focused on developing the fastest possible method that would meet the requirements of labeling with short-lived copper isotopes used in PET. Studied porphyrins included 5,10,15,20-tetrakis(N-methylpyridinium-4-yl)porphine tetratosylate (TMPyP), 5,10,15,20-tetrakis(4-sulfonato phenyl)porphyrin (TSPP) and for microwave synthesis also 5,10,15,20-tetrakis(4-carboxy phenyl)porphyrin (TCPP) (Fig. 1). The reactions were monitored spectrophotometrically.

It is known that large ions, such as Cd^{2+} or Pb^{2+} facilitate the incorporation of smaller ions (Cu^{2+}, Zn^{2+}) into the porphyrin ring. The acceleration of the synthesis of Cu(II)–porphyrin complex with the use of large ions can also be realized with the use of a reducing agent. As far as the radiopharmaceutical application is concerned the choice of an acceptable reductant is important. In our study, ascorbic acid (AA) was employed (Fig. 2). The reaction was conducted at a sufficiently high pH to maintain a deprotonated

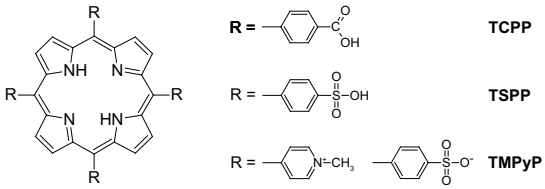

Figure 1: Structures of studied porphyrins.

porphyrin ring. In the first rapid step, copper(II) is reduced to copper(I). As the ionic radius of Cu^{+} (96 pm) is larger than that of Cu^{2+} (72 pm), a complex with Cu^{+} ions remaining out of the ligand plane is formed. This leads to the deformation of the porphyrin ring. Subsequent incorporation of Cu^{2+} ions involves more favorable kinetics leading to almost immediate reaction in optimal conditions.

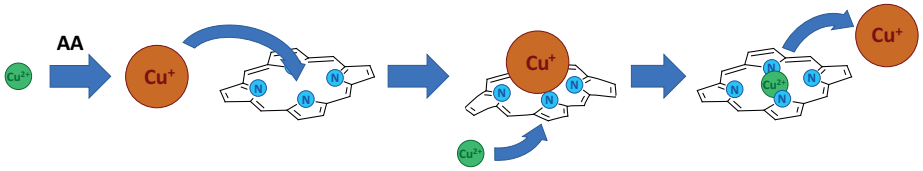

Figure 2: Scheme of synthesis of Cu(II)–poprhyrin complex involving formation of Cu(I) complex.

Synthesis of Cu-TSPP complex in the presence of ascorbic acid (AA) as a reducing agent ran at the highest rate at pH 9 (Fig. 3). Since the [AA]:[Cu] ratio equals 5:1, the maximum of complex absorbance is reached in 1 min. In the case of pH 7, a 20-fold excess of AA is needed to reach a maximum in 10 min or 50-fold (maximum is reached in 8 min). Reaction at pH 4 is the slowest and 20 min is not enough for complete synthesis of the Cu-TSPP complex. The reaction rate for TMPyP is generally higher than for TSPP with maximum absorbance reached at all pH values. Similarly to TSPP, at pH 9 the reaction is the fastest with an almost instant process, and maximum absorbance is reached between mixing the reagents and recording the first spectrum.

Contrary to TSPP, complexation at pH 4 is only slightly inferior to pH 9. From the 10-fold excess of AA upwards the reaction time is about 1 min. For both porphyrins, basic pH led to the deprotonation of pyrrolic nitrogen atoms, which besides the mechanism additionally promoted a high reaction rate of complexation. Strong differences in the behavior of both porphyrins at pH 4 come from the stronger protonation of the porphyrin ring in the case of TSPP. TMPyP remains in a more reactive form with weakly bound protons that can easily be substituted by the incorporation of copper (II) ion into the π system of porphyrin molecules. As for the other porphyrins, in the case of TCPP, which was the object of a previous study [3], complexation at pH 9 is fastest. An almost immediate reaction was achieved with a 10-fold excess of AA. For all studied porphyrins, a significant increase was observed, as the reaction time at room temperature without AA was more than 100 min. The porphyrin ring is notably resistant to harsh conditions, such as high temperatures. For this reason, to increase the reaction rate microwave-assisted synthesis was applied. Microwave heating provides uniform energy transfer that prevents samples from overheating near the reaction vessel walls and the possibility of precise control of

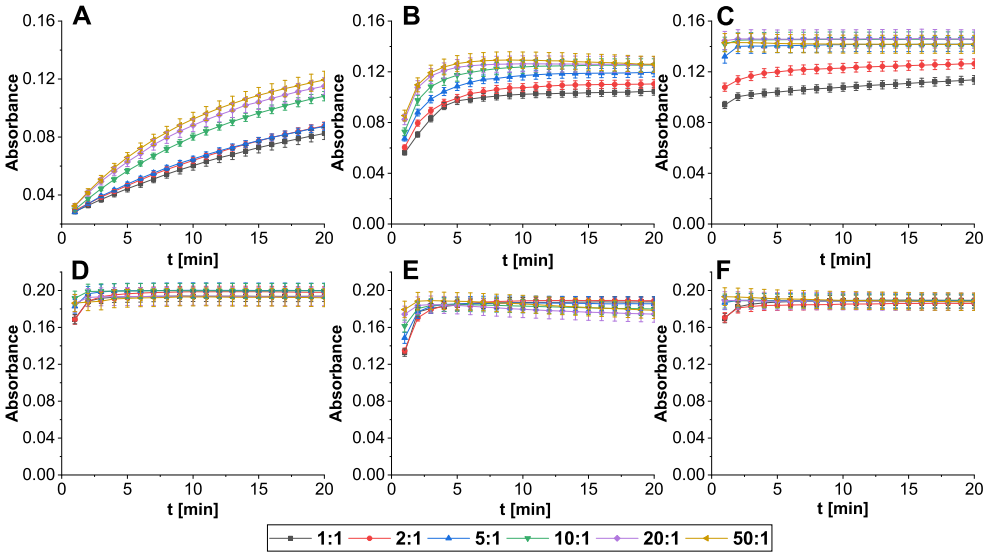

Figure 3: Complexation of Cu with porphyrins in a presence of AA at various [AA]:[Cu] ratios: (A) TSPP (pH 4); (B) TSPP (pH 7); (C) TSPP (pH 9); (D) TMPyP (pH 4); (E) TMPyP (pH 7); (F) TMPyP (pH 9). $[Cu^{2+}] = [TSPP] = [TMPyP] = 10^{-5}$ mol L^{-1}.

reaction parameters. This allowed for a reduction of the reaction time to a minimum, which is vital for possible radiopharmaceutical synthesis.

Microwave heating drastically reduced the time required for the synthesis of the Cu–porphyrin complex without the addition of any other chemicals, which is important in pharmaceutical preparations. Generally, 1–2 min was enough to reach the maximum absorbance of the corresponding complex.Compared to conventional heating, where in many cases 60 min was necessary to complete labeling, microwave-assisted synthesis showed a significant increase in reaction rate.

The studied porphyrins form stable complexes with copper(II) ions. The application of both methods, one with the use of ascorbic acid and the second with microwave heating drastically reduced the time required for the synthesis of Cu(II)–porphyrin complexes. In the case of the method with AA for all studied porphyrins, optimum conditions for fast and efficient complexation at room temperature comprise at least 10-fold excess of AA over Cu. Reactions with TSPP and TCPP should be conducted at pH 9, while for TMPyP pH 4 also offers a satisfying reaction rate. A method with microwave heating would be applicable only for thermally resistant molecules. If the porphyrin acts as a complexing agent attached to an other, thermally sensitive targeting moiety, the method with the use of AA would be more convenient. Both proposed methods are convenient for applications in radiopharmaceutical synthesis as they are one step, fast, and no toxic or harsh chemicals are used that would have to be separated. Additionally, they could be potentially adopted for the synthesis of radiopharmaceuticals labeled with short-lived copper isotopes (^{60}Cu ($t_{1/2}$ = 23.7 min), ^{61}Cu ($t_{1/2}$ = 3.3 h), and even ^{62}Cu($t_{1/2}$ = 9.67 min)).

Bibliography

[1] K. Pyrzyńska, K. Kilian, M. Pęgier, Molecules **27** (2022), 3311.
[2] M. Pęgier, K. Kilian, K. Pyrzyńska, Molecules **28** (2023), 2350.
[3] K. Kilian, M. Pęgier, K. Pyrzyńska, Spectrochim. Acta A Mol. Biomol. Spectrosc. **159** (2016) 123.

B.5 Effects of high-dose electron beam ionizing radiation on an extremophilic alga Cyanidioschyzon merolae

G. Wałpuski[1], M. Zienkiewicz[1], M. Asztemborska[1], A. Rafalski[2], M. Paluch-Ferszt[3], Z. Szefliński[3]

1) Faculty of Biology, University of Warsaw, Warszawa, Poland
2) Institute of Nuclear Chemistry and Technology, Warszawa, Poland
3) Heavy Ion Laboratory, University of Warsaw, Warszawa, Poland

Alongside the development of nuclear physics, researchers have been studying the effect of ionizing radiation (IR) on organisms, including higher plants and algae. As a result of the interaction of γ-quanta and electrons with the cell, numerous ionization processes and dissipation of energy occur, resulting in genetic material damage or disruption of physiological processes [1] . These effects depend mainly on the time exposure, the IR dose and the presence of protection mechanisms against irradiation stress.

Cyanidiophyceae is a class of unicellular algae adapted to acidic hot spring environments which separated evolutionarily from other red algae about 1.5 billion years ago [2]. Our investigation of a member of this class, *Cyanidioschyzon merolae*, covers an original research niche as this extremophilic alga has not yet been analyzed with respect to the influence of IR. The study will provide a better understanding of the evolution of extremophiles exerted by increased physical parameters of the environment in the past, including natural radiation [3].

Throughout the past year's research, we conducted partial analysis of the effects of high doses of IR on physiological parameters and survivability of *C. merolae*. To this purpose, a wild-type strain of alga was exposed, using the "Elektronika" accelerator from the Institute of Nuclear Chemistry and Technology, to an electron beam at seven different approximate dose rates: 2, 4, 6, 8, 10, 20, 40 kGy.

The results obtained indicate the ability of *C. merolae* to survive relatively high doses of IR – 2 and 4 kGy. Depending on the radiation dose, the effects can be observed over the next few days or even immediately after exposure. Results of the observation of algae for the next 2-4 weeks after irradiation indicate a number of differences between the effects of individual doses. These include:

- normal growth, inhibition of cell division, dieback and then restoration of the culture (dose 2-4 kGy);
- initial stimulation of growth followed by inhibition of division and slow death of the cells (dose 6-8 kGy);
- fast, intensive cell death and disintegration of pigments (dose 10-40 kGy).

This pattern of effects caused by distinct IR doses is analogous to one present in the literature [1], except the doses previously used were 3 orders of magnitude lower than in our study. Moreover, post-irradiation cultures were characterized with numerous phenotypic mutations, probably caused by DNA damage and cell cycle disturbances [4]. Among all the mutants, interesting individuals were classified – those of enlarged cell size, and ones with duplicated or multiplicated organelles are worth mentioning. Purification and separation of such mutants is one of the project's future challenges.

The project's preliminary studies and results were presented at the International Conference on Radiation Applications (RAP) 2022 at the poster session [5]. For a continuation of the project and a future manuscript, analyzing other representatives of *Cyanidiophyceae* is an inevitable enhancement to our current data and knowledge.

Bibliography

[1] S. Gudkov *et al.*, J. Environ. Radioact. **202** (2019) 8-24.
[2] E.C. Yang *et al.*, Scientific Reports **6** (2016) 21361.
[3] P.A. Karam, S.A. Leslie, Health Physics **77** (1999) 622-667.
[4] E. R. El-Sayed, A. S. Ahmed, H.K. Abdelhakim, J. Appl. Microbiol. **128** (2020) 747-762.
[5] G. Wałpuski *et al.*, RAP conf. (2022) `https://www.rap-conference.org/22/index.php?page=virtual`.

B.6 The HIL - ICHTJ Collaboration

R. Walczak[1], K. Wawrowicz[1], A. Majkowska-Pilip[1], A. Bilewicz[1], K. Masłowska[1], P. Koźmiński[1], M. Łyczko[1], S. Nosrati[1], M. Pruszyński[1,2] J. Choiński[3], T. Bracha[3], J. Kowalska[3], A. Stolarz[3], Ł. Świątek[3], R. Tańczyk[3]

1) Institute of Nuclear Chemistry and Technology, Warszawa, Poland
2) NOMATEN Centre of Excellence, National Centre for Nuclear Research, Otwock, Poland
3) Heavy Ion Laboratory, University of Warsaw, Warszawa, Poland

There has been close cooperation between HIL and INCT for more than a decade. The last years of joint research were focused on: the production of specific radionuclides, the processes of their separation from irradiated targets, and the search for radiolabeling procedures for molecules acting as isotope carriers. Nuclear reactions induced by protons produced and accelerated in a cyclotron were used to produce radioisotopes.

As part of the cooperation, appropriate targets were produced at the Heavy Ion Laboratory. They were then irradiated with a beam of protons from the PETtrace cyclotron on a special stand connected to the cyclotron. The thickness of the targets prepared for irradiation, regardless of the chemical form of the starting isotope, was selected in such a way that the proton beam was completely stopped in the target. The irradiated targets were then transported to the Institute of Nuclear Chemistry and Technology for further processing.

B.6.1 Production of ^{44}Sc

Continuation of work from 2021

After separation from the target material via the microfiltration method, ^{44}Sc was used for labelling of nanoparticles conjugated with PSMA-617 [C-Fe_3O_4-SiO_2-HPG-NH2-EDTMP@PSMA-617 (NP-EDTMP@PSMA-617) and C-Fe_3O_4-SiO_2-HPG-NH2-DPAPA@PSMA-617 (NP-DPAPA@PSMA-617)]. Labelling was performed at 95°C for 30 min in an environment of 1 M ammonium acetate buffer. The radiolabeling efficiency was found to be almost 98% for EDTMP-PSMA while for DPAPA-PSMA it was found to be almost 97%. For both radiobioconjugates labelling stability in Human serum (HS) and Phosphate buffer (PBS) was checked. Results are shown in Table 1.

	1h	2h	3h	4h	24h
EDTMP HS	93.00	89.67	89.60	90.00	91.67
EDTMP PBS	98.89	97.43	97.34	98.25	96.00
DPAP HS	95.26	94.33	92.13	92.20	84.00
DPAP PBS	98.35	96.79	97.36	97.37	92.31

Table 1: Stability of radiobioconjugates

For radio bioconjugates cell binding affinity was checked
Receptor binding affinity of synthesized bioconjugate was determined with LNCaP cells overexpressing PSMA receptors, as well as with PC-3 cells (PSMA-negative) used as a control.
As presented in Figure 1, both tested compounds bound specifically to PSMA receptors. The significant ($p < 0.05$) decrease in bound fraction confirmed this during the receptor

blocking with excess PSMA. The EDTMP- and DPAPA-based conjugates showed a similar percentage of total bound fraction, calculated as 6.6% (EDTMP) and 5.1% (DPAPA), while the specifically bound fraction was 4.6% and 3.1%, respectively. No binding was observed for PSMA-negative PC-3 cells, which directly shows that synthesized conjugates were successfully conjugated with PSMA, and their biological activity was maintained. PSMA-617-DPAPA/EDTMP NCs are PSMA receptor-specific. Loveless et al. showed that PSMA receptors on LNCaP cells were specifically targeted by using [$^{44/47}$Sc]-PSMA-617 at a molar activity of 10 MBq/nmol.

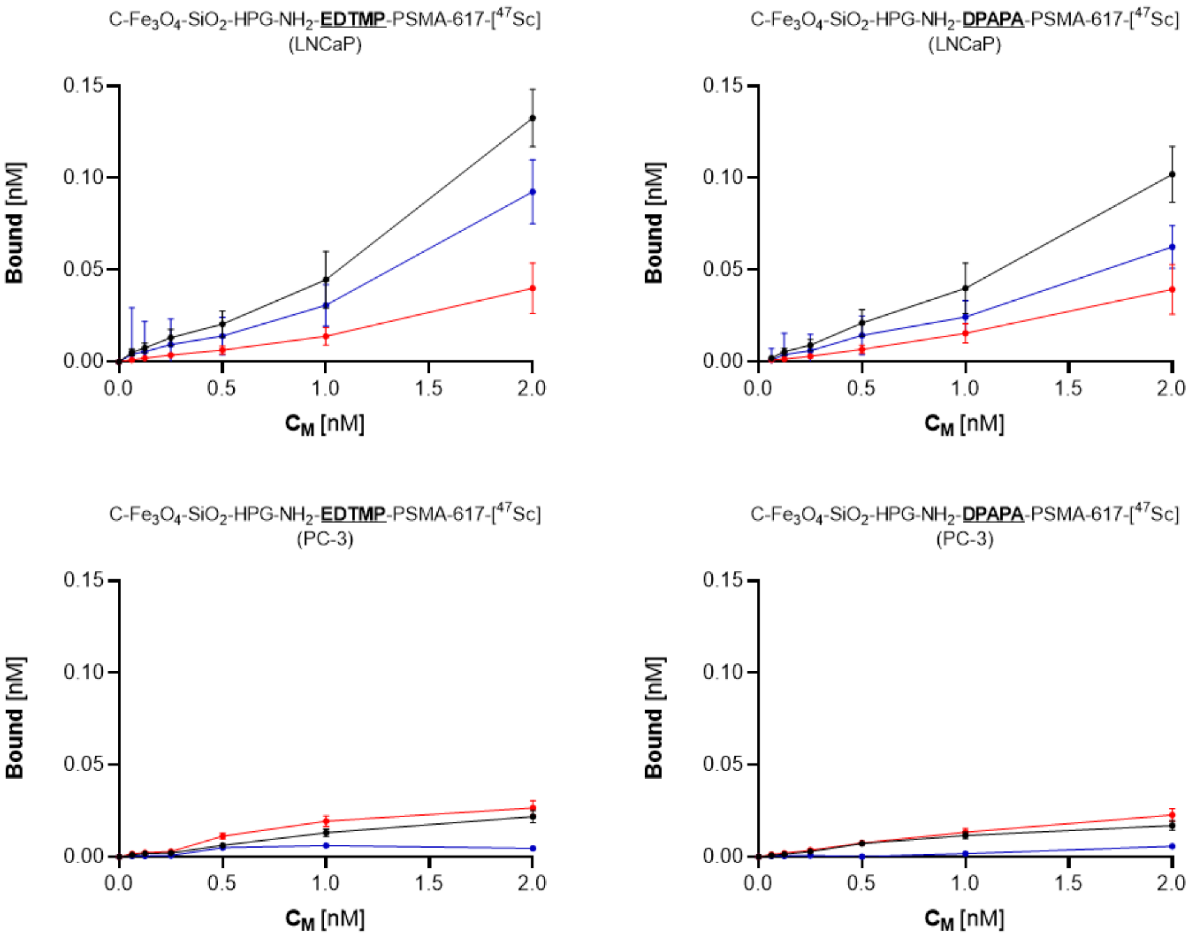

Figure 1: Receptor binding affinity studies of ^{44}Sc labeled EDTMP- and DPAPA-based radiobioconjugates. Upper graphs show data for LNCaP cells; lower graphs show data for PC-3 cells.

New work in 2022

After separation from the target material via the microfiltration method, ^{44}Sc was used for preparing of radiobioconiugates ^{44}Sc-DOTA-Ahx-A7R, Lys(DOTA-^{44}Sc)-A7R, Lys(hArg)-Dab(Ahx-DOTA-^{44}Sc)-Pro-Arg, DR7A-DLys(DOTA-^{44}Sc) which are Peptide and Peptidomimetic Conjugates Targeting Neuropilin-1 Co-Receptor. Labelling was performed in 0.4 M ammonium acetate buffer, pH 4.5, at 95°C.

Results of this work are presented in the paper:
Scandium-44 Radiolabeled Peptide and Peptidomimetic Conjugates Targeting Neuropilin-1 Co-Receptor as Potential Tools for Cancer Diagnosis and Anti-Angiogenic Therapy, Katarzyna Masłowska, Patrycja Redkiewicz, Paweł Krzysztof Halik, Ewa Witkowska, Dagmara Tymecka, Rafał Walczak ,Jarosław Choiński, Aleksandra Misicka, Ewa Gniazdowska, Biomedicines 2023, 11(2), 564;

B.6.2 Production of ^{89}Zr

Pathological angiogenesis, resulting from an imbalance between anti- and pro-angiogenic factors, plays a pivotal role in tumor growth, development and metastasis. The inhibition of the angiogenesis process by the VEGF/VEGFR-2/NRP-1 pathway raises interest in the search for such interaction inhibitors for the purpose of early diagnosis and treatment of angiogenesis-dependent diseases. In this work we designed and tested peptide-based radiocompounds that selectively bind to the neuropilin-1 co-receptor and prevent the formation of the pro-angiogenic VEGF-A165/NRP-1 complex. Three biomolecules, A7R and retro-inverso DR7A peptides, and the branched peptidomimetic Lys(hArg)-Dab-Pro-Arg (K4R), conjugated with macrocyclic chelator through two linker types, were labeled with theranostic scandium-44 radionuclide, and studied in vitro as potential targeted radiopharmaceuticals. ELISA (enzyme-linked immunosorbent assay) studies showed no negative effect of the changes in the introduced biomolecules and high NRP-1 affinity in the case of A7R- and K4R-radiocompounds and a lack affinity for DR7A-radiocompounds. All radiopeptides showed a hydrophilic nature as well as high stability against ligand exchange reactions in cysteine/histidine solutions. Unfortunately, all radiocompounds showed unsatisfactory nano-scale stability in human serum, especially for use as therapeutic radioagents. Further work is ongoing and focused on the search for angiogenesis inhibitors that are more human serum stable.

A separation method based on Zr-resin was performed. Irradiated solid targets made of metallic Y(^{89}Zr) were dissolved in 10 mL of 2 M HCl. The solution of target material was subsequently loaded on a column with 200 mg of Zr resin. After loading the bed was washed with 10 mL of deionized water and ^{89}Zr was eluted with oxalic acid (0.01M, 0.5 mL/min). Results are presented in table 2.

This method allows about 94% of the ^{89}Zr loaded on the column o be obtained.
Separated ^{89}Zr was used for labelling DFO-Infliksimab bioconjugate. Labelling was performed in HEPES buffer (1 M, pH 7.6). The labeling results depending on different amounts of bioconjugate are presented in Table 3.

Unfortunately, labelling efficiency was low which required repetition of the experiment.

B.6.3 Production of ^{135}La

Separation of ^{135}La from $BaCO_3$ target material was performed as in 2021. Separated ^{135}La was used for labelling DOTA-nanobody and DOTATATE.
50 μg of DOTA-nanobody was labelled with 12 MBq of ^{135}La for 1.5 h in 50°C, 0.8 M

Fractions [0.5 mL]	Activity [MBq]
1	0.16
2	75.4
3	45.3
4	5.16
5	1.94
6	1.00
7	0.68
8	0.48
9	0.33
10	0.29
Column	3.6

Table 2: Elution of ^{89}Zr

Sample [nmol]	Efficiency [%]
50	31.2
100	44.6
150	43.5
200	49.2
500	46.1
700	53.3

Table 3

ammonium acetate buffer, pH 4.5. Labelling efficiency was only 9%.
50 nmol of DOTATATE was labelled with 4 MBq of ^{135}La for 1.5 h at 95°C in 0.8 M ammonium acetate buffer pH 4.5. Labelling efficiency was only 97,4%.
Experiments will be continued in the second part of 2023; results was presented at ISTR 2022, Nantes, France.
Poster: Bioconjugates labeled with Auger electron emitter 135La as potential therapeutic radiopharmaceuticals, Rafał Walczak, Sahar Nosrati Shanjani, Emilia Majka, Monika Łyczko, Agnieszka Majkowska-Pilip, Matthias D'Huyvetter, Jarosław Choiński, Marek Pruszyński, Aleksander Bilewicz

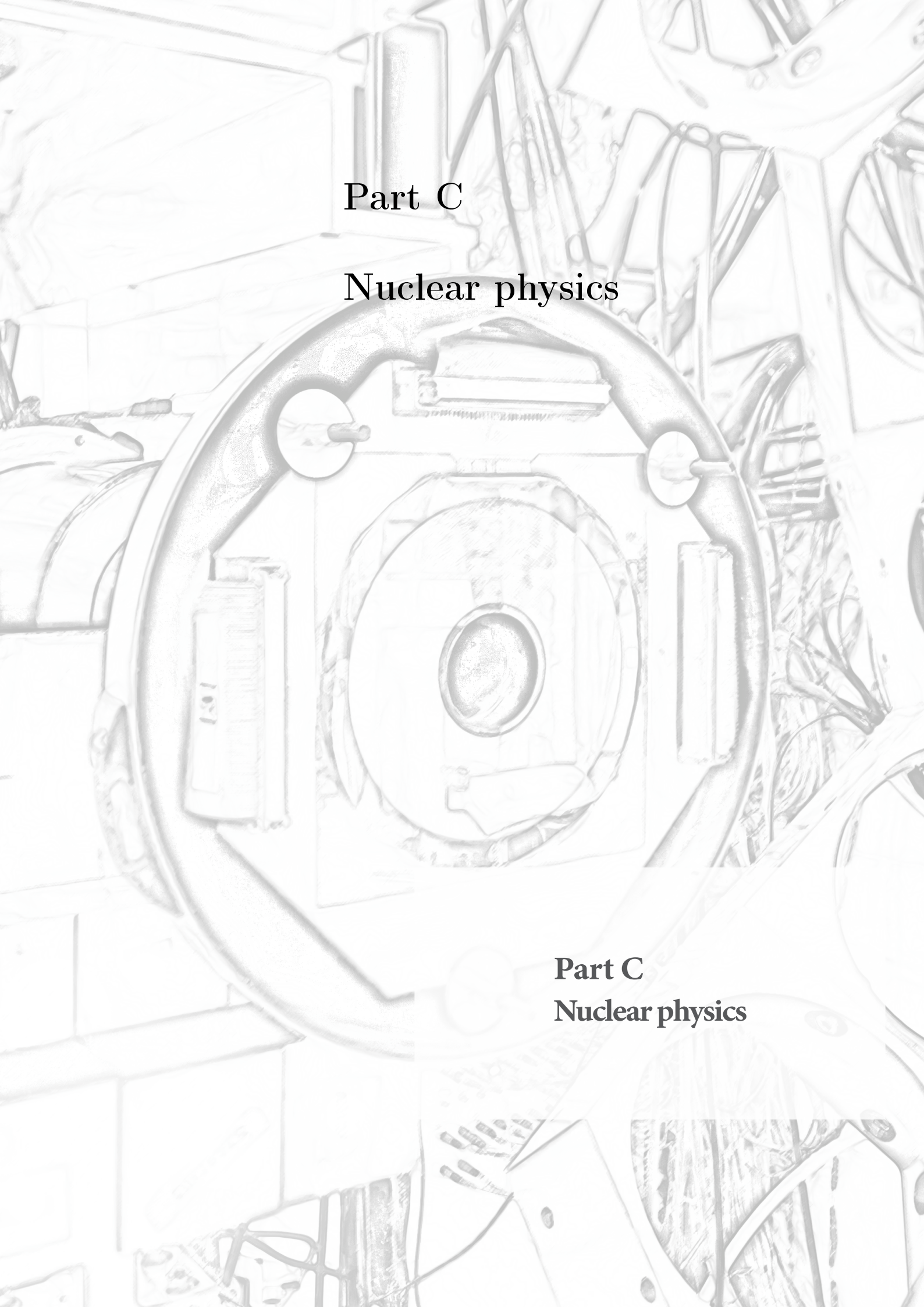

Part C

Nuclear physics

Part C
Nuclear physics

C.1 Dissipation by transfer and its influence on fusion

E. Piasecki[1], G. Colucci[1], A. Trzcińska[1], P. W. Wen[2]

1) Heavy Ion Laboratory, University of Warsaw, Warszawa, Poland
2) China Institute of Atomic Energy, Xinzhen, Fangshan, Beijing, China

The influence of the limited number of projectile and target collective excitations on fusion is a well known phenomenon and can be described using the Coupled Channels (CC) method [1, 2].

Recently, the influence of dissipation (i.e. of the partial conversion of the projectile-target kinetic energy into heat) has become an increasingly frequent topic of discussion. It is relevant to the field of dissipative dynamics in quantum open systems, for which the stationary Schrödinger equation is not adequate because of the irreversibility of the dissipation process and "quantum decoherence" phenomena, present in such systems. New theoretical models, based on the quantum open system method, are under development [3–5].

There are two main mechanisms of dissipation: excitation of non-collective levels by nuclear and electromagnetic interactions [6–8] and mutual projectile-target transfer of light particles. The first phenomenon has been treated by combining the CC method with the Random Matrix Theory (stationary model CCRMT), with promising results [7, 8]. Concerning the transfers, the complicated nature of this many-body phenomenon makes the exact description of it impossible, particularly for heavier systems. Recently we have modified the codes CCQEL and CCFULL [9], upgrading the way they take into account the transfer channels during fusion and backscattering processes. The standard codes assume that two neutron transfer is the dominant transfer channel, especially for positive Q_{gg} (ground state to ground state Q-value). The coupling strength coefficient F_{tr} , employed in the estimation of the transfer coupling form factor $F_{tr} \times dV/dr$ (V – the nuclear potential), is assumed to have a fixed value. Furthermore, the standard model considers only one or a few transfer Q-values, usually corresponding to Q_{gg} or the transfer to a few collective states. In the upgraded model, the $F_{tr}(Q)$ depends on the transferred particle type and Q-value distribution. In [9] we described how of F_{tr} is determined taking simultaneously into account a few coupled transfer channels of different types and the experimental distribution of dissipation. Details of the method and the results obtained will be given in an article in preparation.

We applied the model to the data for ^{24}Mg+^{92}Zr and ^{20}Ne+^{208}Pb, calculating quasielastic barrier distributions (D_{qe}) and fusion barrier distributions (D_{fus}). Interesting discrepancies with respect to the common approximations were observed. In particular, the two neutron transfer, even with a positive Q_{gg} value, does not necessarily dominate the influence on fusion. Moreover, according to the improved model, the fusion enhancement due to transfer is rather moderate and, in contradiction to the standard CCFULL/CCQEL model, concerns mainly the near-barrier region.

Fig. 1 shows the influence of particular transfer channels (1 and 2 neutron pick-up, 1 proton and 1 α stripping) on the fusion excitation function for the ^{24}Mg+^{92}Zr system. Fig. 2 shows the D_{qe} for the same system calculated taking into account 4 transfer channels simultaneously. The calculations show that, according to the model, transfers can also significantly change the barrier distribution shape, smoothing out the structure (a few peaks) resulting from the collective excitations. Unfortunately, at the moment there is no available code able to take into account together non-collective excitations and transfers.

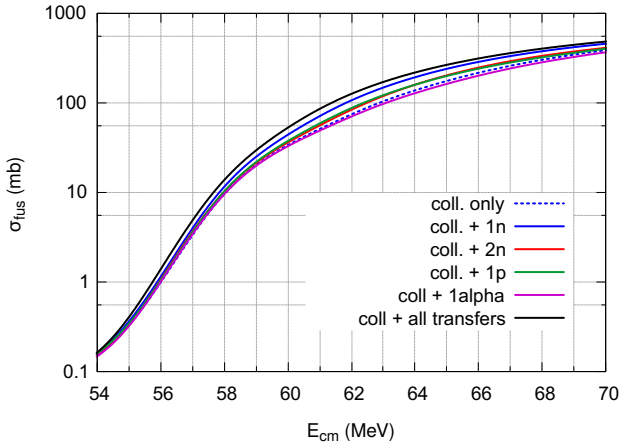

Figure 1: Fusion excitation function for the ^{24}Mg+^{92}Zr system calculated with the improved CCFULL code. Calculations were mode taking into account (separately) particular transfer channels (1 and 2 neutron pick-up, 1 proton, and 1 α stripping) as well as all four transfer channels together – solid lines. In the calculations F_{tr} coefficients resulting from the transfer Q-value distributions were used. These results are compared with the CC calculations taking into account only collective excitations – dashed line.

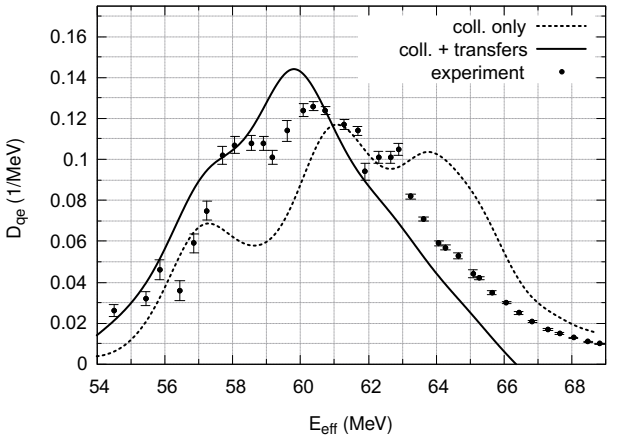

Figure 2: Quasielastic barrier distributions for the ^{24}Mg+^{92}Zr system calculated with the CC method. The solid line describes calculation taking into account simultaneously 4 transfer channels (1 and 2 neutron pick-up, 1 proton and 1 α stripping) and their Q-value distributions, dashed line – the CC calculation taking into account only collective excitations. Theoretical predictions are compared with experimental data – solid circles.

The upgraded CCQEL code was also employed to investigate the influence of transfer channels on the smoothing of the shape of the measured D_{qe} of the ^{20}Ne+^{208}Pb system [8]. Indeed, the ^{208}Pb nucleus is doubly magic and has a relatively low non-collective level density, therefore the dissipation due to non-collective excited states was unable to explain the smoothing of the barrier distribution (see [8], Fig. 6). Including the four dominant transfer channels (1 and 2 neutron pick-up, 1 proton and 1 α stripping) considerably changed the situation (see Fig. 3). One should add that while for the ^{24}Mg+^{92}Zr system the transfer cross sections were measured at one near barrier energy, for ^{20}Ne+^{208}Pb the measurements were made at two beam energies, viz. 92 MeV and 103 MeV [10], which gives us the possibil-

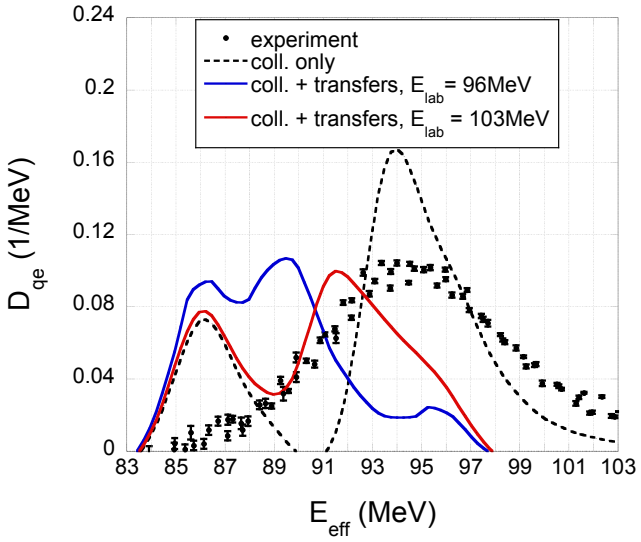

Figure 3: Quasielastic barrier distributions for the ^{20}Ne+^{208}Pb system calculated with the improved CCQEL code. The experimental data (solid black circles) are compared to the theoretical predictions obtained including only collective excitations (dashed black line) and four transfer channels (+1n, +2n, -1p, -1α) measured at beam energies of 96 MeV (blue solid line) and 103 MeV (red solid line).

ity of checking the dependence of F_{tr} on E_{beam}. Thus, the Q-value distributions for various transfer channels were determined for two energies. The $F_{tr}(Q, transfer)$ parameters extracted from the experimental Q-value distributions measured at the two beam energies [9] resulted in significantly different results. This affects the quasielastic barrier distributions as well, which manifest a different shape according to the beam energy measurement, as shown in Fig. 3. Similarly to the case of the ^{24}Mg+^{92}Zr system, the calculations highlight the role of transfer channels in the smoothing of the D_{qe}. However, the calculations obtained from the higher beam energy transfer measurement (red solid line) preserve a two peak structure, while it is strongly damped in the case of the lower energy measurement (blue solid line). This beam energy dependence of the F_{tr}, which according to this model is a consequence of the E_{beam} dependence of dissipation via transfer channels, was not considered before, although it evidently influences the shape of the D_{qe} barrier distribution. Further investigation of this effect requires the transfer cross sections measurements at several beam energies.

Bibliography

[1] M. Dasgupta et al. Annu. Rev. Nucl. Part. Sci. 48 (1998) 401.
[2] B. Back, H. Esbensen, C. Jiang, and K. E. Rehm, Rev. Mod. Phys. 86 (2014) 317.
[3] K. Hagino, priv. comm., "Heavy-ion fusion reactions from a view point of open quantum systems", FUS++ workshop (2022).
[4] A. D. Torres, priv. comm.; I. Lee et al., Phys. Lett. B 827 (2022), 136970.
[5] Sargsyan et al., Physics of Particles and Nuclei, 47(2016) 157.
[6] E. Piasecki et al., Phys. Rev. C 80 (2009) 054613.
[7] S. Yusa, K Hagino, and N. Rowley, Phys. Rev. C 88 (2013) 054621.
[8] E. Piasecki et al., Phys. Rev. C 100 (2019) 014616.
[9] E. Piasecki at al., HIL Annual Report 2021 (2021), 57.
[10] A. Trzcińska at al., HIL Annual Report 2020 (2020), 42.

C.2 Event selection based on a SiC position monitoring system

G. Colucci[1], M. Wolińska-Cichocka[1], M. Kisieliński[1], M. Kowalczyk[1], K. Piasecki[2], B. Zalewski[1], J. Choiński[1], H. M. Jia[3], C. J. Lin[3], M. Matuszewski[1], N. R. Ma[3], E. Piasecki[1], A. Trzcińska[1], L. Yang[3], H. Q. Zhang[3]

1) Heavy Ion Laboratory, University of Warsaw, Warszawa, Poland
2) Faculty of Physics, University of Warsaw, Warszawa, Poland
3) China Institute of Atomic Energy, Xinzhen, Fangshan, Beijing, China

Barrier distributions can be determined directly from the fusion excitation function [1] or the cross sections of quasi elastically back-scattered events [2]. Indeed, barrier transmission and reflection are complementary to each other, therefore the barrier distributions can be determined by detecting the ions which penetrate or are reflected from the barrier. The main advantage of using the quasielastic representation of the barrier distribution is that it yields much smaller experimental uncertainties above the Coulomb barrier than the fusion one and requires much simpler experimental setups for the measurements. On the other hand, the backscattering method has slightly worse resolution and thus may be less sensitive to nuclear structure effects.

The direct observation of evaporation residues (ER) is the most accurate method of determining fusion cross sections. However, the fusion products are strongly focused along the beam direstion, thus this requires the detection of the ER recoil at angles close to the beam direction and suppression of the intense elastic scattering. To this end, the most practical solution is the use of a Wien (velocity) Filter, capable of transmitting ER from heavy ion fusion reactions and suppressing elastic scattering, even at angles as close as 0.5° to the beam direction.

In this perspective, we plan to install at the Heavy Ion Laboratory (HIL) of Warsaw University a new setup for fusion cross section measurements based on a Wien Filter, a static electromagnetic separator. To perform fusion measurement at HIL, the ICARE scattering chamber has been upgraded with an extension, equipped with a moveable platform where the Wien Filter [3, 4] and a Time of Flight (ToF) device, composed of a Microchannel Plate (MCP) and silicon detector, will be placed.

For fusion excitation function measurements, a precise and stable experimental geometry is a necessary condition. Indeed, the angular distribution of the fusion products is very narrow, centred around the beam axis [5]. As a consequence, even a slight change in the beam spot position on the target influences the detection angle and, therefore, the measured cross section. Furthermore, the fusion barrier distributions (D_{fus}) are defined as the second derivative of the excitation function. This amplifies beam-based instabilities considerably [1]. To minimize these instabilities during a D_{fus} measurement, a system that enables the online monitoring of the beam position on the target has been developed at HIL. The device consists of four Silicon Carbide (SiC) detectors placed at small forward angles downstream of the target. This beam monitoring system has been successfully tested at HIL [6], and preliminary analysis proved the ability to ensure a beam position stability with an uncertainty of 0.15 mm in a 7 hours measurement. The sensitivity and stability of the device allow the cyclotron operators to check on-line check and reproduce the beam settings after every change of energy.

Two in-beam tests were performed at the ICARE chamber with ^{32}S and ^{14}N beams of 85 MeV and 35 MeV energies, respectively. Thin targets of ^{nat}Au (0.1 mg/cm^2), ^{nat}Sn

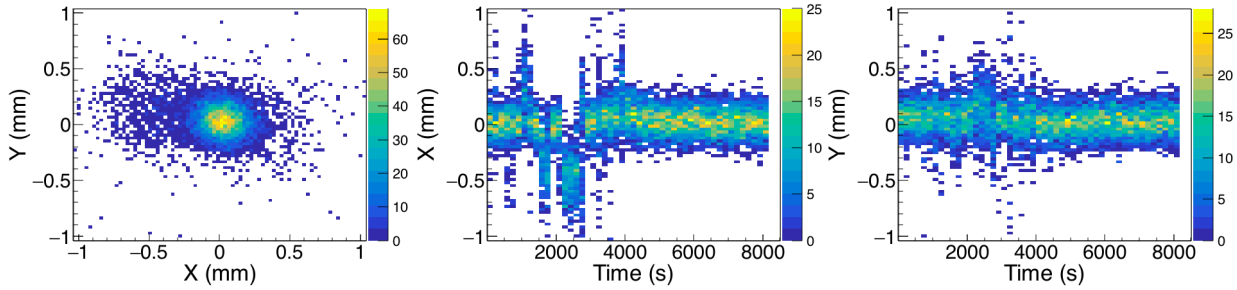

Figure 1: Distribution of the ^{32}S beam spot centre on a ^{nat}Mo target during various steering settings. The left panel shows the X–Y position distribution. Central and right panels show the X and Y beam positions as a function of the time, respectively.

(0.1 mg/cm^2) and ^{nat}Mo (0.6 mg/cm^2) were used. The SiC detectors were placed at 10° and 10 cm downstream the target. The beam passed through a collimator of 2 mm diameter placed 4 cm upstream from the target.

The experiments aimed to verify the device's ability to detect significant displacements in the beam position. To this end, the beam position was intentionally modified by the U200-P cyclotron operator by varying the steering settings. Such modifications lead to a significant variation in the beam position along the horizontal axis. This is shown in Fig. 1 (left panel), where the vertical and horizontal distribution of the centre of the beam position for the ^{32}S scattered on ^{nat}Mo is reported. A significant displacement along the X–axis of about -0.5 mm and +0.3 mm is well visible. The displacements can be distinguished by plotting the horizontal and vertical positions as a function of the time (see Fig. 1, central and right panels).

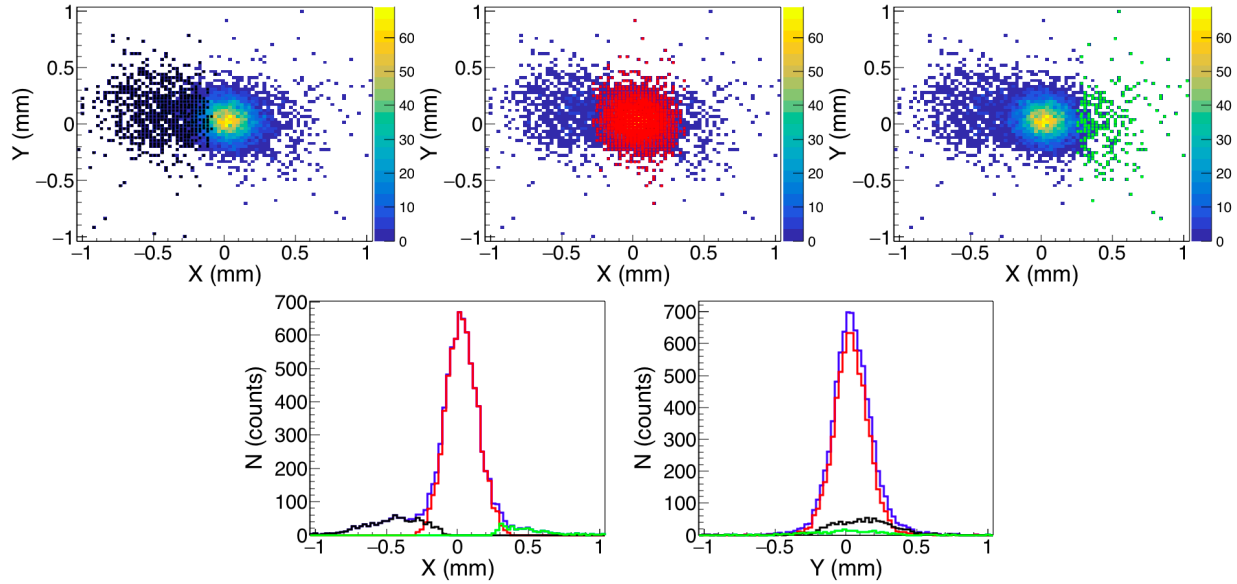

Figure 2: Upper panels: X – Y position distribution for the ^{32}S scattered on ^{nat}Mo target where events corresponding to a beam position along the x-axis at -0.5 mm (black points), 0 mm (red points), and 0.3 mm (green points) are selected. Lower panels: X and Y projection of the beam position distributions, where N is the number of counts. The distributions of the displacement at -0.5 mm and 0.3 mm are indicated in black and green, respectively. The X and Y projections of the beam position distribution centred at 0 mm are in red.

The test proves the device's ability to identify displacements of the beam position within 0.3 mm. Offline analysis allows one to select the events related to these displacements. Figure 2 shows the vertical and horizontal beam position, where the distributions relative to displacements of –0.5 mm (black points) and +0.3 mm (green points) are indicated, as well as the distribution centred at 0 mm (red points). These displacements mainly affect the horizontal position as shown in the X and Y projections (Fig. 2, lower panels), where the different beam positions lead to tails in the X projections.

Therefore, the beam monitoring device is able clearly to identify the displacements of the beam spot centre within 0.3 mm and an offline analysis allows one to select the events related to un-centred beam positions. This is of crucial importance for fusion cross section measurements, since it will allow the rejection of events detected during beam position displacement, minimizing the beam-based instability in fusion barrier distributions measurements.

Bibliography

[1] N. Rowley *et al.*, Phys. Rev. Lett. **B254** (1991) 25.
[2] H. Timmers *et al.*, Nucl. Phys. A **584** (1995)190.
[3] E. V. Pagano *et al.*, LNS Annual Report 2018/2019 (2018).
[4] E. V. Pagano *et al.*, LNS Annual Report 2019 (2019).
[5] J. X. Wei *et al.*, Nucl. Inst. and Meth. A **306** (1991) 557 .
[6] E. Piasecki *et al.*, HIL Annual Report (2021) 25-27.

C.3 Coulomb excitation of ^{110}Cd with a ^{14}N beam

I. Piętka[1], K. Wrzosek-Lipska[2], T. Abraham[2], S. Buck[3], M. Chiari[4], G. Colombi[5,6,7], G. Colucci[2] P.E. Garrett[3], B. Greaves[3], K. Hadyńska-Klęk[2], J. Heery[8], D. Hymers[3], G. Jaworski[2], D. Kalaydjieva[9], M. Komorowska[2], M. Kowalczyk[2], J. Kowalska[2], K. Krutul-Bitowska[2], N. Marchini[4], M. Matejska-Minda[10], C. Michelagnoli[5], A. Nannini[4], P.J. Napiorkowski[2], M. Palacz[2], L. Próchniak[2], M. Rocchini[3,4], A. Stolarz[2], T. Zidar[3], M. Zielińska[9]

1) Faculty of Physics, University of Warsaw, Warszawa, Poland
2) Heavy Ion Laboratory, University of Warsaw, Warszawa, Poland
3) University of Guelph, Guelph, Canada
4) INFN Sezione di Firenze, Firenze, Italy
5) Institut Laue Langevin, Grenoble, France
6) University of Milan, Milano, Italy
7) INFN. Sezione di Milano, Milano, Italy
8) Department of Physics, University of Surrey, Guildford, UK
9) IRFU, CEA, Université Paris-Saclay, Gif-sur-Yvette, France
10) Institute of Nuclear Physics PAN, Kraków, Poland

A Coulomb-excitation study of ^{110}Cd was performed in April 2022 using a 34.75-MeV ^{14}N beam delivered by the Warsaw Cyclotron. This experiment was part of a multi-faceted program of study to ascertain the shapes (charge distributions) of the states in ^{110}Cd. The indication of the presence of multiple shape coexistence in ^{110}Cd comes from previous studies that combined detailed γ-ray spectroscopy with sophisticated beyond-mean-field calculations [1–3]. These investigations suggested that the low-lying 0^+ states in ^{110}Cd possess prolate, triaxial, and oblate shapes with rotational-like bands built upon them. This interpretation would have major implications for structural interpretations of nuclei in the Z=50 region, traditionally considered textbook examples of multiphonon spherical vibrators [5].

As the first step of our experimental programme focused on ^{110}Cd we performed a multistep Coulomb-excitation experiment at the Heavy Ion Laboratory, University of Warsaw, using a 91-MeV ^{32}S beam on a ^{110}Cd target [4]. The following excited states were observed: 2_1^+ (658 keV), 4_1^+ (1542 keV), 2_2^+ (1476 keV), 0_2^+ (1473 keV), 3_1^- (2078 keV), 0_3^+ (1731 keV). The analysis of the ^{32}S +^{110}Cd data was complicated due to the imprecise knowledge of the lifetime of the 2_2^+ state (literature values ranging from 1.07(27) ps [6] to 1.95(+50;-30) ps [1]). This influences the resulting $B(E2)$ values, in particular those involving the 2_2^+ and 0_2^+ states.

Important constraints on multistep Coulomb-excitation analysis can be provided by data collected in measurements performed with lighter ion beams (e.g., ^{14}N). The Coulomb-excitation cross sections depend on the scattering angle, the energy of the projectile, and also the atomic (Z) and mass (A) numbers of the collision partners. With the use of light projectiles single-step excitations are enhanced, dominating the Coulomb-excitation process. Consequently, experimental information from such a measurement is expected to increase the sensitivity for the extraction of the $B(E2)$ values for transitions de-exciting the 2_2^+ state.

The ^{14}N +^{110}Cd experiment was carried out using the EAGLE γ-ray spectrometer [7] and an array of particle detectors (PiN diodes) placed in a compact scattering chamber. The EAGLE array consisted of 16 HPGe detectors with anti-Compton shields, of which 15 had higher efficiency (i.e., 60% relative to a 3″×3″ NaI detector), on loan from Gammapool. To minimize the probability of multi-step excitations, the 47 PiN diodes were placed at

the most forward angles with respect to the beam direction available with this reaction chamber, i.e., from 110 to 131 degrees in the laboratory frame. An isotopically enriched (97%) ^{110}Cd target of 1.04 mg/cm^2 thickness was used. The data were collected in the γ-particle coincidence mode (see, e.g., Ref. [8]).

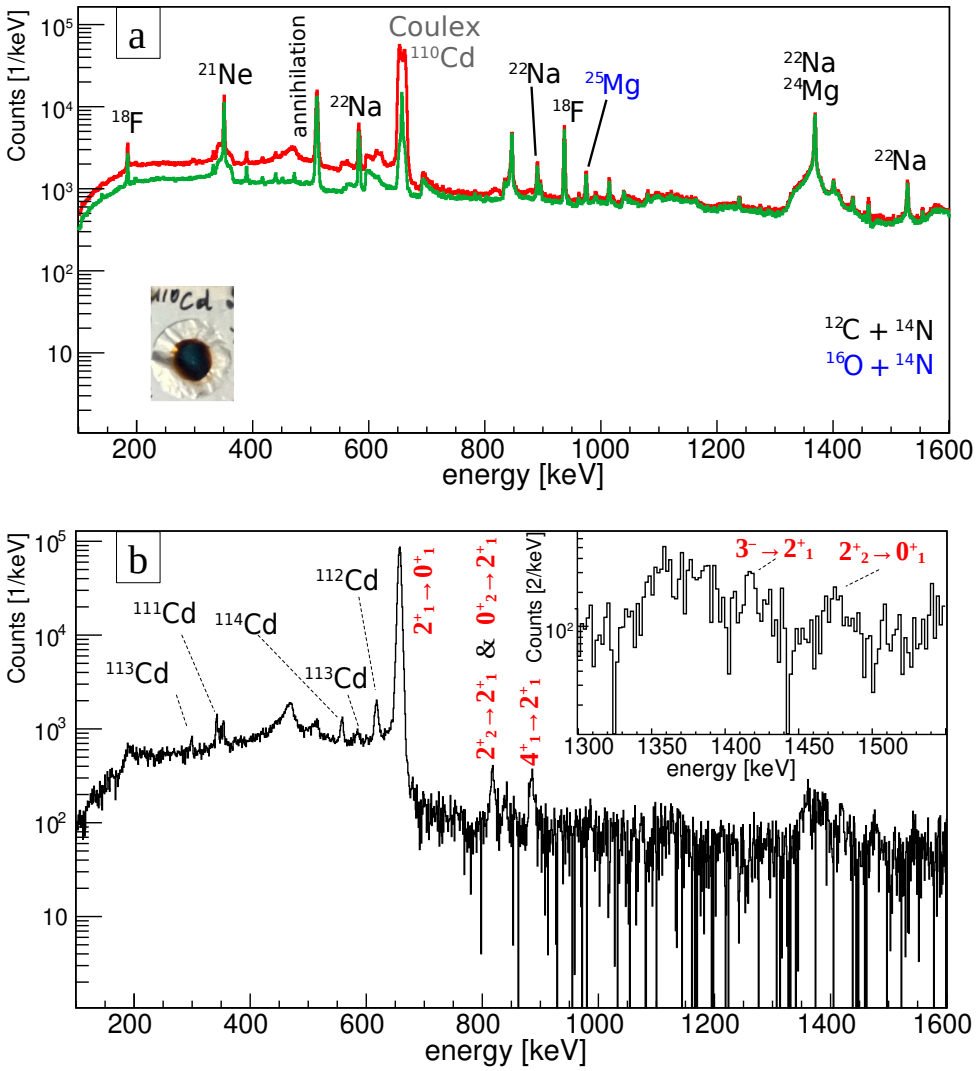

Figure 1: *(a)* Total non-Doppler-corrected γ-ray spectra of prompt (red) and random (green) γ-particle coincidences. The γ rays resulting from the ^{12}C $+^{14}$N and ^{16}O $+^{14}$N reactions are labelled in black and blue, respectively. Inset: the ^{110}Cd target used for the study.
(b) Total Doppler-corrected and background-subtracted γ-ray spectrum of ^{110}Cd. The γ rays originating from ^{110}Cd are labelled in red. The $2^+_2 \rightarrow 2^+_1$ and $0^+_2 \rightarrow 2^+_1$ transitions are observed as a doublet at 818 keV. γ rays resulting from Coulomb excitation of target isotopic impurities ($^{111-114}$Cd) are also visible.

The non-Doppler-corrected γ-ray spectra, collected in the prompt (red) and random (green) particle-γ coincidences are shown in Fig.1(a). In addition to the γ-ray transitions originating from Coulomb excitation of ^{110}Cd, a number of other γ-ray lines are visible as well. The analysis of these additional γ rays revealed that they result from nuclear reactions of the ^{14}N beam with O and C target contaminants [9]. The composition of the ^{110}Cd target used in the Coulomb-excitation measurement at HIL was investigated at the LABEC INFN laboratory in Florence, Italy, using the Rutherford Backscattering Spectrometry

(RBS) method. Details of this method are described in Ref. [10]. The analysis confirmed the presence of oxygen and carbon in the target. While oxidized cadmium layers, which constitute around 6% of the target thickness, were found on each surface of the target, a carbon layer of 10 µg/cm^2 thickness is present only on the side of the target that was facing the beam [11]. The energy loss of ^{14}N ions in these layers, under the conditions of the present experiment, is only about 0.05 MeV. Consequently, the energy range at which Coulomb excitation of ^{110}Cd proceeds is not affected by the presence of oxygen and carbon in the target in any significant way.

The on-going analysis of the ^{14}N $+^{110}$Cd data concentrates on establishing conditions that will minimize the background while retaining the events resulting from Coulomb excitation. The total Doppler-corrected, background-subtracted, particle-γ-ray coincidence spectrum of ^{110}Cd, summed over all HPGe and charged-particle detectors, is presented in Fig. 1(b).

The ongoing analysis is the subject of the Master's thesis of I. Piętka at the Faculty of Physics, University of Warsaw, Poland.

The European Gamma-Ray Spectroscopy Pool (GAMMAPOOL) is acknowledged for providing HPGe detectors.

Bibliography

[1] P.E. Garrett *et al.*, Phys. Rev. C **86** (2012) 044304.
[2] P.E. Garrett *et al.*, Phys. Rev. C **101** (2020) 044302.
[3] P.E. Garrett *et al.*, Phys. Rev. Lett. **123** (2019) 142502.
[4] K. Wrzosek-Lipska *et al.*, Acta Phys. Pol. **B51** (2020) 789.
[5] R.F. Casten, Nuclear Structure from a Simple Perspective (Oxford Univ. Press 1990).
[6] Yu. N. Lobach *et al.*, Eur. Phys. J. **A6** (1999) 131.
[7] J. Mierzejewski *et al.*, Nucl. Inst. and Meth. A**659** (2011) 84.
[8] K. Wrzosek-Lipska *et al.*, HIL Annual Report 2017, page 43.
[9] K. Wrzosek-Lipska *et al.*, HIL Annual Report 2021, page 26.
[10] M. Rocchini *et al.*, Nucl. Instrum. Methods Phys. Res. **B486** (2021) 68.
[11] F. Sansone, B.S. Thesis, University of Naples, Italy (2022).

C.4 Probing shapes and structures ^{100}Ru via Coulomb excitation

P.E. Garrett[1], K. Wrzosek-Lipska[2], M.Rocchini[1,3], M. Zielińska[4], T. Abraham[2], Z. Ahmed[1], V. Bildstein[1], A. Blazhev[5] S. Buck[1], R.Coleman[1], G. Colucci[2], B. Greaves[1], K. Hadyńska-Klęk[2], D. Kalaydjieva[4], M. Komorowska[2], M. Kowalczyk[2], K. Krutul-Bitowska[2], K. Mastakov[1], M. Matejska-Minda[6], C. Michelagnoli[7], P.J. Napiorkowski[2], N. Kopeć[2], M. Palacz[2], S. Pannu[1], I. Piętka[8], J. Samorajczyk-Pyśk[2], A. Stolarz[2], A. Trzcińska[2], A. Tucholski[2], T. Zidar[1]

1) University of Guelph, Guelph, Canada
2) Heavy Ion Laboratory, University of Warsaw, Warszawa, Poland
3) INFN Sezione di Firenze, Firenze, Italy
4) IRFU, CEA, Université Paris-Saclay, Gif-sur-Yvette, France
5) Institut für Kernphysik, Universität zu Köln, Köln, Germany
6) Institute of Nuclear Physics PAN, Kraków, Poland
7) Institut Laue Langevin, Grenoble, France
8) Faculty of Physics, University of Warsaw, Warszawa, Poland

The level schemes of even-even Ru isotopes, especially those with neutron numbers between 54 and 60, are reminiscent of those expected for quadrupole harmonic vibrators. In a survey conducted by Kern et al. [1], that primarily used the level excitation energies as indicators, a number of nuclei in the $Z \approx 50$ region were selected as excellent candidates for spherical vibrational motion. While the Cd isotopes, especially ^{110,112}Cd, stood out as perhaps the best examples, the survey also highlighted the Ru isotopes, albeit with some discrepancies noted. Very recently, an alternative interpretation for the structure of the Cd isotopes has been offered with the suggestion that they exhibit multiple shape coexistence [2, 3]. In a recent update [4] of the survey of Kern et al. [1], it was shown that for many of the previous candidates the spherical vibrational interpretation could be ruled out, and furthermore that the data were suggestive of shape coexistence. This is in particular true for the Ru isotopes with $A \geq$102 (see, e.g., Refs. [4–6]). Further support for the shape-coexistence scenario in the Ru isotopes with N$= 52 - 62$ comes from the most recent beyond-mean-field calculations employing the Gogny D1S energy density functional and the self-consistent configuration mixing (SCCM) method [7].

In light of the recent experimental and theoretical findings, several questions regarding the structure of the Ru isotopes have arisen, i.e., (i) do the light Ru isotopes, especially ^{98,100}Ru, behave as spherical vibrators? (ii) do the Ru isotopes with $N < 60$ display shape coexistence? (iii) if shape coexistence does indeed occur across the Ru isotopic chain, why do the shapes appear to evolve so gradually compared to the Zr and Mo isotopes? (iv) might there be multiple shape coexistence appearing in the Ru isotopes, similar to what has been recently suggested in Cd and Zr isotopes?

In order to address these questions, and firmly establish the degree of deformation that the states possess, detailed Coulomb-excitation measurements are required utilising various projectile-target combinations. This will allow us to access a wide range of yrast and non-yrast states and to extract precisely electromagnetic matrix elements, including static quadrupole moments, and, in consequence, the shape of a nucleus in a given excited state. Investigations along these lines have been initiated, with Coulomb-excitation experiments of ^{100}Ru with ^{14}N and ^{32}S beams approved at the Heavy Ion Laboratory in Warsaw.

The first of these measurements took place in March 2022 and used a 83.4-MeV ^{32}S beam delivered by the Warsaw cyclotron. Measurements were performed in a particle-γ

coincidence mode (see, e.g., Ref. [8] for a particle-γ time coincidence spectrum). The EAGLE γ-ray spectrometer [9], used in the experiment, was coupled to a compact scattering chamber equipped with 47 PIN-diode particle detectors. The EAGLE array consisted of 16 Compton-suppressed HPGe detectors, 15 of which were on loan from Gammapool, and had an efficiency of 60 % relative to a $3'' \times 3''$ NaI detector. The particle detectors were placed at angles between 131 and 167.5 degrees in the laboratory frame with respect to the beam direction. An enriched ^{100}Ru target of 1 mg/cm^2 thickness with a thick Al backing was used. The observed γ-ray transitions in ^{100}Ru were Doppler broadened and shifted in energy.

The low-energy part of the level scheme of ^{100}Ru together with the γ-ray transitions observed in the experiment is shown in Fig. 1, and the total Doppler-corrected and background subtracted γ-ray spectrum is presented in Fig. 2. The spectrum is summed over all HPGe and charged-particle detectors.

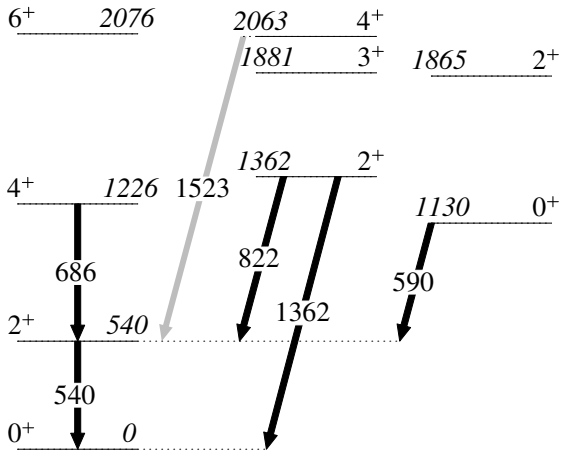

Figure 1: Low-energy part of the ^{100}Ru level scheme highlighting γ-ray transitions observed in the present experiment. The level and transition energies are given in keV. The tentative $4_2^+ \rightarrow 2_1^+$ transition is marked with a gray arrow.

Several states in ^{100}Ru were populated in the present experiment, predominantly via one-step and two-step Coulomb-excitation processes. In addition to the ground-state band, the decays of the lowest-lying non-yrast levels were observed, including the 0_2^+ and 2_2^+ states, which are vital to achieve the physics goals of this project. Some γ-ray transitions that do not originate from Coulomb excitation of ^{100}Ru are visible in the spectrum presented in Fig. 2. In particular, the 1130-keV and 1409-keV transitions likely arise from the decay of ^{54}Fe produced in the ^{27}Al(^{32}S,αp)^{54}Fe reaction on the target backing. Further analysis and verification is required regarding the population of the 4_2^+ state in ^{100}Ru, as its 1523-keV γ-ray decay to the 2_1^+ state lies close in energy to the $2_1^+ \rightarrow 0_1^+$ transition in ^{42}Ca (1525 keV). The latter can be a product of nuclear reactions of the ^{32}S beam with carbon or oxygen contaminants of the target (see, e.g., Refs. [10, 11]).

In summary, the collected experimental data, complemented by a future measurement with the lighter ^{14}N beam, will provide essential information regarding the structure of the low-lying states in ^{100}Ru, in particular the 0_2^+ state.

The European Gamma-Ray Spectroscopy Pool (GAMMAPOOL) is acknowledged for providing HPGe detectors.

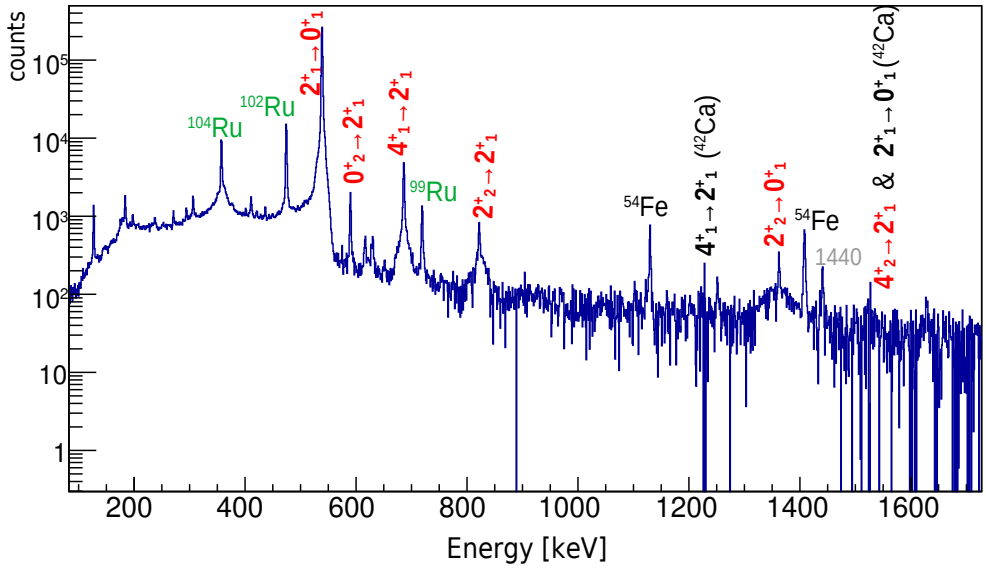

Figure 2: Total Doppler-corrected and background-subtracted γ-ray spectrum from the present Coulomb-excitation experiment. The γ rays originating from ^{100}Ru are labelled in red, and those resulting from the reactions of the ^{32}S beam with ^{12}C, ^{16}O and ^{27}Al in black. Green labels are used for the γ-ray transitions arising from Coulomb excitation of ^{99,102,104}Ru isotopic impurities present in the target.

Bibliography

[1] J. Kern, P.E. Garrett, J. Jolie, and H. Lehmann, Nucl. Inst. and Meth. **593** (1995) 21.
[2] P.E. Garrett *et al.*, Phys. Rev. C **101** (2020) 044302.
[3] P.E. Garrett *et al.*, Phys. Rev. Lett. **123** (2019) 142502.
[4] P.E. Garrett, J.L. Wood, and S.W. Yates, Physica Scripta **93** (2018) 063001.
[5] W. Urban *et al.*, Phys. Rev. C **87** (2013) 031304.
[6] J. Srebrny *et al.*, Nucl. Phys. A **766** (2006) 25.
[7] P.E. Garrett *et al.*, Phys. Lett. B**809** (2020) 135762.
[8] K. Wrzosek-Lipska *et al.*, HIL Annual Report 2017, page 43.
[9] J. Mierzejewski *et al.*, Nucl. Inst. and Meth. A**659** (2011) 84.
[10] K. Wrzosek-Lipska *et al.*, HIL Annual Report 2018, page 49.
[11] K. Hadyńska *et al.*, HIL Annual Report 2008, page 27.

C.5 Lifetime studies in neutron deficient ^{176}Pt using the recoil distance Doppler-shift technique

C. Fransen[1], R. Novak[1], T. Abraham[2], M. Beckers[1], A. Blazhev[1], A. Dewald[1], F. Dunkel[1], K. Hadyńska-Klęk[2], J. Jolie[1], G. Jawroski[2], M. Kowalczyk[2], C.-D. Lakenbrink[1], C. Müller-Gatermann[3], P.J. Napiorkowski[2], M. Palacz[2], B. Radomyski[2], K. Rusek[2], J. Srbrny[2], A. Tucholski[2], K. Wrzosek-Lipska[2], F. Spee[1]

1) Institute for Nuclear Physics, University of Cologne, Germany

2) Heavy Ion Laboratory, University of Warsaw, Warszawa, Poland

3) Argonne National Laboratory, Lemont, Illinois, USA

An experiment on neutron deficient ^{176}Pt was performed at HIL in June 2022 with the Cologne plunger device [1] coupled to the EAGLE γ-ray spectrometer. The aim was the determination of yrast transition strengths in this nucleus from level lifetimes. The latter were measured with the recoil distance Doppler-shift method (RDDS).

In several neutron deficient nuclei in the $A = 180$ mass region experimental findings both on level schemes and absolute $E2$ transition strengths have yielded clear signatures for shape coexistence. These result from low-lying intruding structures, e.g., from excitation of protons over the Z=82 main shell. In neutron deficient Hg isotopes close to neutron midshell, a weakly deformed ground state configuration and a prolate intruder structure were clearly identified (see, e.g., [2, 3]). For the neighboring midshell Pt isotopes (^{178,180}Pt) it was shown that the prolate deformation becomes the ground state configuration, where the corresponding deformation is similar to that of the intruder configuration in Hg [4, 5]. The experimental observables are in agreement with predictions from the interacting boson model (IBM) and mean-field (MF) calculations [6]. For the lighter Pt isotopes these model predictions differ from each other, and exactly at ^{176}Pt a dramatic change towards a spherical ground state configuration is predicted by the IBM, which is supported by

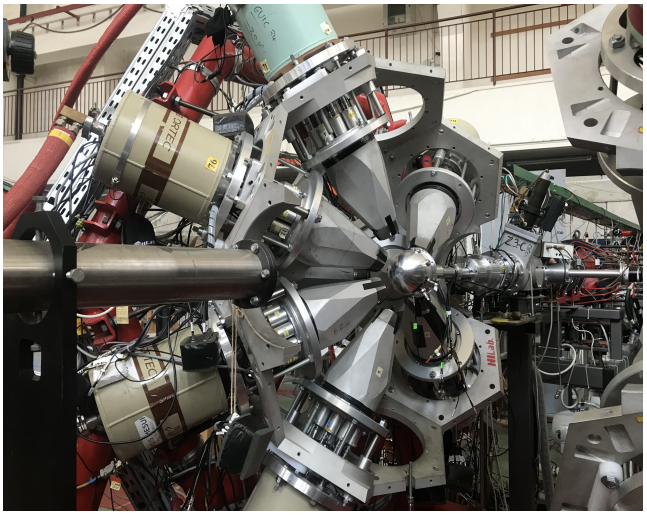

Figure 1: Picture of the Cologne plunger mounted on the EAGLE γ-ray spectrometer at HIL. The plunger was attached to the last valve of the EAGLE beam line and replaced the EAGLE target chamber.

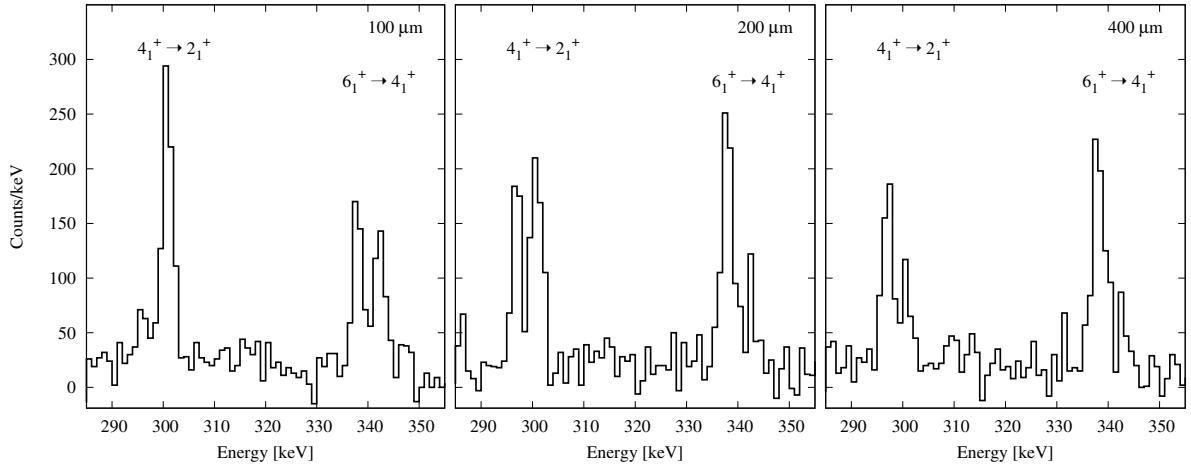

Figure 2: Spectrum from the experiment on ^{176}Pt for the EAGLE detectors at a backward angle of 143 degrees with respect to the beam line gated on the $2_1^+ \rightarrow 0_1^+$ transition for three different target–stopper foil distances: 100 μm, 200 μm, and 400 μm in the energy range of the $4_1^+ \rightarrow 2_1^+$ and $6_1^+ \rightarrow 4_1^+$ transitions. The evolution of the intensities of the stopped and Doppler-shifted components with respect to the the distance of the foils can be clearly seen.

the level scheme. In contrast, MF theory prognosticates almost no change towards even more neutron deficient nuclei. For ^{176}Pt the authors of an earlier publication [7] point out that "^{176}Pt changes from a quasi-vibrational pattern to that of a well deformed rotor, at very low spins, a behaviour similar to that attributed to shape coexistence in the light Hg isotopes" (see also [8]).

The existing data on yrast transition strengths from [7] do not allow us to draw conclusions on the structural evolution within the yrast band of ^{176}Pt, especially as these older data might suffer from unobserved delayed feeding of the levels of interest. Therefore, a high-precision lifetime measurement was performed within this work using the recoil distance Doppler-shift (RDDS) technique in $\gamma\gamma$ coincidence mode. Thus, feeding problems can be excluded, which further reduces systematic errors in comparison to Ref. [7]. By contributing precise B(E2) values, the contradiction between the aforementioned model approaches can be solved and a potential hidden configuration mixing in the Pt isotopes be revealed.

The Cologne plunger was mounted at the EAGLE spectrometer for this experiment (see Fig. 1). We used the ^{148}Sm(^{32}S,4n)^{176}Pt reaction with a ^{32}S beam at an energy of 170 MeV to populate yrast states in ^{176}Pt. The plunger target consisted of a 0.75 mg/cm^2 ^{148}Sm layer evaporated onto a 1.5 mg/cm^2 Ta stretchable support foil facing the beam. A 6.8 mg/cm^2 gold foil was used to stop the recoiling nuclei. The chosen reaction resulted in a mean ^{176}Pt recoil velocity after the target of about $v \approx 1.7\%c$ and thus in a sufficient separation of the Doppler-shifted and unshifted components of the respective γ-ray lines.

The EAGLE spectrometer was equipped with 16 anti-Compton shielded high-purity Germanium detectors arranged in 3 rings with 5 detectors each at angles of 37 degrees, 63 degrees, and 143 degrees with respect to the beam axis, and one detector at an angle of 101 degrees with respect to the beam axis. The data were sorted into $\gamma\gamma$ coincidence matrices aiming for the determination of level lifetimes from direct gates on flight components of feeding transitions to exclude any contribution from delayed feeding. The RDDS experiment was done at 10 target–degrader distances between 15 μm and 600 μm with respect to electrical contact of the foils. Fig. 2 depicts a γ-ray spectrum where shifted and

unshifted components of γ-ray lines of ^{176}Pt can be clearly identified and which proves that the statistics are sufficient to achieve the goal of this work, i.e., the interpretation of the structural evolution within the yrast band of ^{176}Pt.

The data are cuenly being analysed at Cologne and will allow us to determine the life-times of the $2_1^+ - 12_1^+$ states in ^{176}Pt with a precision of $\Delta\tau \leq 10\%$.

Bibliography

[1] A. Dewald, O. Möller, P. Petkov, Prog. Part. Nucl. Phys. **67**, (2012)786.
[2] L.P. Gaffney et al. in Phys. Rev. C **89**, (2014) 024307; Erratum Phys. Rev. C **89**, (2014) 059905.
[3] R. Julin et al., J. of Phys. G **43**, (2016) 024004.
[4] C. Müller-Gatermann *et al.*, Phys. Rev. C **97**, (2018) 024336.
[5] C. Fransen *et al.*, EPJ Web of Conferences **223**, (2019) 01016.
[6] J.E. Garcia-Ramos *et al.*, Phys. Rev. C **89**, (2014) 034313.
[7] G.D. Dracoulis et al., J. Phys. G: Nucl. Phys. **12**, (1986) L97.
[8] B. Cederwall et al., Z. Phys. **A337**, (1990) 283.

C.6 Search for a chiral to not chiral transition by a lifetime measurement of the I=10^+ state in ^{128}Cs with a plunger technique

A. Nałęcz-Jawecki[1], E. Grodner[1], J. Srebrny[2], M. Kowalczyk[2], Ch. Droste[3], A. Stolarz[3], J. Samorajczyk-Pyśk[2], G. Jaworski[2], M. Paluch-Ferszt[2], M. Palacz[2], T. Abraham[2] A. Tucholski[2], A. Kwiatkowska[3], O. Smolira[3], I. Skwira-Chalot[3], A. Podwysocka[3], J. Orliński[3], C. Fransen[4], C.-D. Lakenbrink[4], M. Beckers[4], F. Spee[4],

1) National Centre for Nuclear Research
2) Heavy Ion Laboratory, University of Warsaw, Warszawa, Poland
3) Faculty of Physics, University of Warsaw, Warszawa, Poland
4) Institut für Kernphysik, Universität zu Köln, Köln, Germany

Theory

Exploration of spontaneous time-reversal symmetry breaking in nuclear physics – widely known as nuclear chirality – is one of the main goals of the spectrometric group at HIL UW. Effects of the chirality phenomenon have been found in many odd-odd nuclei [1–5] and the ^{128}Cs isotope is considered the best studied one. However, the mechanisms underpinning the nuclear chirality are still not well established. Chiral doublets, as an effect of stable chiral symmetry breaking, may be recognized based on characteristic gamma selection rules observed in rotational bands formed of these doublets [6–8]. It is not yet clear how the stable chirality emerges with increasing nuclear spin. Such a process has been theoretically discussed [9] but not yet studied/observed experimentally.

^{128}Cs is perfect to trace the development of nuclear chirality with increasing nuclear rotation as it was proven to be non-chiral at low spin values and to be chiral at higher spin values. Recent results of magnetic moment measurements [10] have undoubtedly proven that at spin I=9$\hbar$ this isotope does not have a chiral nature while for spins I>13 nuclear chirality is clearly observed [8] and considered one of the best studied examples of this phenomenon. An experiment carried out at HIL UW in July 2022 aimed to verify the nature of the 10^+ state in ^{128}Cs – the first experimental approach in the search or a non-chiral to chiral collective transition in the atomic nucleus – by measuring its lifetime.

Experiment motivation

During Doppler Shift Attenuation experiments performed previously at HIL, reduced M1 and E2 transition probabilities have been measured in ^{128}Cs[8] B(M1) staggering in states 13$\hbar$<I<20$\hbar$ characteristic of nuclear chirality has been observed. If the staggering remains for $10\hbar \leq I \leq 13\hbar$, then the extrapolated lifetime of the 10^+ state should be around 100-200 ps. On the other hand, theoretical predictions for a non-chiral state suggest that the lifetime should be around 12 ps. Measuring the lifetime of the 10^+ state should be enought to verify its chiral or non-chiral nature. It could also be possible to measure the lifetimes of the 11^+ and 12^+ states, although due to the higher transition energy (349 keV, 273 keV) these lifetemes are expected to be shorter and thus harder to measure.

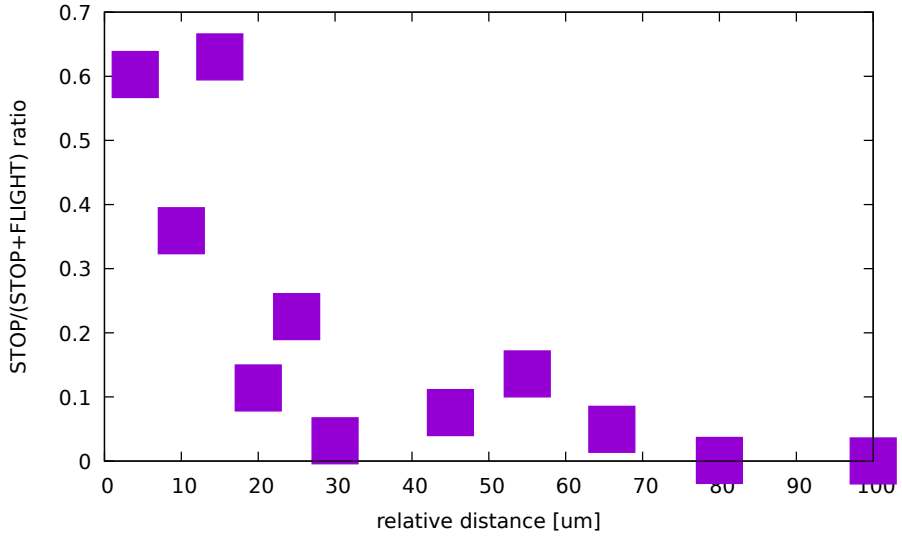

Figure 1: Brief analysis of the lifetime made during the experiment. With a higher distance from the target to the stopper (the diagram doesn't include the offset of around 15 um) we have a lower ratio of non-shifted (STOP) photons to all 143 keV photons detected. From data the lifetime was estimated to be around 17 ps with a very high uncertainty.

Experiment details

Measuring lifetimes the a range of 10-1000 ps is possible using the Recoil Distance Doppler Shift method (RDDS). For the experiment we used the ^{122}Sn(^{10}B,4n)^{128}Cs reaction at a beam energy of 54.2 MeV. The current varied from 2 to 8 nA (0.4 to 1.6 pnA), with 5 nA most of the time. 4 targets were made at HIL of about 0.35 mg/cm^2 ^{122}Sn on a 5 mg/cm^2 gold support. The plunger device was borrowed from the Institut fur Kernphysik, University of Koln.

15 HPGe detectors of the EAGLE setup were used in the unsual way. The low transition energy (143 keV) caused a low Doppler Shift energy – 0.6-0.7 keV, which is lower than the energy resolution of a HPGe – required the use of an additional LOAX germanium detector. The LOAX detector has better resolution ($\sim$0.7 keV) and higher efficiency at energies $<$200 keV. To maximize the Doppler Shift effect we placed the LOAX detector at as low an angle to the beam as possible, instead of the usual angle of 37° of the EAGLE setup. Due to the size of its dewar the lowest possible angle was 28°, which led to a 10% higher energy shift, but still 11% lower than at an angle near 0. Apart from the LOAX half of the EAGLE sphere with 15 HPGe detectors was used for $\gamma-\gamma$ coincidence measurements.

The experiment took place between 4-11.07.2022. After 2 days of dealing with beam problems, the 3 following days were used for 16 measurements at different plunger distances for 4h each. These measurements were meant to determine if the lifetime of the 10^+ state is closer to 10 or 200 ps. A quick analysis (see Fig. 1) showed that the lifetime is 17 ps with a large uncertainty. Therefore, the second part of the experiment was divided between 5 low distances (1-40 um +offset), 1 large distance ($>$500 um) and a measurement in which we flipped the target to measure an un-shifted 143 keV peak.

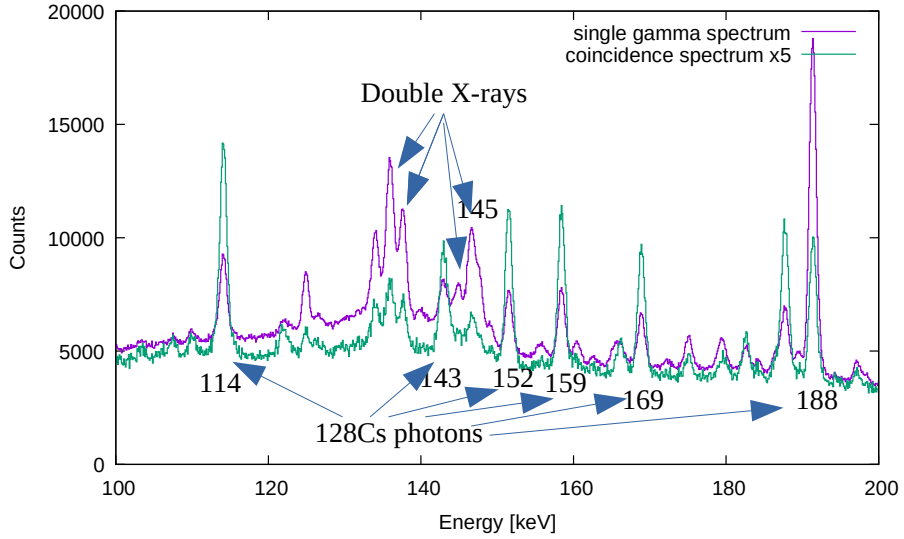

Figure 2: The most interesting range of the spectrum for the LOAX detector. The purple line denots the single-gamma spectrum, the green one the spectrum with any coincidence in any HPGe detector multiplied by a factor 5 for scaling. The 145 keV double X-ray peak is too close to our 143 keV energy of interest to let us analyse it. In coincidence it's highly surpressed, but we still can't see that 143 keV peak should be a double peak of FLIGHT and STOP photons. Only by a comparison to other distances we can tell anything about the STOP/(STOP+FLIGHT) rate.

Analysis

The analysis of the experiment turned out to be much more complex than it seemed before. The LOAX detector, the spectrum of which was the most important one, didn't have any X-ray shields, therefore the intensity of double X-rays was of the order of the 143 keV gammas. One of the double X-rays from gold, which was the material of the beam dump as well as the stopper and target support, is at 145 keV energy. Therefore, it intercepts widely with both stop and flight peaks of 143 keV. There has been developed a way to analyse the experiment anyway (see Fig. 2), but it needs a very good energy calibration, with an uncertainty at the level of 4-20 eV (at 143 keV). Some approaches have been applied, but the analysis is not yet finished.

Bibliography

[1] S. Mukhopadhyay *et al.*, Phys. Rev. Lett. **99** (2007) 172501.
[2] T. Marchlewski *et al.*, Acta Phys. Pol. B **11** (2018) 87.
[3] Wu Xiaoguang *et al.*, Plasma Science and Technology**14** (2012) 526.
[4] T. Marchlewski *et al.*, Acta Phys. Pol. B **46** (2015) 60-66.
[5] E. Grodner *et al.*, Phys. Rev. Lett. B **703** (2011) 46–50.
[6] P. Olbratowski *et al.*, Phys. Rev. Lett. **93** (2004) 052501.
[7] T. Koike *et al.*, Phys. Rev. Lett. **93** (2004) 172502.
[8] E. Grodner *et al.*, Phys. Rev. Lett. **97** (2006) 172501.
[9] P. Olbratowski *et al.*, Phys. Rev. Lett. **93** (2004) 052501.
[10] E. Grodner *et al.*, Phys. Rev. Lett. **120** (2018) 022502.
[11] T. Koike *et al.*, Phys. Rev. C **67** (2003) 044319.

C.7 Collective isovector quadrupole excitation of ^{142}Sm - Identification via a $\gamma - \gamma$-correlation measurement after ϵ/β^+ decay

T. Stetz[1], T. Abraham[2], U. Ahmed[1] G. Colucci[2], M.L. Cortes[1], K. Hadyńska-Klęk[2], G. Jaworski[2], R. Kern[1], M. Kisieliński[2], M. Komorowska[2], M. Kowalczyk[2], P.J. Napiorkowski[2], C. Nickel[1], M. Palacz[2], N. Pietralla[1], G. Rainovski[3], J. Samorajczyk-Pyśk[2], J. Srebrny[2], M. Stoyanova[3] A. Trzcińska[2], V. Werner[1], K. Wrzosek-Lipska[2], B. Zalewski[2], R. Zidarowa[1]

1) Institute for Nuclear Physics, Dept. of Physics, Technische Universität Darmstadt, Germany
2) Heavy Ion Laboratory, University of Warsaw, Warszawa, Poland
3) Sofia University "St. Kliment Ohridski", Sofia, Bulgaria

The 2_3^+ state of ^{142}Sm is a promising candidate for its one-quadrupole phonon mixed-symmetry state. In order to obtain the M1 strength of the $2_3^+ \rightarrow 2_1^+$ transition from a projectile Coulomb-excitation experiment at HIE-ISOLDE at CERN, a complementary β - decay experiment was performed at the Heavy Ion Laboratory in Warsaw with the intention of determining the multipole mixing ratio of the transition of interest.

Scientific motivation - nuclear valence-shell stabilization in N=80 isotones

The origin of quadrupole collectivity in most heavy open-shell nuclei is the attractive quadrupole-quadrupole interaction between valence protons and neutrons. This interaction results in a coherent mixing of collective quadrupole excitations of the proton and neutron subspaces. Geometrical models can describe this collective motion. The nucleus is considered as a homogeneous object with a certain shape which can vibrate or rotate [1]. This approach neglects the nucleonic degrees of freedom to a large extent.

A theoretical approach to the modeling of quadrupole-collective heavy nuclei which provides an attempt to bridge the calculation of nuclear properties from fundamental nucleon-nucleon interactions to the collective model is the interacting boson model (IBM) [2]. The IBM-1 describes the lowest-lying excitations in even-even nuclei, which are called full-symmetry states (FSSs). The IBM-2 [3], which distinguishes between proton and neutron bosons, predicts another class of states, the mixed-symmetry states (MSS). The proton and neutron motions of these states are partly out of phase. To quantify the degree of coherence of the proton-boson and neutron-boson contributions the F spin is introduced. The F spin is the analog of the isopsin for bosons. The F spin of FSSs, $F = F_{max} = (N_\pi + N_\nu)/2$ equals the maximum F spin, whereas MSSs occupy a lower value $F = F_{max} - 1$. MSSs represent a physics case in which the balance and interplay between the nuclear phenomena of collectivity, shell structure, and the isospin degrees of freedom can be studied. In addition, the quality of the F spin as a good quantum number can solely be probed by measuring the mixing between MSSs and FSSs.

According to the IBM-2 the lowest-lying MSS in vibrational nuclei is the $2^+_{1;ms}$ state. The most indicative experimental signature of the $2^+_{1;ms}$ state is a strong M1 transition strength to the full-symmetry 2_1^+ state. In contrast to isoscalar transitions between two FSSs with $\Delta F = 0$, the M1 strength of isovector transitions between MSSs and FSSs with $\Delta F = \pm 1$ is not suppressed. Available information on MSSs in the mass regions $A \approx 90$, 130 of vibrational nuclei has been summarized in a review article [4] and was recently

extended for the mass A ≈ 200 region [5–7]. The determination of the multipole-mixing ratio $\delta(2_i^+ \to 2_1^+)$ is indispensable for the identification of the $2^+_{1;\mathrm{ms}}$ state.

The study of MSSs of the N = 80 isotonic chain reveals an unsolved physics case. The ^{132}Te, ^{134}Xe and ^{136}Ba [8–10] nuclei form isolated $2^+_{1;\mathrm{ms}}$ states. In contrast, the ^{138}Ce $2^+_{1;\mathrm{ms}}$ strongly mixes with a nearby full-symmetry 2^+ state [11]. This dramatic change in the properties of MSSs when only two protons are added to the system, suggests that the strength concentration of collective-isovector excitations in the valence shell reflects the underlying single-particle structure through a mechanism dubbed shell stabilization [11]. The observed mixing in ^{138}Ce is attributed to the lack of shell stabilization at the $\pi(g_{7/2})$ sub-shell closure. All these experimental data lead to the conclusion that a direct experimental confirmation of the mechanism of shell stabilization in the N = 80 isotones, which is a phenomenon related to the proton structure, should be sought for by identifying the MSSs in radioactive ^{140}Nd and ^{142}Sm.

The properties of MSSs of stable N = 80 isotones were theoretically studied with the quasiparticle-phonon model (QPM) [12] and the large-scale shell model (SM) [13]. Both models have demonstrated that the splitting of the M1 strength in ^{138}Ce is a genuine shell effect caused by the specific shell structure and the pairing correlations [12, 13]. The theoretical predictions of the degree of mixing [13] and the experimentally observed mixing [14] of the MSS differ considerably for ^{140}Nd, while they are lacking for ^{142}Sm. To bring full clarity to the evolution of the F-spin mixing in N = 80 isotones, a measurement of the multipole-mixing ratio of the $2^+_3 \to 2^+_1$ transition is essential.

A projectile Coulomb-excitation (CoulEx) experiment was performed at HIE-ISOLDE at CERN, with ^{140}Nd and ^{142}Sm as radioactive ion beams (RIB) [15]. Due to the naturally low statistics of RIBs the determination of the multipole mixing ratio of the $2^+_3 \to 2^+_1$ transition is not feasible; but there are strong indications that the 2^+_3 state is the most promising candidate for the MSS of both isotones. The necessary multipole mixing ratio of ^{140}Nd was determined by a $\gamma-\gamma$ angular-correlation measurement followed a ϵ/β-decay [14]. For ^{142}Sm, the multipole mixing ratio of the $2^+_3 \to 2^+_1$ transition is hoped to be obtained by the evaluation of the present experiment, performed at the Heavy Ion Laboratory in Warsaw.

γ-γ-correlation measurement after ϵ/β^+ decay

The experiment was conducted at the Warsaw Cyclotron at the Heavy Ion Laboratory in Warsaw, Poland. The state of interest is the 2^+_3 of ^{142}Sm at 2140 keV. The population of this state was achieved via the ^{114}Cd(^{32}S,4n)^{142}Gd fusion evaporation reaction followed by two β-decays. A beam of ^{32}S ions impinging on a 4 mg/cm^2 ^{114}Cd target formed the compound nucleus ^{142}Gd ($T_{1/2} \approx 70$ s), which is the grand-mother nucleus of ^{142}Sm. The fusion evaporation reaction was followed by a ϵ/β^+-decay to a short lived isomer of ^{142}Eu ($T_{1/2} \approx 2.4$ s). The ^{32}S beam at 144 MeV was periodically stopped in a cycle of 150 s in order to obtain data in the off-beam periods over a beamtime of 8 days. The high total efficiency of the EAGLE array was ideally suited for the γ-ray detection.

Ongoing analysis and outlook

The multipole mixing ratio of a transition can be determined by its intensity depending on the angle to another coincident transition. The desired $2^+_3 \to 2^+_1$ transition at 1287 keV can be observed in a coincidence spectrum of the 70° angular group with a condition set on the ground-state transition of the 2^+_1 state. The intensities of the $2^+_3 \to 2^+_1$ transition,

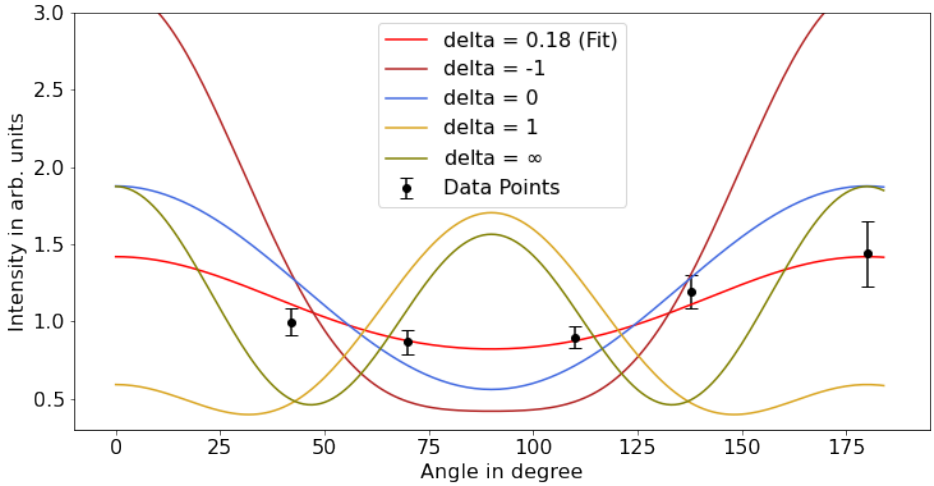

Figure 1: The intensities of the $2_3^+ \rightarrow 2_1^+$ transition for the five angular groups is shown. Using two different fit algorithms, an angular correlation function depending on the angle θ and the multipole mixing ratio δ was adapted to the data. Also shown is the course of angular correlation functions with fixed values of δ.

with the $2_1^+ \rightarrow 0_1^+$ transition used as a quatization axis, can be seen in Fig. 1. An angular correlation function $W(\theta, \delta)$ has been fitted to the data using two different algorithms. The data used for the analysis shown in Fig. 1 contains about one third of the total recorded data. Furthermore, not all detector pairs have been included in the analysis so far.

The analysis of the multipole mixing ratio is currently still in progress. By including the full dataset in the analysis the uncertainty of the intensities of the $2_3^+ \rightarrow 2_1^+$ transition in the different angular groups is expected to decrease significantly. Therefore, a precise determination of the multipole mixing ratio is expected. This is the last missing quantity in obtaining the M1 transition strength of the $2_3^+ \rightarrow 2_1^+$ transition of ^{142}Sm, conclusively to identify its MSS state. This will shed further light on the puzzle of the nuclear valence-shell stabilization for the N = 80 isotonic chain. The data analysis is expected to be completed during 2023. Final results will then be prepared for publication.

Bibliography

[1] A. Bohr and B. Mottelson, **Benjamin, Reading, MA**, vol II (1975).
[2] A. Arima, T. Ohtsuka, F. Iachello, and I. Talmi, Phys. Lett. B **66** (1977) 205-208.
[3] F. Iachello, Phys. Rev. Lett. **53** (1984) 1427-1429.
[4] N. Pietralla *et al.*, Phys. Rev. C **64** (2001) 031301.
[5] D. Kocheva *et al.*, Phys. Rev. C **93** (2016) 011303.
[6] R. Stegmann *et al.* Phys. Lett. B **770** (2017) 77-82.
[7] R. Kern *et al.* Phys. Rev. C **99** (2019) 011303.
[8] M. Danchev *et al.* Phys. Rev. C **84** (2011) 061306.
[9] T. Ahn *et al.* Phys. Lett. B **679** (2009) 19-24.
[10] N. Pietralla *et al.*, Phys. Rev. C **58** (1998) 796-800.
[11] G. Rainovski, Phys. Rev. Lett. **96** (2006) 122501.
[12] N. Lo Iudice, Ch. Stoyanov, and D. Tarpanov, Phys. Rev. C **77** (2008) 044310.
[13] K. Sieja, *et al.*, Phys. Rev. C **80** (2009) 054311.
[14] E. Williams *et al.*, Phys. Rev. C **80** (2009) 054309.
[15] R. Kern *et al.*,EPJ Web Conf., **194** (2018) 03003.

C.8 Effects of deuteron breakup and nucleon-transfer reactions on d+^{11}B elastic scattering

A. Amar[1], Sh. Hamada[1], K. Rusek[2]

1) Faculty of Science, Tanta University, Tanta, Egipt,
2) Heavy Ion Laboratory, University of Warsaw, Warszawa, Poland

Various processes induced by deuterons incident on ^{11}B: elastic scattering, d-breakup, excitation of the target nucleus and n- and p- transfer reactions were studied by means of the continuum-discretized coupled channel (CDCC) and coupled reaction channel (CRC) methods. The influence of the inelastic processes on the elastic scattering was estimated.

It was found that CDCC calculations, taking into account the loosely bound structure of the deuteron, are able to describe the angular distribution of the elastic scattering at forward scattering angles without any adjustable parameters. At backward scattering angles inelastic processes like target excitation and nucleon-transfer reactions significantly modify the CDCC result. Moreover, at these angles, the imaginary parts of the input nucleon-target OM potentials also play an important role. Thus, this kind of study requires a precise knowledge of the nucleon-target interactions at the required energy. For light targets and low energies the existing global nucleon-target OM potentials do not provide precise enough predictions.

Apart from breakup, two inelastic processes, target excitation and the neutron pickup reaction, were found significantly to affect the elastic scattering mostly, at backward angles. An effect from neutron stripping was also encountered, while the virtual processes due to proton-transfer reactions contributed negligibly to the elastic scattering.

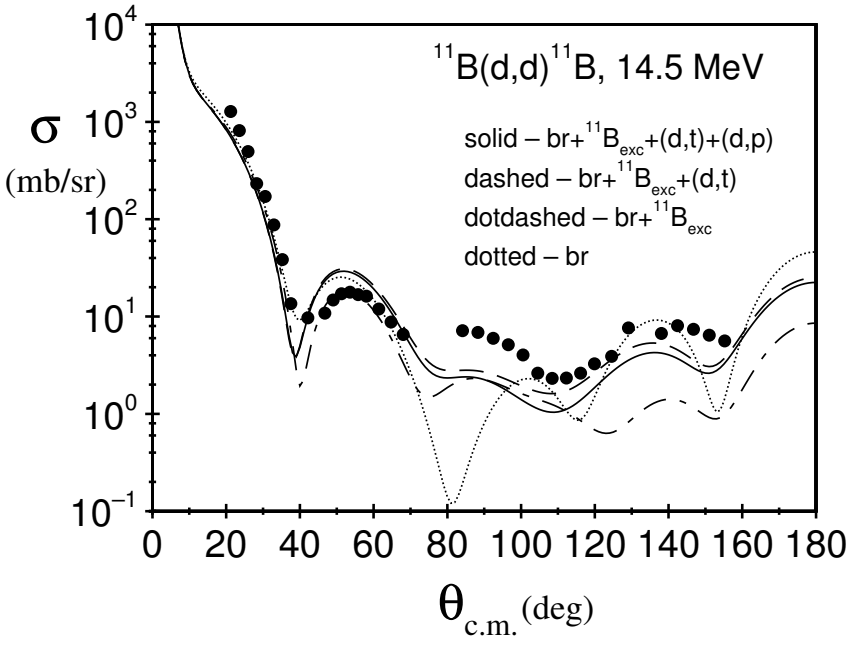

Figure 1: Angular distribution of the differential cross section for elastic scattering of d + ^{11}B compared to the results of model calculations. Experimental data are taken from M. Nassurlla et al., Nucl. Phys. A 1023, 122448 (2022).

Some other observations may be summarized as follows. Breakup of the deuteron reduces the elastic scattering differential cross section at backward angles in comparison with the OM calculations employing a single-folding potential. The contribution related to the quadrupole moment of the deuteron ground state is negligibly small in comparison with the contribution generated by couplings to the states from the $n-p$ continuum. The effect of target excitation on the elastic scattering cross section is similar in character to that of the breakup. However, coupling to the neutron-transfer reactions acts in the opposite way, increasing the elastic scattering cross section at backward scattering angles, thus reducing the difference between the data and the calculations.

C.9 Light Ni isotopes. Search for collective features in low energy excitations

L. Próchniak
Heavy Ion Laboratory, University of Warsaw, Warszawa, Poland

The mean-field theory based on the HFB method is a tool used extensively to describe various properties of nuclei with a wide range of numbers of protons and neutrons. Collective excitations connected to changes of the nuclear mass distribution (in other words a deformation) can be treated within two main approaches: the Generator Coordinate Method or the Adiabatic Time Dependent HFB theory. The latter leads to a collective Hamiltonian dependent on a number of properly chosen variables. The most common excitations in even-even nuclei are connected with changes of the quadrupole deformation. In such a case the collective variables are the well known (β, γ) deformation parameters together with the Euler angles which describe the mutual orientation of the intrinsic and the laboratory system, while the Hamiltonian is often called the General Bohr Hamiltonian [1]. These approaches with various microscopic inputs (Skyrme, Gogny interactions, Relativistic MF) have been applied successfully in many regions of the nuclear chart. However, there are some areas where the mean-field theory fails to describe nuclear properties accurately, e.g. in the vicinity of magic nuclei. Other, more unexpected failures were found elsewhere e.g. in proton-rich Os and W isotopes with quite a large number of valence nucleons. Moreover, light nuclei with mass number below around 70 seem to offer a poor field for this theory, although some successes were obtained even for ^{24}Mg [2].

Here I present the first theoretical results for ^{58,60,62}Ni obtained within the GBH approach with two versions of the microscopic energy functional, UNEDF0 and UNEDF1 [4]. The ^{58,60,62}Ni isotopes are rather light from the mean-field theory perspective and very close to the doubly magic ^{56}Ni. The reason for such a study is twofold. First, there is some interest in looking for an emergence of collectivity in Ni isotopes from the experimental side: new data have appeared, e.g. [3], and new experiments are being planned to study EM properties in more details using the Coulomb excitation method. Second, these isotopes offer a promising area to study the limitations of the mean-field approach and to search for possible extensions towards coupling with single particle degrees of freedom.

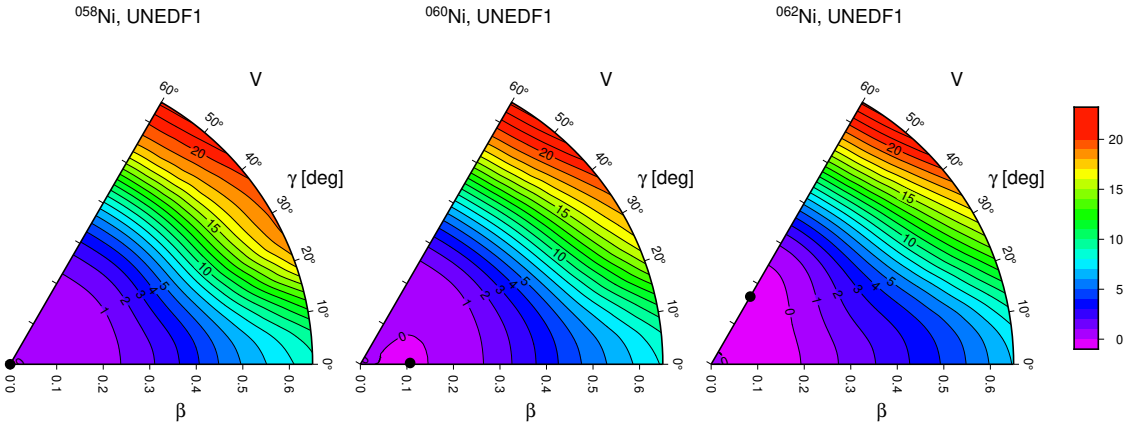

Figure 1: Theoretical potential energy relative to a spherical shape calculated with the UNEDF1 functional for ^{58,60,62}Ni.

Fig. 1 shows the collective potential energy calculated using the UNEDF1 functional. A common feature for the three isotopes is a weak dependence of the energy on the γ variable and a significant flatness around a spherical shape, e.g. the minimum in ^{60}Ni seen on the prolate axis is only around 40 keV. Only for ^{62}Ni is the deformation a bit more pronounced, with a shallow oblate minimum of depth 450 keV. The UNEDF0 functional gives similar landscapes overall but with no traces of an emerging deformation.

Several chosen levels, both experimental and theoretical, are shown in Fig. 2. They comprise the three lowest levels from the yrast band and the 2_2^+ and 0_2^+ states (tentative bandheads of the quasi-γ and quasi-β bands). One can see that the UNDEF1 functional gives results that are closer to the experimental ones. Generally, the agreement with the experimental data is rather good even if some details of the 'two-phonon' triplet are not reproduced exactly. It is worth mentioning that the theory does not contain any parameters fitted to experimental spectroscopic data.

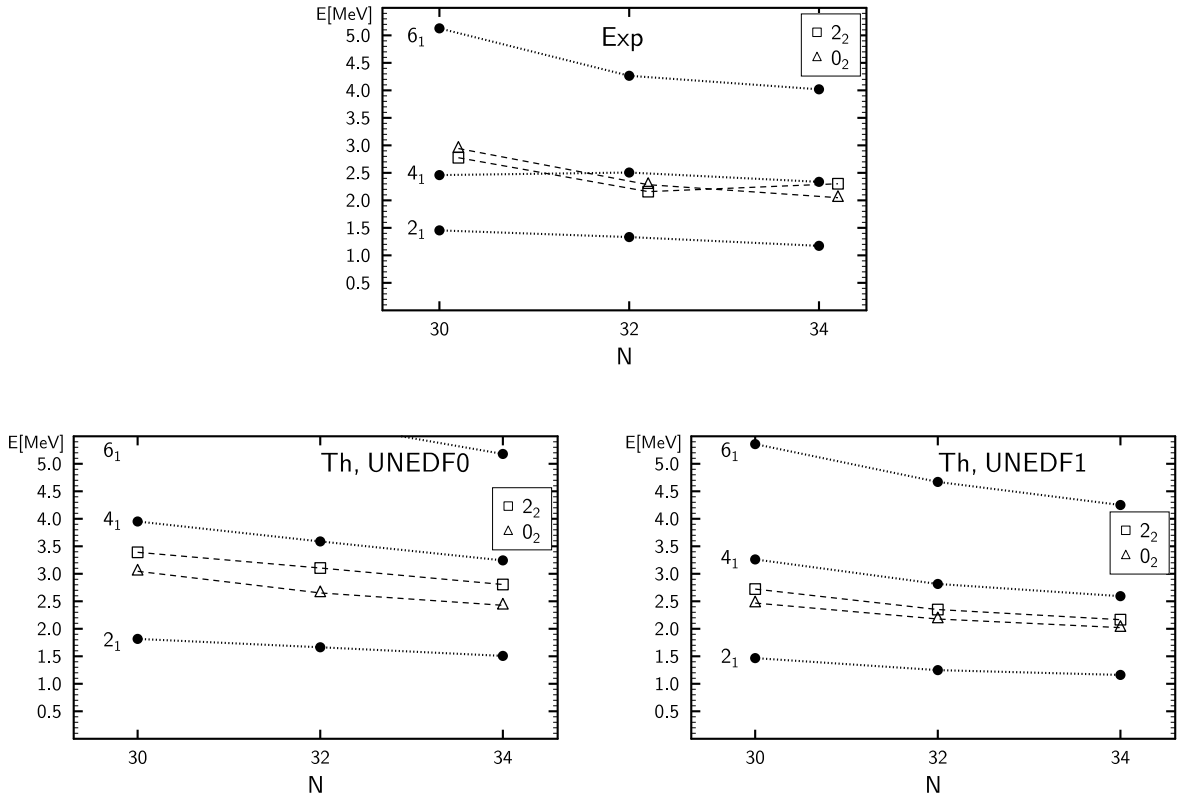

Figure 2: Selected (2_1^+, 4_1^+, 6_1^+, 0_2^+, 2_2^+) experimental [5] and theoretical levels in ^{58,60,62}Ni.

The applied theory also provides detailed information on the matrix elements of the E2 operator connected with changes in the charge distribution. These data can be compared with experimental transition probabilities and spectroscopic moments which are the crucial quantities for an investigation of collective properties. Here I present in Fig. 3 only the B(E2) values for the two lowest transitions in the yrast band: $2_1^+ \to 0_1^+$ and $4_1^+ \to 2_1^+$. Signs of collectivity of the 2_1^+ states can be deduced from experimental values of around 10 W.u. The second transition $4_1^+ \to 2_1^+$ hints at an important change of properties as neutron number increases; unfortunately there are no experimental data on this transition in ^{60}Ni. On the theoretical side, the B(E2)s of the $2_1^+ \to 0_1^+$ transition are reproduced quite well by both functionals. In the case of the $4_1^+ \to 2_1^+$ transition the theory completely fails

for ^{58}Ni but gives a reasonable prediction for ^{62}Ni (with a caveat: a significant experimental uncertainty).

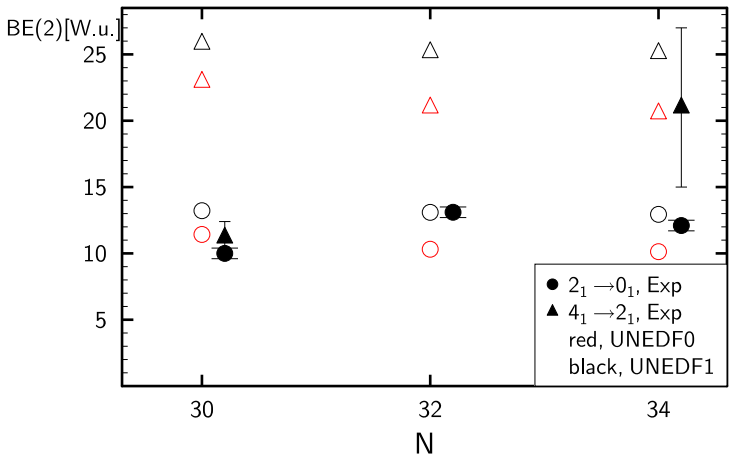

Figure 3: Experimental [5] and theoretical B(E2) values for $2_1^+ \to 0_1^+$ and $4_1^+ \to 2_1^+$ transitions in ^{58,60,62}Ni.

Much remains to be done in order to draw clear-cut conclusions on the emergence of collectivity in light Ni isotopes and the applicability of the mean-field approach in this region. First of all, a detailed analysis of the whole low energy spectrum including EM transitions for which experimental data exist. Such an analysis could indicate which states are of collective character and for which single-particle properties must be taken into account. In addition, research should be extended to heavier Ni isotopes, which would provide a wider area for the study of the evolution of nuclear properties.

Bibliography

[1] L. Próchniak, S.G. Rohoziński, J. Phys. G: Nucl. Phys. **36** (2009) 123101.
[2] S. Peru, M. Martini, Eur. Phys. J. A **88** (2014) 88; J. M. Yao, M. Bender, P.-H. Heenen, Phys. Rev. C **91** (2015) 024301.
[3] L. J. Evitts et al, Phys. Rev. C **99** (2019) 024306.
[4] M. Kortelainen et al., Phys. Rev. C **82** (2010) 024313; M. Kortelainen et al., Phys. Rev. C **85** (2010) 024304.
[5] Data from the NNDC database, revision as of March 2023.

Part D

Appendices

Part D
Appendices

D.1 List of experiments performed at HIL in 2022

A list of the experiments performed in 2022 is presented in the following pages. The following acronyms of institution names are used in the list:

- HIL — Heavy Ion Laboratory, University of Warsaw, Warszawa, Poland;
- CEA UP-S Gif-sur-Yvette — IRFU, CEA, Université Paris-Saclay, Gif-sur-Yvette, France;
- FP UW — Faculty of Physics, University of Warsaw, Warszawa, Poland;
- FS TU Tanta — Faculty of Science, Tanta University, Tanta, Egypt;
- IKP TU Darmstadt — IKP, Technical University Darmstadt, Darmstadt, Germany;
- ILL Grenoble — Institut Laue Langevin, Grenoble, France;
- INFN SF Firenze —INFN Sezione di Firenze, Firenze, Italy;
- INFN SM Milano — INFN. Sezione di Milano, Milano, Italy;
- INP PAN Kraków — Institute of Nuclear Physics PAN, Kraków, Poland;
- INP UK Cologne —Institute for Nuclear Physics, University of Cologne, Germany;
- NCNR Świerk — National Centre for Nuclear Research, Otwock, Poland;
- SU Sofia— Sofia University, Sofia, Bulgaria;
- U Guelph — University of Guelph, Guelph, Canada;
- UM Milano — University of Milan, Milano, Italy;
- US Surrey — Department of Physics, University of Surrey, Guildford, UK;

For each experiment the following information is provided: ion, energy, setup/beam line information, date, proposal number, subject, spokespersons and institutions.

$^{32}S^{5+}$ — 86 MeV — ICARE 15.03 – 18.03

HIL00 — Test of SiC detectors (E.Piasecki, A. Trzcińska)

HIL, FP UW

$^{32}S^{5+}$ — 86 MeV, 93 MeV — EAGLE 20.03 – 05.04

HIL093 — Probing shapes and structures in ^{100}Ru via Coulomb excitation. (P.Garrett, K.Wrzosek-Lipska, M.Rocchini, M. Zielińska)

U Guelph, HIL, CEA UP-S Gif-sur-Yvette, US Surrey, , FP UW, ILL Grenoble, INP PAN Kraków, INFN SF Firenze, INP UK Cologne

$^{14}N^{2+}$ — 34 MeV — EAGLE 06.04 - 13.04

HIL094 — Electromagnetic structure of low-lying states in ^{110}Cd – complementary Coulomb excitation measurements with a ^{14}N beam. (K.Wrzosek-Lipska, P.Garrett, M. Zielińska)

HIL, U Guelph, CEA UP-S Gif-sur-Yvette, FP UW, ILL Grenoble, INP PAN Kraków, INFN SF Firenze, INFN SM Milano, UM Milano, US Surrey

$^{13}N^{3+}$ — 91 MeV — Exposure station 30.05 - 03.06

HIL103 — Semiconductor detectors for low-energy heavy ions. (K. Krutul)

HIL, FP UW

$^{32}S^{7+}$ — 170 MeV — EAGLE 20.06 - 30.06

HIL087 — Lifetime studies in neutron-deficient ^{172}Pt using the RDDS technique EAGLE + Cologne Plunger (C. Fransen, C. Müller-Gatermann)

IKP TU Darmstad, SU Sofia, HIL

$^{10}B^{2+}$ — 54 MeV, 58 MeV — EAGLE 04.07 - 16.07

HIL102 — Search for chiral to not chiral transition by lifetime measurement of I=10+ state in ^{128}Cs with a plunger technique. (A. Nałęcz-Jawecki)

NCNR Świerk, HIL, FP UW, INP UK Cologne, FS TU Tanta

D.2 Degrees and theses completed in 2022 or in progress

D.2.1 PhD theses of students affiliated to HIL, of HIL staff members, and supervised by HIL staff

Mateusz Filipek, Faculty of Physics, University of Warsaw
Wpływ promieniowania α, β, i γ na przeżywalność komórek nowotworowych gruczołu krokowego PC3 i DU145
Effect of α, β, and γ radiation on the survival of PC3 and DU145 prostate cancer cells
Supervisors: dr hab. Z. Szefliński. Expected completion time: 2023.

Michalina Komorowska, Faculty of Physics, University of Warsaw
Korelacje oktupolowe w jądrach atomowych z obszaru $N \sim 88$
Pear-shaped Nuclei in the $N \sim 88$ region
Supervisors: dr hab. L. Próchniak, dr P. Napiorkowski, dr W. Korten, dr M. Zielińska. (program cotutelle) Expected completion time: 2024.

Adam Nałęcz-Jawecki, Graduate School of Physics and Chemistry, National Centre for Nuclear Research, Otwock, Poland
Search for nuclear chirality in low excitation energy states of odd-odd isotopes
Supervisors: dr hab. E. Grodner, dr J. Srebrny. Expected completion time: 2025.

Marcin Pietrzak, Faculty of Physics, University of Warsaw
Nanodosimetric characteristics of a carbon ion beam - experiments and Monte Carlo simulations
Supervisor: dr hab. Z. Szefliński. Expected completion time: 2023.

Łukasz Standyło, National Centre for Nuclear Research, Świerk
Badanie mechanizmu wychwytu i termalizacji strumieni jonów i atomów wprowadzonych do plazmy wytwarzanej metodą elektronowego rezonansu cyklotronowego
Investigation of capture and thermalization mechanisms of ions and atomic beams injected into plasma produced by the electron cyclotron resonance
Supervisor: prof. dr hab. K. Rusek, dr K. Sudlitz. Expected completion time: 2023.

Grzegorz Wałpuski, Faculty of Biology, University of Warsaw
Badanie wpływu promieniowania jonizującego na procesy fizjologiczne ujednokomórkowych glonów z gromady Cyanidiophyceae
Study of the influence of ionizing radiation on physiological processes in single-celled algae from the class Cyanidiophyceae
Supervisors: dr hab. Z. Szefliński. Expected completion time: 2025.

Bogumił Zalewski, Heavy Ion Laboratory, University of Warsaw
Study of the ^{6}He+d interaction
Supervisor: prof. dr hab. K. Rusek. Expected completion time: 2023.

D.2.2 MSc and BSc theses supervised by HIL staff members

Klaudia Koszel, Faculty of Physics, University of Warsaw
Wytwarzanie i kontrola jakości amoniaku znakowanego izotopem ^{13}N
Production and quality control of ammonia labeled with ^{13}N
Supervisor: dr hab. K. Kilian. Expected completion time: 2023.

Grzegorz Wałpuski, Faculty of Biology, University of Warsaw
Wpływ promieniowania jonizującego na procesy fizjologiczne u ekstremofilnej algi Cyanidioschyzon merolae
The influence of ionizing radiationon on physiological processes in the extremophilic alga Cyanidioschyzon merolae
Supervisors: dr M. Asztemborska, dr hab. Z. Szefliński. Thesis completed in July 2022.

Łukasz Łysakowski, Faculty of Physics, University of Warsaw
Badanie korelacji kątowych kwantów γ pochodzących z rozpadu ^{152}Eu
Investigation of angular correlation of gamma rays from radioactive decay of Eu-152
Supervisors: dr J. Samorajczyk-Pyśk, dr G. Jaworski. Thesis completed in December 2022.

Iwona Piętka, Faculty of Physics, University of Warsaw
Badanie struktury elektromagnetycznej jądra ^{110}Cd metodą wzbudzeń kulombowskich
Study of the electromagnetic structure of ^{110}Cd using the Coulomb excitation method
Supervisor: dr K. Wrzosek-Lipska. Expected completion time: 2023.

Justyna Sykuła, Faculty of Physics, University of Warsaw
Badanie zanieczyszczeń radionuklidowych w procesie produkcji radiofarmaceutyków znakowanych ^{18}F
Determination of radionuclidic impurities in the production of ^{18}F labelled radiopharmaceuticals
Supervisor: dr hab. K. Kilian. Expected completion time: 2023.

D.3 Publications

D.3.1 Publications in Web of Knowledge and/or Scopus data bases

[1] S.V. Artemov, R. Yarmukhamedov, N. Burtebayev, B.K. Karakozov, F.K. Ergashev, M. Nassurlla, S.B. Igamov, N. Amangeldi, A. Morzabayev, J. Burtebayeva, V.S. Zhdanov, G. Yergaliuly, E. Piasecki, K. Rusek, S.B. Sakuta, A. Demyanova, O.R. Tojiboev, A. Trzcińska, A. Sabidolda, R. Khojayev, K.I. Tursunmakhatov, M. Nassurlla, M. Wolińska-Cichocka, T.K. Sadykov, and N. Saduyev. Asymptotic normalization coefficient for ^{12}C + p$\rightarrow$ ^{13}N from the ^{12}C (^{10}B , ^{9}Be) ^{13}N reaction and the ^{12}C (p, γ) ^{13}N astrophysical s factor. *Eur. Phys. J. A*, 58(2), 2022.

[2] C. Ciampi, S. Piantelli, G. Casini, G. Pasquali, J. Quicray, L. Baldesi, S. Barlini, B. Borderie, R. Bougault, A. Camaiani, A. Chbihi, D. Dell'Aquila, M. Cicerchia, J.A. Dueñas, Q. Fable, D. Fabris, J.D. Frankland, C. Frosin, T. Génard, F. Gramegna, D. Gruyer, M. Henri, B. Hong, S. Kim, A. Kordyasz, T. Kozik, M.J. Kweon, J. Lemarié, N. Le Neindre, I. Lombardo, O. Lopez, T. Marchi, S.H. Nam, A. Ordine, P. Ottanelli, J. Park, J.H. Park, M. Pârlog, G. Poggi, A. Rebillard-Soulié, A.A. Stefanini, S. Upadhyaya, S. Valdré, G. Verde, E. Vient, M. Vigilante, and INDRA-FAZIA Collaboration. First results from the indra-fazia apparatus on isospin diffusion in ni ^{58,64}Ni + ^{58,64}Ni systems at fermi energies. *Phys. Rev. C*, 106(2), 2022.

[3] A.A. Ciemny, C. Mazzocchi, W. Dominik, A. Fijałkowska, J. Hooker, C. Hunt, H. Jayatissa, Ł. Janiak, G. Kamiński, E. Koshchiy, M. Pfützner, M. Pomorski, B. Roeder, G.V. Rogachev, A. Saastamoinen, S. Sharma, N. Sokołowska, W. Satuła, and J. Singh. β -delayed charged-particle decay of ^{22,23}Si. *Phys. Rev. C*, 106(1), 2022.

[4] M. Del Fabbro, A.M. Stefanini, G. Montagnoli, G. Colucci, P. Čolović, L. Corradi, E. Fioretto, F. Galtarossa, A. Goasduff, J. Grebosz, M. Heine, G. Jaworski, M. Mazzocco, T. Mijatović, S. Szilner, M. Bajzek, D. Brugnara, M. Siciliano, and I. Zanon. Fusion hindrance and pauli blocking in ^{58}Ni + ^{64}Ni. *Nuovo Cimento Soc. Ital. Fis. C*, 45(5), 2022.

[5] F.Kh. Ergashev, S.V. Artemov, O.R. Tojiboev, A.A. Karakhodzhaev, K. Rusek, A. Trzcińska, M. Wolińska-Cichocka, E.Piasecki, N. Burtebayev, S.B. Sakuta, M.N.M. Nassurlla, and R.F. Rumi. Asymptotic normalization coefficients for the ^{17}F $\rightarrow$ ^{16}O + p configuration from the ^{16}O(^{10}B, ^{9}Be)^{17}F reaction and estimation of the ^{16}O(p, γ)^{17}F astrophysical s-factor. *Acta. Phys. Pol. B*, 53(9), 2022.

[6] P.E. Garrett, M. Zielińska, A. Bergmaier, T.R. Rodríguez, D. Kalaydjieva, M. Siciliano, H. Bidaman, V. Bildstein, C. Burbadge, A.D. Varela, D.T. Doherty, T. Faestermann, K. Hadyńska-Klęk, R. Hertenberger, N. Keeley, A. Laffoley, A.D. MacLean, M. Mahgoub, A.J. Radich, M. Rocchini, P. Spagnoletti, S. Triambak, M. Vandebrouck, and K. Wrzosek-Lipska. Coulomb excitation of ^{102}Ru with ^{12}C and ^{16}O. *Phys. Rev. C*, 106(6), 2022.

[7] T.J. Gray, J.M. Allmond, R.V.F. Janssens, W. Korten, A.E. Stuchbery, J.L. Wood, A.D. Ayangeakaa, S. Bottoni, B.M. Bucher, C.M. Campbell, M.P. Carpenter, H.L. Crawford, H. David, D.T. Doherty, P. Fallon, M.T. Febbraro, A. Galindo-Uribarri, C.J. Gross, M. Komorowska, F.G. Kondev, T. Lauritsen, A.O. Macchiavelli, P. Napiorkowsi, E. Padilla-Rodal, S.D. Pain, W. Reviol, D.G. Sarantites, G. Savard, D. Seweryniak, C.Y. Wu, C.-H. Yu, and S. Zhu. E2 rotational invariants of 0_1^+ and 2_1^+ states for ^{106}Cd: The emergence of collective rotation. *Phys. Lett. B and High-Energy Physics*, 834, 2022.

[8] E. Grodner, M. Kowalczyk, M. Kisieliński, J. Srebrny, L. Próchniak, C. Droste, S.G. Rohoziński, Q.B. Chen, M. Ionescu-Bujor, C.A. Ur, F. Recchia, J. Meng, S.Q. Zhang, P.W. Zhao, G. Georgiev, R. Lozeva, E. Fiori, S. Aydin, and A. Nałęcz-Jawecki. Examination of nuclear chirality with a magnetic moment measurement of the i=9 isomeric state in ^{128}Cs. *Phys. Rev. C*, 106(1), 2022.

[9] N. Keeley, K.W. Kemper, and K. Rusek. Compatibility of the asymptotic normalization coefficient for the ^{14}C$\rightarrow$ ^{13}B+p overlap extracted from the ^{14}C(^{11}B, ^{12}C)^{13}B reaction with ^{14}C(d, ^{3}He)^{13}B data.

Phys. Rev. C, 106(1), 2022.

[10] G.G. Kiss, A. Vitéz-Sveiczer, Y. Saito, A. Tarifeño-Saldivia, M. Pallas, J.L. Tain, I. Dillmann, J. Agramunt, A. Algora, C. Domingo-Pardo, A. Estrade, C. Appleton, J.M. Allmond, P. Aguilera, H. Baba, N.T. Brewer, C. Bruno, R. Caballero-Folch, F. Calvino, P.J. Coleman-Smith, G. Cortes, T. Davinson, N. Fukuda, Z. Ge, S. Go, C.J. Griffin, R.K. Grzywacz, O. Hall, A. Horváth, J. Ha, L.J. Harkness-Brennan, T. Isobe, D. Kahl, T.T. King, A. Korgul, S. Kovács, R. Krücken, S. Kubono, M. Labiche, J. Liu, J. Liang, M. Madurga, K. Miernik, F. Molina, A.I. Morales, M.R. Mumpower, E. Nacher, A. Navarro, N. Nepal, S. Nishimura, M. Piersa-Siłkowska, V. Phong, B.C. Rasco, B. Rubio, K.P. Rykaczewski, J. Romero-Barrientos, H. Sakurai, L. Sexton, Y. Shimizu, M. Singh, T. Sprouse, T. Sumikama, R. Surman, H. Suzuki, T.N. Szegedi, H. Takeda, A. Tolosa, K. Wang, M. Wolińska-Cichocka, P. Woods, R. Yokoyama, and Z. Xu. Measuring the β-decay properties of neutron-rich exotic Pm, Sm, Eu, and Gd isotopes to constrain the nucleosynthesis yields in the rare-earth region. *Astrophys. J.*, 936(2), 2022.

[11] K.Z. Krutul-Bitowska, P.J. Napiorkowski, K. Hadyńska-Klęk, P. Horodek, M. Komorowska, A. Olejniczak, M. Paluch-Ferszt, K. Siemek, Z. Szefliński, M. Wróbel, and K. Wrzosek-Lipska. Radiation resistance studies of pin diode detectors irradiated with heavy ions. *Acta. Phys. Pol. A*, 142(6):783–788, 2022.

[12] X. Liu, B. Cederwall, C. Qi, R.A. Wyss, Ö. Aktas, A. Ertoprak, W. Zhang, E. Clément, G. De France, D. Ralet, A. Gadea, A. Goasduff, G. Jaworski, I. Kuti, B.M. Nyakó, J. Nyberg, M. Palacz, R. Wadsworth, J.J. Valiente-Dobón, H. Al-Azri, A. Ataç Nyberg, T. Bäck, G. De Angelis, M. Doncel, J. Dudouet, A. Gottardo, M. Jurado, J. Ljungvall, D. Mengoni, D.R. Napoli, C.M. Petrache, D. Sohler, J. Timár, D. Barrientos, P. Bednarczyk, G. Benzoni, B. Birkenbach, A.J. Boston, H.C. Boston, I. Burrows, L. Charles, M. Ciemala, F.C.L. Crespi, D.M. Cullen, P. Désesquelles, C. Domingo-Pardo, J. Eberth, N. Erduran, S. Ertürk, V. González, J. Goupil, H. Hess, T. Huyuk, A. Jungclaus, W. Korten, A. Lemasson, S. Leoni, A. Maj, R. Menegazzo, B. Million, R.M. Perez-Vidal, Z. Podolyàk, A. Pullia, F. Recchia, P. Reiter, F. Saillant, M.D. Salsac, E. Sanchis, J. Simpson, O. Stezowski, C. Theisen, and M. Zielińska. Evidence for spherical-oblate shape coexistence in ^{87}Tc. *Phys. Rev. C*, 106(3), 2022.

[13] B.F. Lv, C.M. Petrache, R. Budaca, A. Astier, K.K. Zheng, P. Greenlees, H. Badran, T. Calverley, D.M. Cox, T. Grahn, J. Hilton, R. Julin, S. Juutinen, J. Konki, J. Pakarinen, P. Papadakis, J. Partanen, P. Rahkila, P. Ruotsalainen, M. Sandzelius, J. Saren, C. Scholey, J. Sorri, S. Stolze, J. Uusitalo, B. Cederwall, A. Ertoprak, H. Liu, S. Guo, J.G. Wang, H.J. Ong, X.H. Zhou, Z.Y. Sun, I. Kuti, J. Timár, A. Tucholski, J. Srebrny, and C. Andreoiu. Experimental evidence for transverse wobbling bands in ^{136}Nd. *Phys. Rev. C*, 105(3), 2022.

[14] B.F. Lv, C.M. Petrache, E.A. Lawrie, S. Guo, A. Astier, K.K. Zheng, H.J. Ong, J.G. Wang, X.H. Zhou, Z.Y. Sun, P.T. Greenlees, H. Badran, T. Calverley, D.M. Cox, T. Grahn, J. Hilton, R. Julin, S. Juutinen, J. Konki, J. Pakarinen, P. Papadakis, J. Partanen, P. Rahkila, P. Ruotsalainen, M. Sandzelius, J. Sarén, C. Scholey, J. Sorri, S. Stolze, J. Uusitalo, B. Cederwall, A. Ertoprak, H. Liu, I. Kuti, J. Timár, A. Tucholski, J. Srebrny, and C. Andreoiu. Evidence against the wobbling nature of low-spin bands in ^{135}Pr. *Phys. Lett. B and High-Energy Physics*, 824, 2022.

[15] H.M. Maridi, K. Rusek, and N. Keeley. Calculation of coulomb breakup cross sections using a new coulomb dynamical polarization potential. *Phys. Rev. C*, 106(5), 2022.

[16] H.M. Maridi, K. Rusek, and N. Keeley. Comparison of coulomb breakup effects on the elastic scattering of ^{6}He and ^{8}He using a coulomb dipole polarization potential. *Eur. Phys. J. A*, 58(3), 2022.

[17] S.Y. Mezhevych, N. Keeley, A.T. Rudchik, K. Rusek, K.W. Kemper, A.A. Rudchik, O.A. Ponkratenko, E.I. Koshchy, and S.B. Sakuta. Extracting the asymptotic normalization coefficient for the ^{14}C$\rightarrow$ ^{13}B+p overlap from the ^{14}C(^{11}B, ^{12}C) ^{13}B reaction. *Phys. Rev. C*, 105(2), 2022.

[18] S.Yu. Mezhevych, A.T. Rudchik, O.A. Ponkratenko, K. Rusek, K.W. Kemper, V.M. Kyrianchuk, A.A. Rudchik, Y.M. Stepanenko, and V.V. Uleshchenko. Potentials of interaction of ^{10,11,12,13}B isotopes with ^{12}C. *Nucl. Phys. At. Energy*, 23(3):164–171, 2022.

[19] S.Yu. Mezhevych, A.T. Rudchik, K. Rusek, K.W. Kemper, A.A. Rudchik, O.A. Ponkratenko, and E.I. Koshchy. Reaction ^{14}C(^{11}B,^{12}C)^{13}B at E$_{lab}$(^{11}B) = 45 MeV, interaction of ^{13}B+^{12}C versus that of ^{10,11,12}B +^{12}C. *Nucl. Phys. At. Energy*, 23(1):12–19, 2022.

[20] S. Neupane, J. Heideman, R. Grzywacz, M. Cooper, J. Hooker, K.L. Jones, T.T. King, N. Kitamura, M. Madurga, K. Siegl, C.R. Thornsberry, P. Wagenknecht, Z.Y. Xu, L.H. Heilbronn, M.M. Rajabali, A. Chester, A. Richard, Y. Alberty-Jones, J. Derkin, T.N. Massey, D. Soltesz, N.T. Brewer, B.C. Rasco, K.P. Rykaczewski, M. Wolińska-Cichocka, J. Clark, D. Santiago-Gonzales, and G. Savard. Demonstration of the neutron tracking capability of next array in time-of-flight measurements to improve energy resolution. *Phys. Rev. C*, 106(4), 2022.

[21] E.Yu. Nikolskii, I.A. Muzalevskii, A.A. Bezbakh, V. Chudoba, S.A. Krupko, S.G. Belogurov, D. Biare, A.S. Fomichev, E.M. Gazeeva, A.V. Gorshkov, L.V. Grigorenko, G. Kamiński, M. Khirk, O. Kiselev, D.A. Kostyleva, M.Yu. Kozlov, B. Mauyey, I. Mukha, Yu.L. Parfenova, W. Piątek, A.M. Quynh, V.N. Schetinin, A. Serikov, S.I. Sidorchuk, P.G. Sharov, N.B. Shulgina, R.S. Slepnev, S.V. Stepantsov, A. Swiercz, P. Szymkiewicz, G.M. Ter-Akopian, R. Wolski, B. Zalewski, and M.V. Zhukov. ^{6}H states studied in the ^{2}H(^{8}He, ^{4}He) reaction and evidence of an extremely correlated character of the ^{5}H ground state. *Phys. Rev. C*, 105(6), 2022.

[22] A. Pakou, O. Sgouros, V. Soukeras, J. Casal, and K. Rusek. Reaction mechanisms of the weakly bound nuclei ^{6,7}Li and ^{7,9}Be on light targets at near barrier energies. *Eur. Phys. J. A*, 58(1), 2022.

[23] V.H. Phong, S. Nishimura, G. Lorusso, T. Davinson, A. Estrade, O. Hall, T. Kawano, J. Liu, F. Montes, N. Nishimura, R. Grzywacz, K.P. Rykaczewski, J. Agramunt, D.S. Ahn, A. Algora, J.M. Allmond, H. Baba, S. Bae, N.T. Brewer, C.G. Bruno, R. Caballero-Folch, F. Calviño, P.J. Coleman-Smith, G. Cortes, I. Dillmann, C. Domingo-Pardo, A. Fijalkowska, N. Fukuda, S. Go, C.J. Griffin, J. Ha, L.J. Harkness-Brennan, T. Isobe, D. Kahl, L.H. Khiem, G.G. Kiss, A. Korgul, S. Kubono, M. Labiche, I. Lazarus, J. Liang, Z. Liu, K. Matsui, K. Miernik, B. Moon, A.I. Morales, P. Morrall, N. Nepal, R.D. Page, M. Piersa-Siłkowska, V.F.E. Pucknell, B.C. Rasco, B. Rubio, H. Sakurai, Y. Shimizu, D.W. Stracener, T. Sumikama, H. Suzuki, J.L. Tain, H. Takeda, A. Tarifeño-Saldivia, A. Tolosa-Delgado, M. Wolińska-Cichocka, P.J. Woods, and R. Yokoyama. β -delayed one and two neutron emission probabilities southeast of ^{132}Sn and the odd-even systematics in r -process nuclide abundances. *Phys. Rev. Lett.*, 129(17), 2022.

[24] D.A. Pietak, P. Bilski, and P.J. Napiorkowski. Ah method: a novel routine for vicinity examination of the optimum found with a genetic algorithm. *INTERNATIONAL JOURNAL OF ELECTRONICS AND TELECOMMUNICATIONS*, 68(4):695–708, 2022.

[25] K. Pyrzyńska, K. Kilian, and M. Pęgier. Porphyrins as chelating agents for molecular imaging in nuclear medicine. *Molecules*, 27(10), 2022.

[26] K. Pyrzyńska and A. Sentkowska. Biosynthesis of selenium nanoparticles using plant extracts. *J. Nanostruct. Chem.*, 12(4):467–480, 2022.

[27] B.C. Rasco, K.P. Rykaczewski, A. Fijalkowska, M. Karny, M. Wolińska-Cichocka, R.K. Grzywacz, D.W. Stracener, E.F. Zganjar, J.C. Batchelder, J.C. Blackmon, N.T. Brewer, M.P. Cooper, K.C. Goetz, J.W. Johnson, T. King, A. Laminack, J.T. Matta, K. Miernik, M. Madurga, D. Miller, M.M. Rajabali, T. Ruland, P. Shuai, M. Stepaniuk, and J. Winger. Deciphering ^{98}Nb β decay with the modular total absorption spectrometer at ORNL. *Phys. Rev. C*, 105(6), 2022.

[28] A. Rebillard-Soulie, D. Gruyer, G. Verde, FAZIA Collaboration, and FAZIACOR Expt. Study of the hoyle state in ^{12}C produced by ^{20}Ne. *Nuovo Cimento Soc. Ital. Fis. C*, 45(3), MAY-JUN 2022.

[29] A.T. Rudchik, A.A. Rudchik, O.O. Chepurnov, K.W. Kemper, N. Keeley, K. Rusek, E.I. Koshchy, S. Kliczewski, S.Y. Mezhevych, V.M. Pirnak, O.A. Ponkratenko, R. Siudak, H.M. Maridi, A.P. Ilyin, B.V. Mishchenko, Y.M. Stepanenko, V.V. Uleshchenko, Y.O. Shyrma, K.A. Chercas, and B. Zalewski. Comparison of ^{10}B + ^{6}Li and ^{10}B + ^{7}Li elastic scattering: The role of ground state reorientation and breakup. *Phys. Rev. C*, 106(1), 2022.

[30] A.T. Rudchik, A.A. Rudchik, V.V. Khejlo, K. Rusek, K.W. Kemper, E. Piasecki, A. Stolarz, A. Trzcińska, V.M. Pirnak, O.A. Ponkratenko, E.I. Koshchy, O.E. Kutsyk, S.Yu. Mezhevych, A.P. Ilyin, Yu.M. Stepanenko, V.V. Uleshchenko, and Yu.O. Shyrma. Elastic and inelastic scattering of ^{15}N ions by ^{10}B at energy 81 MeV. isotopic effects in scattering of ^{15}N +^{10}B, ^{15}N +^{11}B,^{14}N +^{10}B nuclei. *Nucl. Phys. At. Energy*, 23(3):153–158, 2022.

[31] A. Sentkowska. The potential of traditionally used medicinal plants for the synthesis of selenium nanoparticles. *Nat. Prod. Res.*, 2022.

[32] A. Sentkowska and K. Pyrzyńska. Does the type matter? verification of different tea types' potential in the synthesis of senps. *Antioxidants*, 11(12), 2022.

[33] A. Sentkowska and K. Pyrzyńska. The influence of thiol addition on selenium stability and antioxidant activity of beetroot juice. *Appl. Sci.*, 12(24), 2022.

[34] A. Sentkowska and K. Pyrzyńska. Stability of selenium compounds in aqueous extracts of dietary supplements during storage. *J. Pharm. Biomed. Anal.*, 214, 2022.

[35] A. Sentkowska and K. Pyrzyńska. The influence of synthesis conditions on the antioxidant activity of selenium nanoparticles. *Molecules*, 27(8), 2022.

[36] A. Sentkowska and K. Pyrzyńska. Polyphenols in herbal extracts. *Ref. Ser. Phytochem.*, pages 19–33, 2022.

[37] P. Shuai, B.C. Rasco, K.P. Rykaczewski, A. Fijałkowska, M. Karny, M. Wolińska-Cichocka, R.K. Grzywacz, C.J. Gross, D.W. Stracener, E.F. Zganjar, J.C. Batchelder, J.C. Blackmon, N.T. Brewer, S. Go, M. Cooper, K.C. Goetz, J.W. Johnson, C.U. Jost, T.T. King, J.T. Matta, J.H. Hamilton, A. Laminack, K. Miernik, M. Madurga, D. Miller, C.D. Nesaraja, S. Padgett, S.V. Paulauskas, M.M. Rajabali, T. Ruland, M. Stepaniuk, E.H. Wang, and J.A. Winger. Determination of β -decay feeding patterns of ^{88}Rb and ^{88}Kr using the Modular Total Absorption Spectrometer at ORNL HRIBF. *Phys. Rev. C*, 105(5), 2022.

[38] P. Spagnoletti, P.A. Butler, L.P. Gaffney, K. Abrahams, M. Bowry, J. Cederkäll, T. Chupp, G. De Angelis, H. De Witte, P.E. Garrett, A. Goldkuhle, C. Henrich, A. Illana, K. Johnston, D.T. Joss, J.M. Keatings, N.A. Kelly, M. Komorowska, J. Konki, T. Kröll, M. Lozano, B.S.N. Singh, D. O'Donnell, J. Ojala, R.D. Page, L.G. Pedersen, C. Raison, P. Reiter, J.A. Rodriguez, D. Rosiak, S. Rothe, M. Scheck, M. Seidlitz, T.M. Shneidman, B. Siebeck, J. Sinclair, J.F. Smith, M. Stryjczyk, P. Van Duppen, S. Viñals, V. Virtanen, K. Wrzosek-Lipska, N. Warr, and M. Zielińska. Coulomb excitation of ^{222}Rn. *Phys. Rev. C*, 105(2), 2022.

[39] B. Wasilewska, M. Kmiecik, M. Ciemała, A. Maj, F.C.L. Crespi, A. Bracco, M.N. Harakeh, P. Bednarczyk, S. Bottoni, S. Brambilla, F. Camera, I. Ciepał, N. Cieplicka-Oryńczak, M. Csatlos, B. Fornal, V. Gaudilla, J. Grębosz, J. Isaak, Ł.W. Iskra, M. Jeżabek, A.J. Krasznahorkay, S. Kihel, M. Krzysiek, P. Lasko, S. Leoni, M. Lewitowicz, J. Łukasik, M. Matejska-Minda, K. Mazurek, P.J. Napiorkowski, W. Parol, P. Pawłowski, L.Q. Qi, M. Saxena, C. Schmitt, Y. Sobolev, B. Sowicki, M. Stanoiu, A. Tamii, O. Wieland, and M. Zięblíński. γ decay to the ground state from the excitations above the neutron threshold in the ^{208}Pb(p, p'γ) reaction at 85 MeV. *Phys. Rev. C*, 105(1), 2022.

[40] J. Wu, S. Nishimura, P.-A. Söderström, A. Algora, J.J. Liu, V.H. Phong, Y.Q. Wu, F.R. Xu, J. Agramunt, D.S. Ahn, T.A. Berry, C.G. Bruno, J.J. Bundgaard, R. Caballero-Folch, A.C. Dai, T. Davinson, I. Dillmann, A. Estrade, A. Fijałkowska, N. Fukuda, S. Go, R.K. Grzywacz, T. Isobe, S. Kubono, G. Lorusso, K. Matsui, A.I. Morales, N. Nepal, S.E.A. Orrigo, B.C. Rasco, K.P. Rykaczewski, H. Sakurai, Y. Shimizu, D.W. Stracener, T. Sumikama, H. Suzuki, J.L. Tain, H. Takeda, A. Tarifeño-Saldivia, A. Tolosa-Delgado, M. Wolińska-Cichocka, and R. Yokoyama. First observation of isomeric states in ^{111}Zr, ^{113}Nb, and ^{115}Mo. *Phys. Rev. C*, 106(6), 2022.

D.4 Seminars

D.4.1 Seminars organised at HIL

J. Choiński — Heavy Ion Laboratory, University of Warsaw, Warszawa, Poland — 01 January 2022

Informacje o aparaturze pozyskanej z Uppsali
Information about the apparatus acquired from Uppsala

U. Kaźmierczak — Heavy Ion Laboratory, University of Warsaw, Warszawa, Poland — 18 March 2022

Pracownia radiobiologiczna w ŚLCJ UW - jej powstanie i badania wstępne
The radiobiology laboratory at ŚLCJ UW - its creation and preliminary research

N. Kopeć — Heavy Ion Laboratory, University of Warsaw, Warszawa, Poland — 20 April 2022

Symulacje procesów fragmentacji ciężkich jonów w zakresach energii SPS, CERN
Simulations of fragmentation processes of heavy ions in the energy range of SPS, CERN

H. Maridi — Heavy Ion Laboratory, University of Warsaw, Warszawa, Poland — 08 May 2022

Coulomb breakup of exotic nuclei studied by means of dynamic polarization potential

S. K. Chamoli — Saha Institute of Nuclear Physics, Kolkata, India — 15 July 2022

Nuclear structure studies with lifetime measurements at IUAC Delhi

S. Bhattacharjee — Saha Institute of Nuclear Physics, Kolkata, India — 06 September 2022

Probing the reaction dynamics of strongly and weakly bound projectiles eith rare-earth target nuclei

B. Zalewski — Heavy Ion Laboratory, University of Warsaw, Warszawa, Poland — 12 October 2022

1,2H+6He reactions at ACCULINNA2

Z. Szefliński — Heavy Ion Laboratory, Univ. of Warsaw, Warszawa, Poland — 09 November 2022

Jak zlekceważyć Nagrodę Nobla. Test nierówności Bella dla splątanych kwantów gamma
How to disregard the Nobel Prize. Bell inequality test for entangled gamma quanta

D.4.2 Seminars co-organised by HIL

Warsaw Nuclear Physics Seminar

Seminars organised jointly by the divisions of Nuclear Physics and Nuclear Structure Theory of the Faculty of Physics, University of Warsaw and the Heavy Ion Laboratory, University of Warsaw

K. Rykaczewski — Oak Ridge National Lab., Oak Ridge, TN, USA 13 February 2022

R. Grzywacz — Dep. of Physics and Astronomy, Univ. of Tennessee, Knoxville, TN, USA
A. Korgul, M. Pfützner — Inst. of Exp. Physics, Univ. of Warsaw, Warsaw, Poland
Spotkanie specjalne z okazji Th(orowego) jubileuszu prof. Jana Żylicza
Special meeting on the occasion of Prof. Jan Żylicz's Th(orowy) jubilee

K. Grzelak — Inst. of Exp. Physics, University of Warsaw, Warszawa, Poland 27 January 2022
Neutrina sterylne. Status poszukiwań i nowe wyniki dotyczące zagadki LSND/MiniBooNE, anomalii antyneutrin reaktorowych i anomalii galowej
Sterile neutrinos LSND/MiniBooNE puzzle. Reactor Antineutrino Anomaly. Gallium Anomaly

P. Magierski — Faculty of Physics, Warsaw Univ. of Technology 03 March 2022
Mody Nambu-Goldstonea i Higgsa w zderzeniach jąder atomowych
Nambu-Goldstone and Higgs modes in nuclear collisions

R. Han — Department of Physics, University of Jyväskylä, Finland 10 March 2022
Scission configuration in self-consistent calculations with neck constraint

M. Zielińska — IRFU, CEA, Université Paris-Saclay, Gif-sur-Yvette, France 17 March 2022
AGATA wraca do Legnaro
AGATA is coming back to Legnaro

A. Tolosa-Delgado — Department of Physics, University of Jyväskylä, Finland 24 March 2022
High accuracy neutron emission measurements of nuclei around 78Ni for nuclear astrophysics

D. Vretenar — Faculty of Science, University of Zagreb 31 March 2022
Induced fission dynamics

J. E. García-Ramos — University of Huelva, Huelva, Spain 21 April 2022
On the nature of the shape coexistence and the quantum phase transition phenomena in the zirconium and lead region

M. Kuźniak — AstroCeNT: Particle Astrophysics Science and Technology Centre, Warsaw, Poland 28 April 2022
Poszukiwanie ciemnej materii przy pomocy detektorów ciekło-argonowych
Searching for dark matter with liquid-argon detectors

P. Moskal — Inst. of Phys., Jagiellonian Univ., Kraków, Poland 19 May 2022
Positronium imaging with the J-PET tomograph

U. Kaźmierczak — Heavy Ion Laboratory, University of Warsaw, Warszawa, Poland — 26 May 2022

Pracownia radiobiologiczna w ŚLCJ UW
Radiobiology laboratory at ŚLCJ UW

A. Kankainen — Department of Physics, University of Jyväskylä, Finland — 02 June 2022

Studies for nuclear structure and astrophysics with the JYFLTRAP Penning trap

A. Ciemny — Institute of Experimental Physics, University of Warsaw, Warszawa, Poland — 09 June 2022

Exotic decay modes of medium-mass proton drip-line nuclei

M. Pfützner — Institute of Experimental Physics, University of Warsaw, Warszawa, Poland — 06 October 2022

Egzotyczne rozpady z emisją cząstek naładowanych
Exotic Decays with Emission of Charged Particles

B. Hong — Center for Extreme Nuclear Matters (CENuM), Korea University — 07 October 2022

Radioactive-ion-beam (RIB) accelerator complex RAON

K. Łasocha — Jagiellonian Univ., Kraków, Poland — 20 October 2022

Non-invasive Beam Diagnostics with Schottky Signals and Cherenkov Diffraction Radiation

A. Wrońska — Jagiellonian Univ., Kraków, Poland — 27 October 2022

Prompt-gamma radiation in proton therapy - activities of the SiFi-CC collaboration

R. Mikołajczak — National Centre for Nuclear Research, Institute of Atomic Energy POLATOM, Otwock-Świerk, Poland — 03 November 2022

CERAD – cyklotron 30 MeV w infrastrukturze badawczej NCBJ
ERAD – 30 MeV cyclotron in the NCBJ research infrastructure

J. W. Mitelski — The H. Niewodniczański Institute of Nuclear Physics PAN, Kraków, Poland — 10 November 2022

The Oklo natural reactor in Gabon: 50 years from the discovery

B. Jurado — LP2I, Bordeaux-Gradignan, France — 17 November 2022

Indirect measurements of neutron-induced reaction cross sections at storage rings

Z. Szefliński — Heavy Ion Laboratory, Univ. of Warsaw, Warszawa, Poland — 24 November 2022

Jak zlekceważyć Nagrodę Nobla. Test nierówności Bella dla splątanych

kwantów gamma
How to disregard the Nobel Prize. Bell inequality test for entangled gamma quanta

T. Cap — National Centre for Nuclear Research 01 December 2022
Możliwości wytworzenia pierwiastków o Z > 118
Possibilities of producing elements with Z > 118

M. Stepaniuk — Inst. of Exp. Physics, University of Warsaw, Warszawa, Poland 08 December 2022
Badanie rozpadów beta neutrono-nadmiarowych jąder bromu za pomocą Modularnego Spektrometru Pełnej Absorpcji
Study of beta decays of neutron-redundant bromine nuclei using the Modular Full Absorption Spectrometer

P. Horodek — The H. Niewodniczański Institute of Nuclear Physics PAN, Kraków, Poland 15 December 2022
Spektroskopia anihilacji pozytonów w badaniach materiałowych
Positron annihilation spectroscopy in materials research

D.4.3 External seminars given by HIL staff

K. Hadyńska-Klęk 31 May 2022
Shapes in the stable Xe isotopic chain
Shapes and Symmetries in Nuclei: from Experiment to Theory (SSNET'22 Conference), IJCLab in Orsay, France

K. Wrzosek-Lipska 5 June 2022
Shape coexistence and E0 transitions in neutron-deficient Hg isotopes studied through Coulomb excitation
Shapes and Symmetries in Nuclei: from Experiment to Theory (SSNET'22 Conference), IJCLab in Orsay, France

A. Sentkowska 22 June 2022
Problemy analityczne w analizie specjacyjnej selenu z wykorzystaniem chromatografii cieczowej w trybie HILIC
Analytical problems in speciation analysis of selenium using liquid chromatography in the HILIC mode
XI Polska Konferencja Chemii Analitycznej, Łódź

G. Jaworski 03 September 2022
NEEDLE — fast neutron detection in the service of the gamma spectroscopy of neutron-deficient nuclei at HIL
The 55th Zakopane Conference on Nuclear Physics, Zakopane, Poland

L. Próchniak 23 September 2022
Quadrupoles, octupoles, invariants and ... syzygies
28^{th} Nuclear Physics Workshop, 24-28 September, Kazimierz Dolny

J. Srebrny 23 September 2022
Quadrupole Triaxiality Softness-collective models from simple phenomenological model to fully microscopic General Bohr Hamiltonian
28^{th} Nuclear Physics Workshop, 24-28 September, Kazimierz Dolny

M. Paluch-Ferszt 26 October 2022
Nuclear Power as an opportunity for low-cost and clean energy
EGT 2022 Energy, Environmental technology, Green transformation, Warsaw, Poland

K. Hadyńska-Klęk 15 November 2022
Nuclear deormation in excited states
Workshop of the COLL-AGAIN (France - Italy), COPIGAL (France - Poland), and POLITA (Italy - Poland), IJCLab in Orsay, France

M. Palacz 15 November 2022
Nuclear structure close to N=Z=50 with AGATA
Workshop of the COLL-AGAIN (France - Italy), COPIGAL (France - Poland), and POLITA (Italy - Poland), IJCLab in Orsay, France

G. Colucci 16 November 2022
Fusion barrier distribution studies
Workshop of the COLL-AGAIN (France - Italy), COPIGAL (France - Poland), and POLITA (Italy - Poland), IJCLab in Orsay, France

K. Wrzosek-Lipska 16 November 2022
Nuclear deformation in excited states - Shape coexistence
Workshop of the COLL-AGAIN (France - Italy), COPIGAL (France - Poland), and POLITA (Italy - Poland), IJCLab in Orsay, France

K. Rusek 18 November 2022
Reaction dynamics studies with light exotic beams
Workshop of the COLL-AGAIN (France - Italy), COPIGAL (France - Poland), and POLITA (Italy - Poland), IJCLab in Orsay, France

D.4.4 Poster presentations

M. Wolińska-Cichocka 30 August 2022
IBeta decay of A=142 isobars improved by means of MTAS array
The 55th Zakopane Conference on Nuclear Physics, Zakopane, Poland

D.4.5 Lectures for students and student laboratories

K. Kilian summer semester of the academic year 2021/2022, 15 hours
Radiofarmaceutyki — synteza, wytwarzanie i zastosowania
Radiopharmaceuticals — synthesis, production and applications
Faculty of Chemistry, University of Warsaw, Warszawa, Poland

K. Kilian summer semester of the academic year 2021/2022, 60 hours
Pracownia radiofarmaceutyków
Laboratory of Radiopharmaceuticals
Faculty of Physics, University of Warsaw, Warszawa, Poland

K. Kilian winter semester of the academic year 2021/2022, 30 hours
Metody izotopowe i chemia radiofarmaceutyków
Radiochemistry and radiopharmacy
Faculty of Chemistry, University of Warsaw, Warszawa, Poland

A. Sentkowska winter semester of the academic year 2021/2022, 45 hours
Analityka środowiska - laboratorium
Environmental Analysis Laboratory
Faculty of Chemistry, University of Warsaw, Warszawa, Poland

A. Sentkowska winter semester of the academic year 2021/2022, 45 hours
Pracownia specjalizacyjna
Specialization Laboratory
Faculty of Chemistry, University of Warsaw, Warszawa, Poland

Z. Szefliński summer semester of the academic year 2021/2022, 30 hours
Techniki jądrowe w diagnostyce i terapii medycznej
Nuclear Techniques in Medical Diagnostics and Therapy
Faculty of Physics, University of Warsaw, Warszawa, Poland

B. Zalewski summer semester of the academic year 2021/2022, 45 hours
Pracownia Technik Pomiarowych dla Astronomów
Laboratory of measurement techniques for astronomers
Faculty of Physics, University of Warsaw, Warszawa, Poland

D.4.6 Science popularization lectures

Z. Szefliński Uniwersytet Otwarty UW 08.03.22

Czy bać się elektrowni atomowej?
Should you be afraid of a nuclear power plant?

M. Paluch-Ferszt radio broadcast "Network Effect" DELab UW 24.03.2022

Czym grożą podróże w kosmos?
What are the risks of space travel?

M. Paluch-Ferszt radio broadcast "Network Effect" DELab UW 07.04.2022

Jak odległy jest kosmos?
How far away is space?

Z. Szefliński Guest lecture at the FUW May 2022

Fizyka w diagnostyce medycznej PET-SPECT
Physics in PET-SPECT medical diagnostics

M. Paluch-Ferszt radio broadcast "Network Effect" DELab UW 02.06.2022

Wyjaśnianie z uzyciem metody Monte Carlo
Explaining using the Monte Carlo method.

A. Sentkowska Dzień Otwarty kampusu Ochota 11.06.22

Przypadki chodzą po ludziach- o przypadkowych odkryciach w chemii
Coincidences happen to people - about accidental discoveries in chemistry

A. Sentkowska Dzień Otwarty kampusu Ochota 11.06.22

Czy na pewno wiesz jak parzyć herbatę? O zdolnościach antyutleniających słów kilka
Do you know how to brew tea? A few words about antioxidant abilities

M. Paluch-Ferszt radio broadcast "Network Effect" DELab UW 16.06.2022

Monte Carlo, Las Vegas czyli interdyscyplinarne szacowanie prawdopodobieństwa
Monte Carlo, Las Vegas or interdisciplinary probability estimation

A. Sentkowska III meeting of the Heavy Ion Laboratory Council 24.06.22

Co wspólnego ma herbata Zhejiang i cyklotron?
What do Zhejiang tea and a cyclotron have in common?

A. Sentkowska Meeting of the Scientific Council of the Faculty of Chemistry, UW 07.07.22

Aspekty metodologiczne w oznaczaniu specjacji selenu
Methodological aspects in the determination of selenium speciation

Z. Szefliński Festiwal Nauki 16-30.09.22

Promieniowanie, kóre leczy
The radiation that heals

A. Sentkowska Festiwal Nauki 16-30.09.22

Czy na pewno wiesz jak parzyć herbatę? O zdolnościach antyutleniających słów kilka
Do you know how to brew tea? A few words about antioxidant abilities

M. Paluch-Ferszt radio broadcast "Network Effect" DELab UW 20.10.2022

Czy elektrownie jądrowe są bezpieczne?
Are nuclear power plants safe?

M. Paluch-Ferszt radio broadcast "Network Effect" DELab UW 03.11.2022

Czy łatwo zaatakować elektrownię jądrową?
Is it easy to attack a nuclear power plant?

M. Palacz Guest lecture for the Faculty of Physics, Warsaw Univ. of Technology 16.12.2022

Śrdowiskowe Laboratorium Ciężkich Jonów
Heavy Ion Laboratory

D.5 Honours and Awards

The Rector of the University of Warsaw awards

In 2022 the following employees of the Heavy Ion Laboratory received the Rector of the University of Warsaw award:

Mariusz Antczak,
Eliza Balcerowska,
Anna Błaszczyk-Duda,
Jarosław Choiński,
Antoni Dąbkowski,
Piotr Jasiński,
Wiesław Kalisiewicz,
Maciej Kisieliński,
Robert Kopik,
Mariusz Matuszewski,
Paweł Napiorkowski,
Bogusław Paprzycki,
Bogdan Radomyski,
Lidia Strzelczyk,
Katarzyna Włodarczyk,
Bogumił Zalewski,
Magdalena Zawal.

D.6 Laboratory staff

Director: Paweł Napiorkowski
Deputy director: Jarosław Choiński, Leszek Próchniak
Financial executive: Eliza Balcerowska

Senior scientists:

Krzysztof Kilian, Andrzej Kordyasz[a], Marcin Palacz, Ernest Piasecki[a], Krzysztof Rusek[a], Anna Stolarz, Zygmunt Szefliński[a]

Scientific staff and engineers:

Tomasz Abraham, Andrzej Bednarek, Giulia Colucci, Przemysław Gmaj, Katarzyna Hadyńska-Klęk, Grzegorz Jaworski, Grzegorz Kamiński[b], Urszula Kaźmierczak, Maciej Kisieliński, Marian Kopka, Michał Kowalczyk, Katarzyna Krutul-Bitowska, Ireneusz Mazur, Jan Miszczak, Wojciech Okliński[a], Monika Paluch-Ferszt, Serhii Panasenko[c], Mateusz Pęgier, Wojciech Piątek[bd], Bogdan Radomyski, Olga Saeed Mohamed Nassar, Justyna Samorajczyk-Pyśk, Aleksandra Sentkowska, Julian Srebrny[a], Roman Tańczyk, Agnieszka Trzcińska, Andrzej Tucholski, Marzena Wolińska-Cichocka, Katarzyna Wrzosek-Lipska

Doctoral candidates:

Michalina Komorowska, Łukasz Standyło, Bogumił Zalewski

Technicians:

Mariusz Antczak, Tomasz Bracha, Piotr Jasiński, Bartosz Kalisiewicz, Wiesław Kalisiewicz, Robert Kopik, Wojciech Kozaczka, Zbigniew Kruszyński[a], Piotr Krysiak, Krzysztof Łabęda, Kamil Makowski, Mariusz Matuszewski, Bogusław Paprzycki, Krzysztof Pietrzak, Robert Ratyński[e], Mariusz Szperkiewicz, Łukasz Świątek

Administration and support:

Anna Błaszczyk-Duda, Antoni Dąbkowski, Maciej Durkiewicz, Jan Getka[f], Andrzej Giziński, Radosław Jaielski, Tadeusz Jagielski, Rafał Klęk[g], Barbara Kowalska[ah], Joanna Kowalska, Jolanta Matuszczak, Aleksander Morantowicz, Anna Odziemczyk, Jolanta Ormaniec, Anna Ratyńska, Mirosław Rogalski[i], Ewa Sobańska, Nurullo Sobirov, Lidia Strzelczyk, Edyta Szeląg, Lech Szeląg, Andrzej Wiechowski[j], Katarzyna Włodarczyk[a], Magdalena Zawal

Voluntary scientists:

Martyna Araszkiewicz[kl], Jędrzej Iwanicki, Jan Kownacki, Iwona Piętka[lm], Andrzej Wojtasiewicz, Irena Żejmo

[a]part time
[b]on leave
[c]since 1 May
[d]until 31 Auust
[e]since 1 March
[f]until 28 February
[g]since 1 September
[h]until 26 November
[i]since 1 April
[j]until 30 May
[k]since 23 May
[l]until 30 September
[m]since 12 May

D.7 Laboratory Council

1. Prof. dr hab. Józef Andrzejewski
Nuclear Physics Division
University of Łódź, Łódź
2. Prof. dr hab. Mieczysław Budzyński
Institute of Physics
Maria Curie-Skłodowska University, Lublin
3. Prof. dr hab. Ewa Bulska
Biological and Chemical Research Centre
University of Warsaw, Warszawa
4. Dr Jarosław Choiński
Heavy Ion Laboratory
University of Warsaw, Warszawa
5. Prof. dr hab. Zbigniew Czerski
Institute of Physics
University of Szczecin, Szczecin
6. Prof. dr hab. inż. Andrzej Chmielewski
(**Member of the Council Presidium**)
Institute of Nuclear Chemistry
and Technology, Warszawa
7. Prof. dr hab. Bogdan Fornal
The Henryk Niewodniczański
Institute of Nuclear Physics
Polish Academy of Sciences, Kraków
8. Dr hab. Krzysztof Kilian
Heavy Ion Laboratory
University of Warsaw, Warszawa
9. Prof. dr hab. Stanisław Kistryn
(**Member of the Council Presidium**)
M. Smoluchowski Institute of Physics
Jagiellonian University, Kraków
10. Dr hab. Agnieszka Korgul
Faculty of Physics
University of Warsaw, Warszawa
11. Dr hab. inż. Michał Kowal, prof. NCNR
The National Centre for Nuclear Research
Świerk
12. Prof. dr hab. Leszek Królicki
Department of Nuclear Medicine
Medical University of Warsaw, Warszawa
13. Prof. dr hab. inż. Krzysztof Kurek
(**Member of the Council Presidium**)
The National Centre for Nuclear Research
Świerk k/Warszawy
14. Prof. dr hab. Adam Maj
(**Chairman of the Council**)
The Henryk Niewodniczański
Institute of Nuclear Physics
Polish Academy of Sciences, Kraków
15. Prof. dr hab. inż Piotr Magierski
Faculty of Physics
Warsaw University of Technology,
Warszawa
16. Dr hab. Krzysztof Miernik
Faculty of Physics
University of Warsaw, Warszawa
17. Dr Paweł Napiorkowski
(**Director of HIL**)
Heavy Ion Laboratory
University of Warsaw, Warszawa
18. Dr hab. Marcin Palacz
Heavy Ion Laboratory
University of Warsaw, Warszawa
19. Dr hab. Leszek Próchniak
Heavy Ion Laboratory
University of Warsaw, Warszawa
20. Prof. dr hab. Krzysztof Rusek
Heavy Ion Laboratory
University of Warsaw, Warszawa
21. Prof. dr hab. Wojciech Satuła
(**Deputy Chairman of the Council**)
Faculty of Physics
University of Warsaw, Warszawa
22. Dr hab. Elżbieta Stephan, prof. US
Institute of Physics
University of Silesia, Katowice
23. Dr Agnieszka Trzcińska
(representative of the HIL staff)
Heavy Ion Laboratory
University of Warsaw, Warszawa

D.8 Programme Advisory Committee

PAC members

- Piotr Bednarczyk (The H. Niewodniczański Institute of Nuclear Physics PAN, Kraków, Poland)
- Gilles de France (GANIL, Caen, France)
- Nicholas Keeley (National Centre for Nuclear Research, Otwock, Poland)
- Marco Mazzocco (Padova University, Padova, Italy)
- Chiara Mazzocchi (Faculty of Physics, University of Warsaw, Warszawa, Poland)
- Leszek Próchniak (Heavy Ion Laboratory, University of Warsaw, Warszawa, Poland)
- Władysław Trzaska (Department of Physics, University of Jyväskylä, Finland)

The international Programme Advisory Committee of the Heavy Ion Laboratory usually meets twice a year, in spring and autumn. The deadline for submitting proposals is 3 - 4 weeks before a PAC meeting. PAC approved experiments are scheduled at the meetings of the Users' Committee, which also serves as a link between cyclotron users and the Laboratory. The Users' Committee is chaired by Jarosław Perkowski (the University of Łódź).

D.9 External HIL users

In 2022 there were **41** external HIL users and visitors from **17** scientific institutions, including 12 people from 4 institutes in Poland, 14 people from 8 institutions in the European Union and associated countries and 15 people from 5 institutes in other countries.

External HIL users and visitors were from:

Poland

- Faculty of Physics, University of Warsaw, Warszawa, Poland
- Faculty of Biology, University of Warsaw, Warszawa, Poland
- The H. Niewodniczański Institute of Nuclear Physics PAN, Kraków, Poland
- National Centre for Nuclear Research, Otwock, Poland

European Union and associated countries

- Institute for Nuclear Physics, University of Cologne, Germany
- Institut Laue Langevin, Grenoble, France
- INFN Sezione di Firenze, Firenze, Italy
- INFN. Sezione di Milano, Milano, Italy
- IRFU, CEA, Université Paris-Saclay, Gif-sur-Yvette, France
- IKP, Technical University Darmstadt, Darmstadt, Germany
- Sofia University, Sofia, Bulgaria
- University of Milan, Milano, Italy

Other countries

- Department of Physics, University of Surrey, Guildford, UK
- Eurasian National University, Institute of Nuclear Phisics, Nur-Sultan, Kazakhstan
- Faculty of Science, Tanta University, Tanta, Egypt
- Saha Institute of Nuclear Physics, Kolkata, India
- University of Guelph, Guelph, Canada

List of Authors

www.slcj.uw.edu.pl

RAPORT ROCZNY 2022
ŚRODOWISKOWE LABORATORIUM CIĘŻKICH JONÓW
UNIWERSYTET WARSZAWSKI